SF 298 MASTER COPY KEEP THIS COPY FOR REPRODUCTION PURPOSES

REPORT DOCUMENTATION PAGE

Form Approved OMB NO. 0704-0188

1. AGENCY USE ONLY *(Leave blank)*	2. REPORT DATE	3. REPORT TYPE AND DATES COVERED
	April 15, 2003	April 1999 to March 2003 01 Apr 99 - 31 Oct 02

4. TITLE AND SUBTITLE

Experimental Characterization and Modeling of Damage in Composites under Ballistic Impact

5. FUNDING NUMBERS

FAMU account 37-1906-~~[illegible]~~ 712

Grant No. DAAD19-99-1-0166

6. AUTHOR(S)

Dr. Namas Chandra (P. I.)

7. PERFORMING ORGANIZATION NAMES(S) AND ADDRESS(ES)

Florida A&M University
Division of Sponsored Research
400 Foote Hilyer Administration Center
Tallahassee, FL 32307

8. PERFORMING ORGANIZATION REPORT NUMBER

9. SPONSORING / MONITORING AGENCY NAME(S) AND ADDRESS(ES)

U.S. Army Research Office
P.O. Box 12211
Research Triangle Park, NC 27709-2211

10. SPONSORING / MONITORING AGENCY REPORT NUMBER

38718.1-MS-SAH

11. SUPPLEMENTARY NOTES

The views, opinions and/or findings contained in this report are those of the author(s) and should not be construed as an official Department of the Army position, policy or decision, unless so designated by other documentation.

12a. DISTRIBUTION / AVAILABILITY STATEMENT

Approved for public release; distribution unlimited.

20030509 058

13. ABSTRACT *(Maximum 200 words)*

The primary focus of our research is to understand the ballistic behavior of composites. It is shown that the shock response of composites is quite different from that of the metals, and the presence of heterogeneous interfaces in composites can be attributed to this fact. The interfaces cause multiple scattering, and the magnitude of scattering depends on the level of heterogeneity as indicated by impedance mismatch. In this research work we have developed an analytical model for the plate impact of a bilaminate material system by considering explicitly material heterogeneity and the equation of state. Comparison of the model with experimental data and numerical results show good agreement.

Further, a comprehensive analysis of cohesive zone models has been carried out to study its applicability to represent damage and fracture from a micromechanical perspectives. Thus cohesive zone models can be used within the framework of continuum mechanics to analyze damage in the composites under ballistic loading conditions.

14. SUBJECT TERMS			15. NUMBER IF PAGES
			16. PRICE CODE
17. SECURITY CLASSIFICATION OR REPORT	18. SECURITY CLASSIFICATION OF THIS PAGE	19. SECURITY CLASSIFICATION OF ABSTRACT	20. LIMITATION OF ABSTRACT
UNCLASSIFIED	UNCLASSIFIED	UNCLASSIFIED	UL

NSN 7540-01-280-5500

Enclosure 1

Standard Form 298 (Rev. 2-89)
Prescribed by ANSI Std. 239-18
298-102

EXPERIMENTAL CHARICTERIZATION AND MODELING OF DAMAGE IN COMPOSITES UNDER BALLISTIC IMPACT

FINAL REPORT

Namas Chandra and Xianglei Chen

March 2003

U.S. ARMY RESEARCH OFFICE

Grant No. DAAD19-99-1-0166

Department of Mechanical Engineering
FAMU-FSU College of Engineering
Florida State University
2525 Pottsdamer Street, Room 229
Tallahassee, FL 32310

APPROVED FOR PUBLIC RELEASE
DISTRIBUTION UNLIMITED

PUBLICATIONS DURING THE PROJECT PERIOD
1999-2002

1. X.Chen and N. Chandra, Material heterogeneity and the structure of the stress wave of layered material system, (to be submitted).

2. X.Chen, N. Chandra and A.M. Rajendran, Analytical Solution to the Plate Impact Problem of Layered Heterogeneous Material Systems, (to be submitted).

3. N. Chandra, X. Chen and A.M. Rajendran, The Effect of Material Heterogeneity on the Shock Response of Layered Systems in Plate Impact Tests, Journal of Composites Technology & Research, 24 (4): 232-238, (2002).

4. Oscillatory structure of stress wave profile in layered systems under plate impact loading conditions, X. Chen, N. Chandra, A.M. Rajendran, Proceedings of the 2th international Conference on Structural Ability and Dynamics, December 16-18, 981-987, (2002).

5. X. Chen, N. Chandra, A.M. Rajendran, The shock response of layered systems in plate impact tests, Proceedings of the Shock wave processes in condensed matter, Edinburgh, 19-24 May 2002.

6. X. Chen and N. Chandra, The effect of material heterogeneity on high amplitude wave propagation in layered material system. Fourteenth U.S. National Congress of Theoretical and Applied Mechanics (USNCTAM14), June 23-28, Blacksburg, Virginia USA, 2002.

7. Temperature Effects on the Localization and Mode of Failure of Al 5083, John D. Watts, Xianglei Chen, Anthony Belvin, Z. Chen and N. Chandra. Material Science Forum, Vols. 357-359, 599-606, (2000).

GRADUATE STUDENTS

XIANGLEI CHEN
ANTHONY BELVIN
JOHN WATTS

Contents

1 Introduction **6**

1.1. Motivation 6

1.2. Outline of the Report 8

2 Wave propagation in solids **10**

2.1. Wave equation and wave velocity 11

2.1.2. Plastic wave propagation 15

2.1.3. Shock wave equations 16

2.2. Plate Impact Tests and the State of Uniaxial Strain 17

3 The impact response of layered heterogeneous systems subjected to plate impact loadings **25**

3.1. An analytical model to study the rise characteristics based on multiple reflections in layered composites 28

3.1.1. Solution method 28

3.1.2. Numerical/Analytical Solution to the Cu/Al multi-layered system . . . 35

3.1.3. Some consequences of the analytical solution 37

3.1.4. Summary 37

3.2. Late time solution to the plate impact problem 39

3.2.1. Background 39

3.2.2. Problem formulation and solution methods 43

3.2.3. Solution to the plate impact problem 50

3.2.4. Approximate Solution for shock loading 58

3.2.5. Results and discussions 63

3.2.6. Summary 67
Appendix: Dremin's theory in finding effective wave speed 68

4 Controlling parameters for layered materials **71**
4.1. Material Heterogeneity factors 71
4.1.1. Impedance mismatch 73
4.1.2. Number of layers/Interface density 75
4.1.3. Thickness ratio 77
4.2. Numerical analysis of elastic-plastic response of layered systems 78
4.3. Structure of the stress wave profiles of periodic layered structures 80
4.3.1. Rise characteristics 80
4.3.2. Oscillations 83
4.4. Velocity c_0 and Arrival time 84

5 Composites **96**
5.1. Constitutive Relation 97
5.2. Modes of failure of composites 100
5.3. Simulating composite damage under impact using LS-DYNA3D 102
Damage of composites by plate impact (modeling) 104
5.4. Modeling the engineering GRP as layered structures 106

6 Conclusions **111**

List of Figures

2-1 Schematic illustration of wave propagation in the bar 13

2-2 Schematic X-T diagram of elastic-plastic plate impact (same materials) . . . 15

2-3 Stress profile of elastic-plastic plate impact (a) $\sigma_x - \epsilon_x$ for uniaxial strain (b) $\sigma_x - T$ 22

2-4 Schematic of plate impact experiments to investigate shock wave profiles in laminated materials 23

2-5 Stress-strain curve for uniaxial strain 23

2-6 Stress - strain relation of ideal elastic-plastic material. 24

3-1 X-T diagram of aluminum plate impacts another aluminum plate 26

3-2 Normal stress profile of Al-Al elastic 27

3-3 Schematic of layered system. 30

3-4 Reflection/transmission at an Interface 31

3-5 Head wave and successive wave trains in a layered system 31

3-6 Stress intensity of head wave in a layered system 32

3-7 Rise characteristics of alternating layered Al - Cu (a) Schematic configuration, (b) 2L=4, (c) 2L=8, (d) 2L=16 36

3-8 (a) Schematic configuration (b) Definition of the rising angle (c) Results . . . 38

3-9 Schematic wave profiles of homogeneous metals and layered composites for a finite thickness flyer plate. 40

3-10 Schematic of the configuration for impact problem(a) two half spaces of homogeneous materials, (b) general plate impact problem of layered systems (c) plate impact problem of two half spaces with target being layered (d) The layered media under unit step loading. 44

3-11 Solution to the Unit step loading condition in PMMA-Cu. 50
3-12 Multi-step loading method (a) The wave trains that reach the impact plane from inside of the target due to reflections. 53
3-13 Comparison of the stress history at the boundary of the layered systems between analytical solution and 54
3-14 Comparison of solutions for Al impacting PMMA26/Al36 at x=10mm. Comparison between FEM results and Analytical solutions using n=1,3,5 respectively. 59
3-15 The normalized mean stress as a function of volume fraction in different systems. 64
3-16 The effect of EOS in velocity and impedance mismatch. 65
3-17 Comparisons of the experimental data and the analytical solutions in layered PC/GS. (a) Experiment 1, and (b) Experiment 2. 70

4-1 Structure of 2D woven GRP. (a) Fiber fabric, (b) micrograph of the lay-up structure 72
4-2 The relation between impedance mismatch I and impedance ratio R. 74
4-3 Impedance mismatch of selected material combinations 87
4-4 The strength of the head wave and the second wave train as a function of I with 2L=16. 88
4-5 The effect of thickness ratio on the rise characteristics of Al-Cu structures. (a) Configuration, (b) The third wave trains of different ratio, (c) (d) , (e) , and (f) 89
4-6 The effect of interface on spatial wave dispersion and attenuation in alternating glass/resin system. 90
4-7 The effect of yield stress/strength on wave profile for fixed Young's modulus, failure strain and strain hardenging coefficient. Impacting velocity 273m/s. (a)1.0×10^7 Pa, (b) 1.0×10^8 Pa, (c) 5.0×10^8 Pa, (d) 1.0×10^9 Pa. 91
4-8 The elastic-plastic response of homogeneous resin. 92
4-9 The analytical solutions to the normalized stress history (with respect to in PMMA-PC, PMMA-Al and PMMA-Cu. (a) Flyer plate is PMMA and (b) Flyer plate is Al. 93

4-10 The shock responses of two material systems. (a) Epoxy/Epoxy-graphite by Clements et al, (b) Cu-PMMA by Oved et al. 94
4-11 The frequency factors of different systems. 95
4-12 The effective velocity of different systems. 95

5-1 Material properties of CFRP T300/914 98
5-2 Copper impacting an elastic orthotropic plate 99
5-3 Failure modes of composites 102
5-4 The failure evolution including fiber failure and matrix crack 104
5-5 Damage modes and the corresponding stresses update 105
5-6 Experimental results of GRP subjected to plate impact [1]. 107
5-7 Lamina of 2D woven GRP and wave refelctions in a curved interface. 110

Chapter 1

Introduction

1.1. Motivation

The understanding of the behavior of materials under very high strain rate loading conditions is vital to many areas of civilian applications ranging from explosive forming, welding, cutting, compaction, and hardening, to oil well exploration and micrometeorite impact on space stations; military applications are also numerous and range from armor and anti-armor structures/vehicles to ballistic designs. There are many other additional applications of high strain-rate deformation, such as machining, accidental impact of vehicles and crashworthiness studies, earthquakes and the associated damage to structures, and explosive devices. All these applications require a thorough knowledge of the mechanics of high strain rate deformation, and the dynamic response of materials under those conditions. A number of material systems ranging from metals, ceramics, polymers in both monolithic and composite forms are being used to achieve a combination of characteristics specific to meet the goals in each of those applications. Composite materials with organic matrices reinforced by synthetic or ceramic fibers either individually or in combination with monolithic ceramic layers are being used to achieve light weight and enhanced ballistic impact resistance [2][3][4][5]. These material systems promise light weight armors which are structurally robust and are being contemplated for the future combat vehicles for defense applications, e.g., as in US Army. However, the ballistic response of these heterogeneous materials are very poorly understood because a number of microscopic based mechanisms are activated simultaneously

or in succession to yield the macroscopically observed shock response.

Controlled shock wave experiments are usually carried out in a plate impact test where a plate of known material is impacted on the target material under investigation at a specified impact velocity. Shock wave data are acquired in the form of either stress vs. time or velocity vs. time at intermediate locations or at the free surface of the target plate. These data are then used to compute the engineering dynamic strength and equation-of state properties as well as shock-induced motion histories for validation of theoretical and computational models. They are rich in features that can help in understanding the underlying physics [6] responsible for the process. While the shock wave profile in homogeneous metallic materials have been well documented and understood, the same cannot be said for the case of heterogeneous materials. This is partly due to the very nature of composites, which is a conglomerate of matrix, fibers, and interfaces between fiber and matrix and between different laminae, various lay-up sequences with different ply orientations and different forms of fiber arrangements within the matrix (particulate, planar, 2D/3D woven). The very heterogeneity that allows an engineer to alter the stiffness and strength response to meet the design need, makes it challenging to predict the overall structural and acoustic properties from the details of the construction. But this task of linking micromechanics to dynamic response needs to be accomplished to meet our goal of optimizing the composite constituents and lay-up sequence for decreased weight and increased performance. This *bottom-up* approach is very challenging but the only way out for an optimal design.

When studying composites, homogenization remains one of the most widely used methodologies, in which the microstructure is assumed to smear out. The whole material is considered homogeneous with certain "effective" elastic constants or other overall properties. Some studies indicate that this theoretical predictions agrees well with the experimental data only at low frequencies (when the wavelength is large compared to fiber diameter) and at low fiber volume concentration [7][8][9]. At higher frequencies and fiber volume concentrations, the internal factors such as phase impedance mismatch, the geometry of the fiber fabric, lay-up sequence and interface properties as well as manufacturing defects such as voids are all expected to have pronounced effect on the characteristics of wave profiles of composites. Very little work has been done to link modeling microstructural details or interface effect of

composites with the high velocity impact response of materials. We know that for a plate impact problem that the higher the impact velocity, the higher the frequency content and the shorter the wavelength. Therefore, it is the "interaction scale" that determines the problem solving methodology, that is the scale of the applied loading rate versus the length scales of composites. Different loading rates will necessitate the consideration of different length scales in composites.

It is recognized based on available experimental data, that the impact behavior of composites is strongly influenced by constituent materials, geometric details of the composite, the method of manufacture and the rate of loading. There is a clear need to develop a better understanding of the high velocity impact behavior of composites, and a need for a computations based model that links the microstructural details of GRP with the overall observed behavior. In view of the current research state of the shock response of layered heterogeneous materials, three fundamental aspects have been investigated in an attempt to build a micromechanics based computational model.

- Layered configuration with alternating fiber bundle layer/pure matrix layer have already been identified as the model system to study the inherent material heterogeneity effects to the level of subl-amina. Micromechanics based computational model for engineering 2-D woven composites was explored.

- Wave dispersion and attenuation in bilaminated material systems was studied based on linear and nonlinear wave interactions in one dimensional analysis. Numerical and Analytical analysis were conducted.

- The Effects of material orthotropy and material heterogeneity on the impact response of laminated composites have been examined, both analytically and numerically.

1.2. Outline of the Report

This report is organized into 6 chapters. Chapter 2 mainly provides a review of wave propagation in solids. General governing equations will first be presented to describe the constitutive relationship of the impact response in three regimes: elastic, elastic-plastic and shock. Specifically plate impact configuration will be introduced and then the uniaxial strain state will be

analyzed in details. Chapter 3 focused on the stress wave propagation in periodically layered systems based on one-dimensional analysis. Two analytical solutions will be presented. The first one is based on the initial effort of building up the rise characteristics of the stress profiles by taking into account the multiple transmission and reflections at interfaces. The idea of this solution is general and helps the development of the second analytical solution. For the second solution, Floquet's theory of ODEs with periodic coefficients and mixture theory are invoked. Chapter 4 aims to analyze the material heterogeneity factors and the structure of the stress wave profiles. This chapter is largely a parametric study based on the analytical solutions developed in chapter 3. Numerical results are also included for the purpose of comparison and validation. Chapter 5 aims to evaluate the proposed periodic layered model for engineering woven composites. Preliminary micromechanics based study on the 2D woven composites are included. Also, as a important mechanisms, failure analysis of the composites based on homogenized model is also provided. Summary is included in Chapter 6.

Chapter 2

Wave propagation in solids

When a material is stressed with a suddenly applied load (impact), the deformations and stresses are transmitted to the remote portion through wave propagation. A thorough knowledge of wave propagation in materials is essential to the understanding of the various aspects of deformation and mechanisms of failure of materials under impact loading conditions. In this report, the basic concepts involved in the state of uniaxial stress and strain and their influence on elastic and plastic behavior are examined. Further, these theories are applied to both homogeneous and inhomogeneous material systems. Numerical simulations are carried out to model plate impact problems involving single and multiple plates of different materials, including composites.

This chapter comprises two sections. The first section focuses on the basic theory on longitudinal wave propagation, mainly the governing equations for elastic, elastic-plastic and shock regime respectively. The second section briefly introduces the plate impact test and uniaxial strain state. The objective of this chapter is to go through the basic concepts such as elastic stress wave propagation, Hugoniot Elastic limit, and the state of uniaxial strain etc. In this way, material behavior under high strain rate can be better understood.

2.1. Wave equation and wave velocity

As we know, one dimensional elastic wave equation is as follows [10]:

$$c^2 \frac{\partial^2 u}{\partial x^2} = \frac{\partial^2 u}{\partial t^2} \tag{2.1}$$

From the equation of equilibrium when body force is absent, we have

$\frac{\partial \sigma}{\partial x} = \rho \frac{\partial^2 u}{\partial t^2}$

The left side of the above equation can be rewritten as

$\frac{\partial \sigma}{\partial x} = \frac{\partial \sigma}{\partial \epsilon}\frac{\partial \epsilon}{\partial x} = \frac{\partial \sigma}{\partial \epsilon}\frac{\partial^2 u}{\partial x^2}$ $\quad (\frac{\partial \epsilon}{\partial x} = \frac{\partial^2 u}{\partial x^2}$ $\quad$ since $\epsilon = \frac{\partial u}{\partial x})$

$\frac{\partial \sigma}{\partial \epsilon}\frac{\partial^2 u}{\partial x^2} = \rho \frac{\partial^2 u}{\partial t^2}$

That is, $(\frac{1}{\rho}\frac{\partial \sigma}{\partial \epsilon})\frac{\partial^2 u}{\partial x^2} = \frac{\partial^2 u}{\partial t^2}$

From wave equation (2.1),we have $c^2 = \frac{1}{\rho}\frac{\partial \sigma}{\partial \epsilon}$

For longitudinal wave, assume elastic compression, so Hooke's law holds.

That is, $\sigma = E\epsilon$ $\quad$ so, $\frac{d\sigma}{d\epsilon} = E$

From above, we obtain the elastic wave velocity in one dimensional stress state:

$$C_L = \sqrt{\frac{E}{\rho_0}} \tag{2.2}$$

The general one dimensional solution of 2.1 is in the form:

$$u = f(x - ct) + g(x + ct) \tag{2.3}$$

For general *plane irrotational wave*, its volume changes harmonically as a particle oscillates. So the wave is also known as dilatational wave. The motion is in the form

$$u_1 = \epsilon \sin \frac{2\pi}{l}(x_1 - c_L t),\ u_2 = 0,\ u_3 = 0$$

$$E_{11} = \epsilon \cos \frac{2\pi}{l}(x_1 - c_L t)$$

$$E_{22} = E_{23} = E_{12} = E_{13} = E_{33} = 0$$

$$e = E_{11} + 0 + 0 = E_{11}$$

The stress components are

$$T_{11} = (\lambda + 2\mu)\, E_{11} = (\lambda + 2\mu)\, \frac{\partial u_1}{\partial x_1}$$

$$T_{22} = T_{33} = \lambda E_{11} = \lambda \frac{\partial u_1}{\partial x_1}$$

$$T_{12} = T_{13} = T_{23} = 0$$

Substituting $T_{ij}$and u_i into the equations of motion in the absence of body forces, i.e.,

$$\rho_0 \frac{\partial^2 u_i}{\partial t^2} = \frac{\partial T_{ij}}{\partial x_j} \tag{2.4}$$

The first equation demands that

$$\rho_0 \frac{\partial^2 u_1}{\partial t^2} = \frac{\partial T_{11}}{\partial x_1} = (\lambda + 2\mu)\, \frac{\partial^2 u_1}{\partial x_1^2}$$

$$-\rho_0 \epsilon \left(\frac{2\pi}{l}\right)^2 c_L^2 \sin \frac{2\pi}{l}(x_1 - c_L t) = -(\lambda + 2\mu)\, \epsilon \left(\frac{2\pi}{l}\right)^2 \sin \frac{2\pi}{l}(x_1 - c_L t)$$

So the sound velocity of the longitudinal wave is given by

$$C_L = \sqrt{\frac{\lambda + 2\mu}{\rho_0}} = \sqrt{\frac{k + \frac{4}{3}G}{\rho_0}} \tag{2.5}$$

2.1.1. Intensity of Elastic Stress Wave

If a bar (initially at rest) was impacted by another bar at time $t = 0$ as shown in Figure

2-1.At time $t = 0$, a compressive pulse starts to strike the bar .

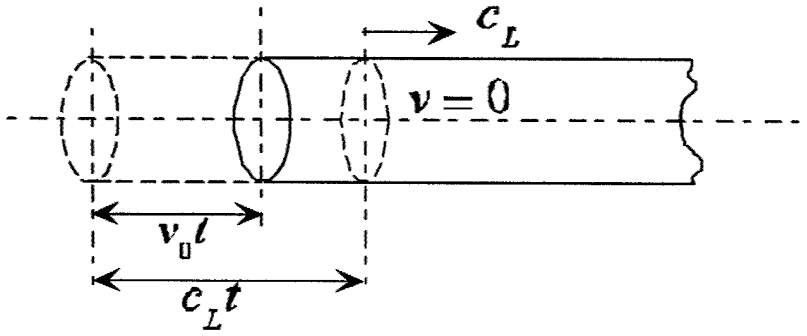

Figure 2-1: Schematic illustration of wave propagation in the bar

At time$t = t$:

Compressive wave has moved forward by distance $c_L t$;

Distance of left end of the bar moving rightward is $v_0 t$.

Equate the change of momentum to impulse:

$(\rho_0 A_0 c_L t)\, v_0 = (\sigma A_0)\, t$

So, the stress intensity of the elastic wave is

$$\sigma = \rho_0 c_L v_0 \tag{2.6}$$

Reflection of plane elastic waves at an interface

Typically, when an incident wave(no matter it is dilatational wave or distortional wave) hits an interface at an arbitrary angle, two waves (dilatational wave and distortional wave) will be reflected and two waves (dilatational wave and distortional wave) will be transmitted.

Incident pulse $\sigma_I = \rho_1 c_1 v_I$

Reflected pulse: $\sigma_R = -\rho_1 c_1 v_R$

Transmitted pulse: $\sigma_T = \rho_2 c_2 v_T$

$$V_I = V_R + V_T$$

$$F_1 = F_2 \qquad \Longrightarrow \qquad (\sigma_I + \sigma_R)A_1 = \sigma_T A_2$$

$$\frac{\sigma_T}{\sigma_I} = \frac{2\rho_2 c_2}{\rho_1 c_1 + A\rho_2 c_2} \qquad A = \frac{A_2}{A_1}$$

If $A = 1 \Rightarrow$

$$\frac{\sigma_T}{\sigma_I} = \frac{2\rho_2 c_2}{\rho_1 c_1 + \rho_2 c_2} \tag{2.7}$$

$A = 1 \Rightarrow$

$$\frac{\sigma_R}{\sigma_I} = \frac{\rho_2 c_2 - \rho_1 c_1}{\rho_1 c_1 + \rho_2 c_2} \tag{2.8}$$

Three special cases based on the above equations:

Case 1: If $\rho_2 c_2 = 0$ (free surface)

$$\sigma_T = 0 \qquad \sigma_R = -\sigma_I$$

Case 2: If $\rho_2 c_2$ is infinite (rigid wall)

$$\sigma_R = \sigma_I$$

Case3: two objects of the same material and the same cross section, we have $\rho_1 c_1 = \rho_2 c_2$

$$\frac{\sigma_R}{\sigma_I} = \frac{\rho_2 c_2 - \rho_1 c_1}{\rho_1 c_1 + \rho_2 c_2} = 0 \tag{2.9}$$

$$\frac{\sigma_T}{\sigma_I} = \frac{2\rho_2 c_2}{\rho_1 c_1 + \rho_2 c_2} = 1 \tag{2.10}$$

So, no reflection wave for this case.

It should be noted that this reflection law at an interface is valid for elastic wave. For nonlinear wave propagation, energy dissipation need to be considered if necessary [11].

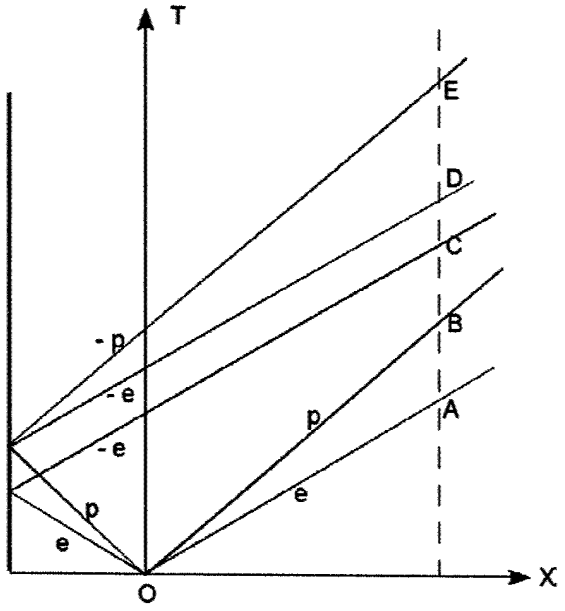

Figure 2-2: Schematic X-T diagram of elastic-plastic plate impact (same materials)

2.1.2. Plastic wave propagation

When HEL is reached, plastic wave will be generated. However, on contrary to elastic wave, it is not possible to solve plastic wave propagation through solving a simple constitutive equation. In plate impact, when the plastic wave impinges on a boundary of the solid, both elastic wave and plastic wave will be generated as shown in Fig. 2-2. It should be noted that the unloading elastic wave which is of much larger amplitude than that of the initial elastic wave can significant change the state of the material, which can be see Fig. ?? (a).

For strain rate independent material, the stress-strain relationship can be expressed as

$$\sigma = \sigma_0 + k\varepsilon^n \tag{2.11}$$

The velocity of the plastic wave is equal to

$$V_p = \left(\frac{d\sigma/d\varepsilon}{\rho}\right)^{1/2} \tag{2.12}$$

where $d\sigma/d\varepsilon$ is the slope of the plastic region of the stress-strain curve. So for bilinear

elastic-plastic material, the one-dimensional plastic wave velocity is

$$V_p = \sqrt{\frac{E_T}{\rho}} \tag{2.13}$$

Because in general the sound speed decreases with decreasing work-hardening rate, the tendency is for the front of the wave to "spread out" or disperse.

2.1.3. Shock wave equations

Consider a plate of compressible materials that [12][13] has an initial state of internal energy E_0, pressure P_0, and the material is at rest ahead of shock. A uniform pressure P_1, is suddenly applied to one face of the plate, would result in a wave traveling at velocity U_s if no failure occurs. The application of P_1 compresses the plate material to a new state of internal energy E_1, density ρ_1 and particle velocity U_P. Across the shock front, mass, momentum and energy must be conserved.

Conservation of mass: After a short time period dt, the mass of material encompassed by the shock wave, $\rho_0 U_s A dt$, with A being cross-sectional area, now occupies the volume $\rho_1 [U_s - U_p] A dt$ at density ρ_1, so we have

$$\rho_0 U_s = \rho_1 [U_s - U_p] \tag{2.14}$$

Conservation of momentum is expressed by noting that the rate of change of momentum of a mass of material $\rho_0 U_s A dt$ is accelerated to a velocity of U_p in time dt from $U_p = 0$ by a net force $P_1 - P_0$ is given by

$$P_1 - P_0 = \rho_0 U_s U_p \tag{2.15}$$

Conservation of energy across the shock front is expresses by equating the work done by the shock wave with the sum of the increase of both kinetic and internal energy of the system. Thus

$$P_1 U_p = \frac{1}{2}\rho_0 U_s U_p^2 + \rho_0 U_s (E_1 - E_0) \tag{2.16}$$

Equations (2.14)-(2.16) contain a total of 8 parameters (ρ_0, ρ_1, P_0, P_1, U_s, U_p, E_1, E_0). If the initial state (ρ_0, P_0, E_0) is assumed to be known, then five unknowns (ρ_1, P_1, U_s, U_p, E_1) remain.

Equations 2.14-2.16 are the "jump conditions" that must be satisfied by materials parameters on the two sides of a shock front. Elimination of the particle velocity from the mass and momentum equations results in an expression for the shock velocity of the form

$$U_s^2 = \frac{\rho_1 (P_1 - P_0)}{\rho_0 (\rho_1 - \rho_0)} \tag{2.17}$$

As we can see from above, changes in pressure, density and thus internal energy across a shock front can be calculated by measurement of just two parameters, the shock velocity U_s and particle velocity U_p.

2.2. Plate Impact Tests and the State of Uniaxial Strain

In order to characterize the dynamic behavior of materials under impact loading, diagnostic experiments are usually carried out using a plate impact test configuration under a one-dimensional strain state, and the experimental measurements from this configuration form the basis for the shock response characterization. The plate impact test serves the exact purpose of characterizing materials under high-pressure dynamic loading analogous to that of uniaxial tensile tests under quasi-static loading conditions and split Hopkinson bar tests under high strain rate loading conditions. Conventionally, a stress versus strain plot under one-dimensional strain condition is generated from measured particle velocity or stress history data from a number of plate impact tests performed at various impact velocities. This plot is referred to as the Hugoniot. The stress response is usually measured at intermediate locations within a given specimen using embedded manganin or PVDF gauges. The velocity measurements are typically carried out using a velocity interferometry (VISAR) system at the stress free back surface of the target plate or at the interface of a transparent window glued to the back of the target plate. These measured well-structured wave profiles in metals and ceramics provide a wealth of information about the shock response of the material. Plate impact tests are the test configuration used to investigate the impact response of materials

throughout this research (The schematic set-up is shown in Figure 2-4) since plate impact can generate high pressure state and provide a range of controlled impact velocities. Also, this configuration offers a unique opportunity for design of appropriate experiments to study wave propagation in complicated microstructures.

When a material is subjected under shock loading, the deformation is restricted to one dimension, with the lateral strains being zero. The stress strain curve is shown below.

In general, the three principal strains can be divided into an elastic part and a plastic part:

$$\varepsilon_1 = \varepsilon_1^e + \varepsilon_1^p$$

$$\varepsilon_2 = \varepsilon_2^e + \varepsilon_2^p$$

$$\varepsilon_3 = \varepsilon_3^e + \varepsilon_3^p$$

In one dimension deformation

$$\varepsilon_2 = \varepsilon_3 = 0$$

$$\varepsilon_2^p = -\varepsilon_2^e \text{ and } \varepsilon_3^p = -\varepsilon_3^e$$

Since the plastic part of the total strain is assumed to be incompressible, so that

$$\varepsilon_1^p + \varepsilon_2^p + \varepsilon_3^p = 0 \tag{2.18}$$

From equation (2.18) which we can have

$$\varepsilon_1^p = -\varepsilon_2^p - \varepsilon_3^p = -2\varepsilon_2^p$$

Due to symmetry, we have $\varepsilon_2^p = \varepsilon_3^p$

so, $\varepsilon_1^p = 2\varepsilon_2^e$

Therefore, the total strain $\varepsilon_2$can be written as

$$\varepsilon_1 = \varepsilon_1^e + \varepsilon_1^p = \varepsilon_1^e + 2\varepsilon_2^e$$

The elastic strain can be expressed using Hooke's law:

$\varepsilon_1^e = \frac{\sigma_1}{E} - \frac{v}{E}(\sigma_2 + \sigma_3) = \frac{\sigma_1}{E} - \frac{2v}{E}\sigma_2$ (Since $\sigma_2 = \sigma_3$)

$\varepsilon_2^e = \frac{\sigma_2}{E} - \frac{v}{E}(\sigma_1 + \sigma_3) = \frac{1-v}{E}\sigma_2 - \frac{v}{E}\sigma_1$

$\varepsilon_3^e = \frac{\sigma_3}{E} - \frac{v}{E}(\sigma_2 + \sigma_1) = \frac{1-v}{E}\sigma_3 - \frac{v}{E}\sigma_1$

From above, we have

$$\varepsilon_1 = \varepsilon_1^e + \varepsilon_1^p = \varepsilon_1^e + 2\varepsilon_2^e = \frac{\sigma_1(1-2v)}{E} + \frac{2\sigma_2(1-2v)}{E} \tag{2.19}$$

The yield criterion for either the Von Mises or Tresca for this case is

$$\sigma_1 - \sigma_2 = Y_0 \tag{2.20}$$

using above as the definition of σ_2, insert this to Eqn. (2.19),

$\left(\frac{E}{1-2v}\right)\varepsilon_1 = 3\sigma_1 - 2Y_0$

or $\sigma_1 = \frac{E}{3(1-2v)}\varepsilon_1 + \frac{2}{3}Y_0 = K\varepsilon_1 + \frac{2Y_0}{3}$

For the special case of elastic one-dimensional strain:

$\varepsilon_1 = \varepsilon_1^e$

$\varepsilon_2 = \varepsilon_2^e = \varepsilon_3 = \varepsilon_3^e = 0$

$\varepsilon_1^p = \varepsilon_2^p = \varepsilon_3^p = 0$

From Hooke's law, we have

$\varepsilon_2^e = \frac{\sigma_2}{E} - \frac{v}{E}(\sigma_1 + \sigma_3) = 0$

and $\sigma_2 = \sigma_3$

$$\sigma_2 = \left(\frac{v}{1-v}\right)\sigma_1 \tag{2.21}$$

So, $\varepsilon_1 = \varepsilon_1^e = \frac{\sigma_1}{E} - \frac{v}{E}(\sigma_2 + \sigma_3) = \frac{\sigma_1}{E} - \frac{2v}{E}\sigma_2 = \frac{\sigma_1}{E} - \frac{2v^2\sigma_1}{E(1-v)}$

That is,

$$\sigma_1 = \frac{1-v}{(1-2v)(1+v)}E\varepsilon_1 \tag{2.22}$$

Under uniaxial strain, the effective stress can be obtained by using Von-mises Criterion,

$$\begin{aligned}\sigma_{eff} &= \frac{1}{\sqrt{2}}\left[(\sigma_1-\sigma_2)^2+(\sigma_1-\sigma_3)^2+(\sigma_2-\sigma_3)^2\right]^{\frac{1}{2}} \\ &= \frac{1}{\sqrt{2}}\left\{\left[\sigma_1-\left(\frac{v}{1-v}\right)\sigma_1\right]^2+\left[\sigma_1-\left(\frac{v}{1-v}\right)\sigma_1\right]^2+0\right\}^{\frac{1}{2}} \\ &= \frac{1}{\sqrt{2}}\left\{2\left[\frac{1-2\nu}{1-\nu}\sigma_1\right]^2\right\}^{\frac{1}{2}} = \frac{1-2\nu}{1-\nu}\sigma_1\end{aligned} \tag{2.23}$$

From 2.23, we can obtain Hugoniot elastic limit (The critical normal stress beyond which inelastic wave will be generated under the state of uniaxial strain):

$$HEL = \frac{1-\nu}{1-2\nu}Y_0 \tag{2.24}$$

Experiments on shock-loaded metals have shown that relation 2.24 works very well and ratio between HEL and Y_0 is around $2\nu \approx 1/3$ for most metals. However, for brittle materials, Rosenberg , based on the studies of shock waves on ceramics, suggested that Griffith's yield criterion should be used. Griffith's biaxial-stress criterion gives the following equation for the yield surface:

$$(\sigma_1-\sigma_2)^2+8\sigma_0(\sigma_1+\sigma_2)=0 \tag{2.25}$$

Realizing that the compressive strength, according to this relation is $Y_0 = 8\sigma_0$, so the Hugoniot elastic limit in this case is

$$HEL = \frac{1-\nu}{(1-2\nu)^2}Y_0 \tag{2.26}$$

which differs from 2.24 by an additional factor of $1/(1-2\nu)$. Recent studies suggest that HEL may not be an elastic limit, but rather, may be a transition in failure mechanisms.

More generally, the Von Mises yield condition states that the materials is behaving elastically if

$$J_2 < \frac{1}{3}Y^2 \tag{2.27}$$

and behaving plastically if

$$J_2 > \frac{1}{3}Y^2 \tag{2.28}$$

where J_2 is the second invariant of the stress deviation tensor.

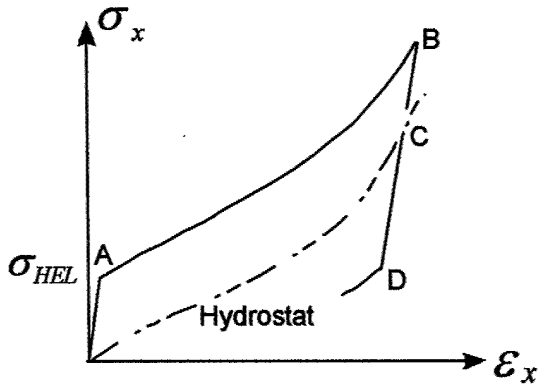

(a) Loading cycle in uniaxial strain

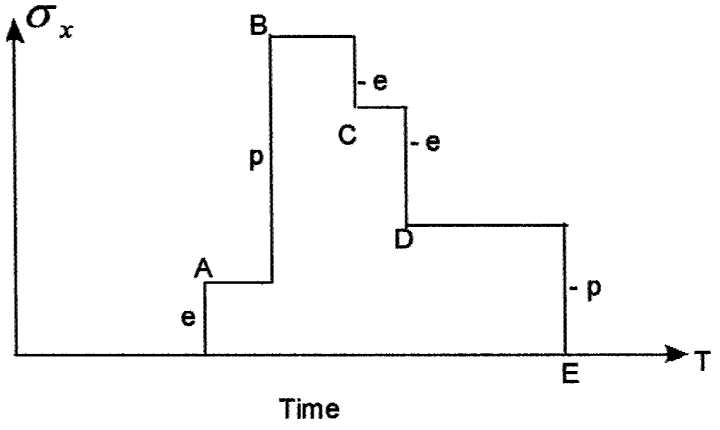

(b)

Figure 2-3: Stress profile of elastic-plastic plate impact (a) $\sigma_x - \epsilon_x$ for uniaxial strain (b) $\sigma_x - T$

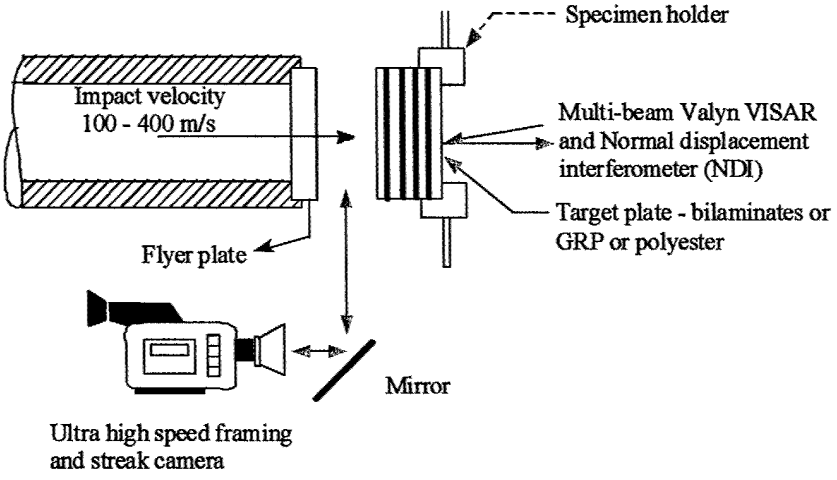

Figure 2-4: Schematic of plate impact experiments to investigate shock wave profiles in laminated materials

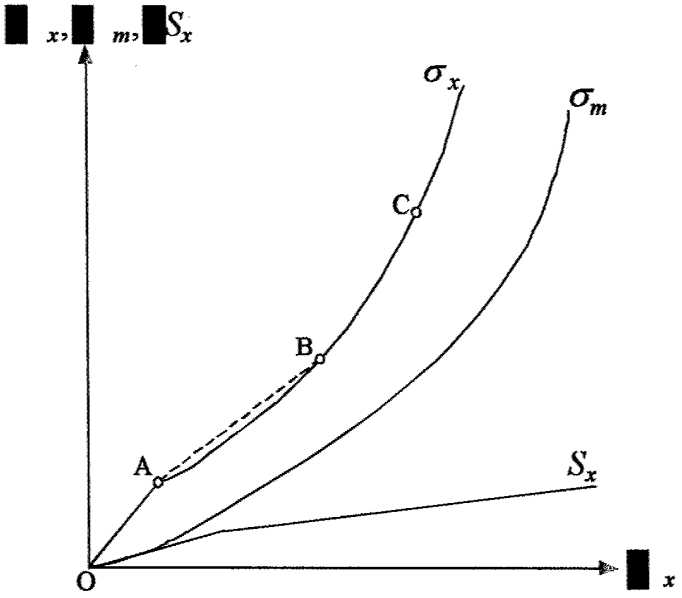

Figure 2-5: Stress-strain curve for uniaxial strain

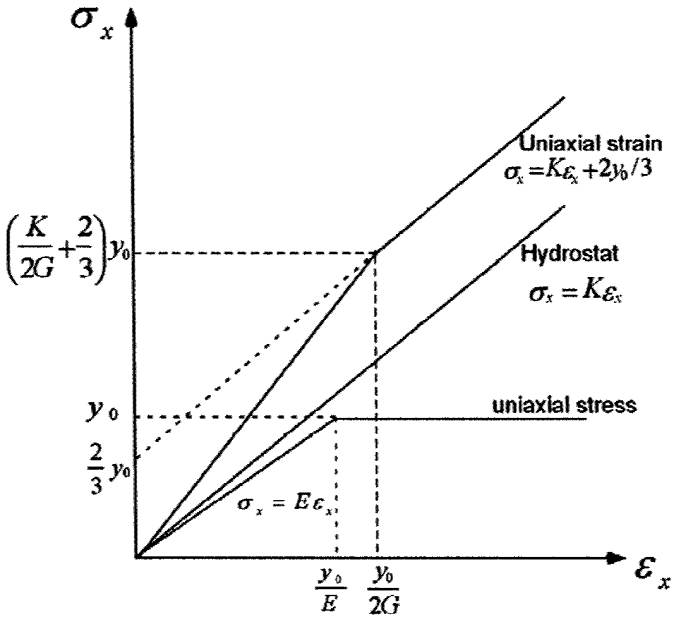

Figure 2-6: Stress - strain relation of ideal elastic-plastic material.

Chapter 3

The impact response of layered heterogeneous systems subjected to plate impact loadings

Before investigation of the impact response of heterogeneous materials, it is convenient to demonstrate an example of simple elastic stress response in homogeneous materials under plate impact for the purpose of comparison. Fig. 3-1 shows one example of aluminum impactor impacts another aluminum plate with initial velocity of 300m/s. It is assumed that this impact velocity is low such that the HEL of the material is not reached, and thus the material exhibits elastic response.

The maximum stress for elastic wave propagation, as mentioned before, for two plates made of the same materials, the particle velocity for target plate (initially at rest) $\sigma = \rho c_L v_{partical} = 2.7 \times 10^3 \times 6.623 \times 10^3 \times (\frac{1}{2} \times 300)\ m/s = 26.8\ kbar$. Time to reach the back of the target plate (the thickness is 20mm): $t = \frac{l}{c_L} = \frac{20mm}{6.62 \times 10^3 m/s} = 3.02\mu s$. Time to reach the back of the flyer plate (the thickness is 5mm): $t = \frac{l}{c_L} = \frac{5mm}{6.62 \times 10^3 m/s} = 0.755\mu s$. The corresponding X-T plot of wave propagation is shown in Fig. 3-1. From this figure, we can see again that, for plates of the same materials, no reflected wave is created in the interface, incident wave is transmitted completely. And the stress in point G (where the distance to the back surface is equal to the thickness of the flyer plate) is tension and 2σ in the amplitude, in many cases for brittle materials, this is where spall will happen.

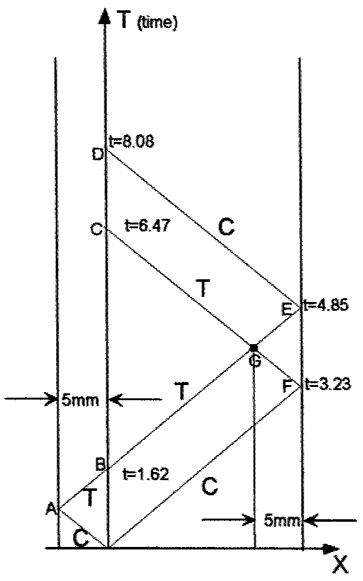

Figure 3-1: X-T diagram of aluminum plate impacts another aluminum plate

From Fig. 3-2, it is obvious that the stress amplitude remain exactly at the same level before the incident compressive wave reaches the back surface of the target plate. After that, however, the release wave created from the free surfaces or the corner tend to cause dispersion.

In order to study the effect of planar interfaces, as is the case in laminated composite systems, it is appropriate to simulate a layered configuration, and this approach is taken in this work. In this paper, we examine only the rise characteristics of the signal, i.e., the slope $\frac{\partial \sigma}{\partial t}\big|_x$. For the time being, we will focus our attention on elastic materials, hence one should be cautious in extending the results to a generic nonlinear material system. We have developed an analytical solution to the problem of multiple reflections/transmissions in the layered system. The solution relates the cumulative amplitude of the stress wave arriving at a given section in the body as a function of time when the body is subjected to a shock wave at the front surface. Such a study will not only provide a fundamental understanding on the shock response of heterogeneous materials but also provide a better guideline for postulating a physically acceptable equation of state. It is noteworthy to realize if the target plate were to be a homogeneous material (for example a metal), then the head of the shock front will be planar (vertical stress rise with zero rise time), followed by a dwell time corresponding to

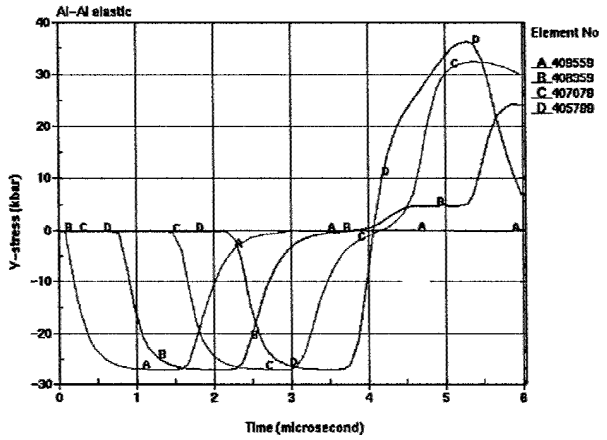

Figure 3-2: Normal stress profile of Al-Al elastic

the arrival of release wave from impactor back surface, and a sloping pull back signal. The dwell time and pull back signal shape are affected by a number of factors including arrival of release waves from different sources (e.g. target back surface, corners, internal damage surfaces and the acceleration of wave speed with pressure). The rise portion of the response is primarily affected by the shock front behavior, with the exception of damage and viscous effects. Thus we are concerned here only with the rise characteristics of the layered structure under plate impact and examine why it is different from that of a monolithic metal.

Our approach in this work is to examine the response of elastic wave as it encounters an interface, be it be fiber/matrix or different laminae and compute the multiple reflection/transmissions. For this purpose, we develop an analytical model for a two-material layered system in section 3.1.1. This section is rather long but self-contained in providing a relationship between the number of layers, properties of the materials, the arrival times of transmitted/reflected wave trains at a given location. Further we provide numerical solution to selected material/layers combination. This section is used to illustrate the possibility that rise time may comprise of many wave trains arriving at a given section over time leading to the observed slope. we present the comparison of finite element solution with the analytical solution. In section 3.1.3., we present certain consequences of the analytical solutions. In section 3.2, a late time analytical solution is presented and this solution is based on the solution for unit step loading condition. Equation of state is incorporated for shock loading

conditions. In the final section we summarize the results.

3.1. An analytical model to study the rise characteristics based on multiple reflections in layered composites

3.1.1. Solution method

Consider a layered composite system with alternate layers of materials A and B arranged in succession as shown in Figure 3-3. Let us assume that materials A and B are both isotropic with known stiffness, strength and acoustic properties, denoted with subscripts A and B; for example, E_A represents the Young's modulus of material A and ρ_B the density of material B. If there are 2L+1 layers in the system, then there are L+1 layers of material A and L layers of material B with 2L interfaces. Let σ_I be the incident amplitude of stress in the first layer of A. This can be construed as the magnitude of high amplitude compressive shock wave imposed as a result of a plate impact condition. As the wave travels through material A, it encounters the first interface $A \longrightarrow B$. At the interface because of acoustic impedance mismatch, there will be partial transmission and rest reflection, as shown in Figure 31. Let σ_{T1}be the transmitted wave into material B, and σ_{R1} be the reflected wave. Here the second subscript 1 represents the wave interaction event 1 at the first interface between A and B. The ratio of $\frac{\sigma_{T1}}{\sigma_I}$ and $\frac{\sigma_{R1}}{\sigma_I}$can be written as,

$$\frac{\sigma_{T1}}{\sigma_I} = \frac{2\rho_B C_B}{\rho_A C_A + \rho_B C_B} \equiv m_1 \tag{3.1}$$

$$\frac{\sigma_{R1}}{\sigma_I} = \frac{\rho_B C_B - \rho_A C_A}{\rho_A C_A + \rho_B C_B} \equiv m_2 \tag{3.2}$$

Hence after the first interaction with the interface $A \longrightarrow B$ we have,

$$\sigma_{T1} = m_1 \sigma_I \qquad \text{and} \qquad \sigma_{R1} = m_2 \sigma_I \tag{3.3}$$

We note that with every layer, as a wave interacts two waves emerge, one transmitted and one reflected. Let us now proceed with the transmitted wave designated with the amplitude σ_{T1} interacting with $B \rightarrow A$. Let σ_{T2} be the transmitted wave and σ_{R2} the reflected wave as a result of the second interaction. We now introduce two more constants m_3 and m_4 as

$$\frac{\sigma_{T2}}{\sigma_{T1}} = \frac{2\rho_A C_A}{\rho_A C_A + \rho_B C_B} \equiv m_3 \qquad \frac{\sigma_{R2}}{\sigma_{T1}} = \frac{\rho_A C_A - \rho_B C_B}{\rho_A C_A + \rho_B C_B} \equiv m_4 \tag{3.4}$$

$$\sigma_{T2} = m_3 \sigma_{T1} = m_1 m_3 \sigma_I \tag{3.5}$$

$$\sigma_{R2} = m_4 \sigma_{T1} = m_1 m_4 \sigma_I \tag{3.6}$$

Proceeding with the same argument, the next interaction will be with that of $A \longrightarrow B$ leading to

$$\sigma_{T3} = m_1 \sigma_{T2} = m_1^2 m_3 \sigma_I \tag{3.7}$$

$$\sigma_{R3} = m_2 \sigma_{T2} = m_1 m_2 m_3 \sigma_I \tag{3.8}$$

and with the next interaction at $B \rightarrow A$ stress levels

$$\sigma_{T4} = m_3 \sigma_{T3} = m_1^2 m_3^2 \sigma_I \tag{3.9}$$

$$\sigma_{R4} = m_4 \sigma_{T3} = m_1^2 m_3 m_4 \sigma_I \tag{3.10}$$

are reached.

A. First Transmitted wave after 2L layers

We are now ready to generalize the magnitude of transmitted wave after $2L$ interactions for a system comprising alternating L layers of A and L layers of B. This transmitted wave represents the head of the shock wave and the first to reach any given point in the downstream of the wave propagation, as shown in Figure 3-5.

$$\sigma_{T2L} = m_3 \sigma_{T(2L-1)} = m_1^L m_3^L \sigma_I \tag{3.11}$$

which is intuitively obvious since there are L interaction from $A \longrightarrow B$ and another L

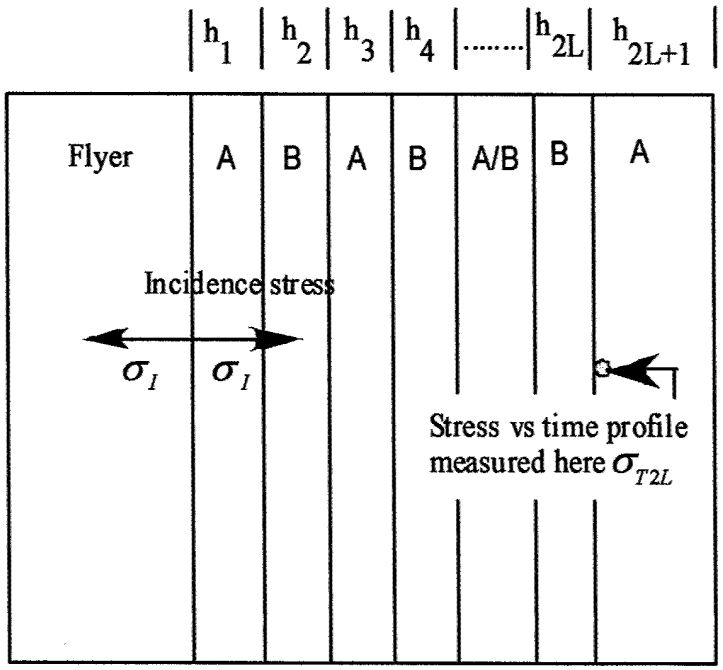

Figure 3-3: Schematic of layered system.

interactions with $B \rightarrow A$ interfaces.

We focus our attention on the head wave (see Figure 3-5) which is the very first wave to arrive at a given section. This head wave represents the wave that is always transmitted at all the interfaces as shown by equation (3.11). For the purpose of illustration, we analyze a combination of material systems that are used for a variety of applications. The table below shows the value of m_1, m_2, m_3 and the product $m_1 m_3$. For the sake of convenience, let us define an impedance mismatch factor $I \equiv 1 - m_1 m_3$,($I = 1$ represents infinite impedance mismatch and $I = 0$ leads to no mismatch) which is a function of a given pair of materials. I represents the fraction of transmitted energy to that of incident one, after a pair of transmissions at A/B and B/A interfaces. For example in the case of Aluminum-S2 Glass this product is 0.996, while in Tungsten-Plexiglas it is only 0.108. While the former system allows most of the energy to be transmitted, the latter system will reflect most of it for dissipation in many more scattering events. Hence the stress amplitude in the Aluminum-S-2 Glass the head wave will be quite high and that in Tungsten-Plexiglas system it will be low. It is also to easy to see that with a low initial head wave, further arrivals will build additional stress

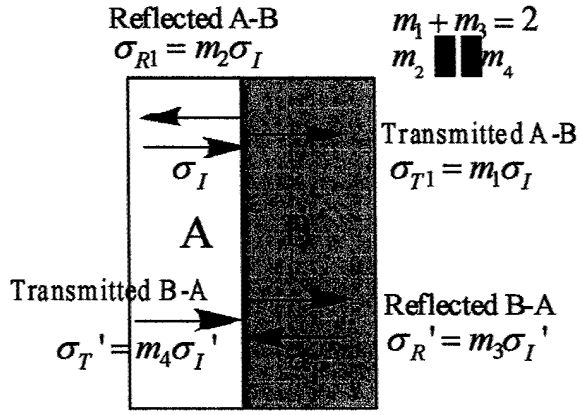

Figure 3-4: Reflection/transmission at an Interface

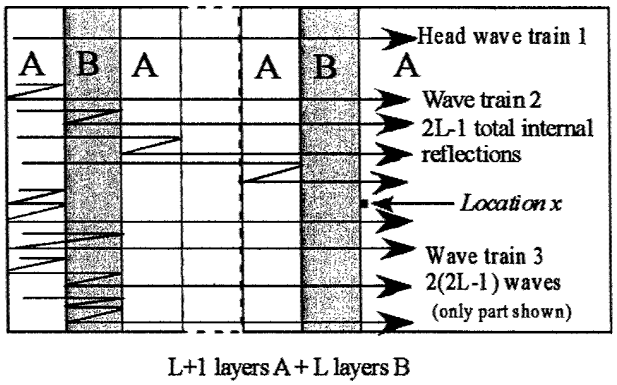

Figure 3-5: Head wave and successive wave trains in a layered system

over time resulting in stress build up over time, leading to a slower starting rising slope.

Table: Material impedance mismatch.

Figure 3-6 shows the intensity of the first transmitted wave train (head wave) for different material systems as a function of the number of layers. The behavior can be classified into three distinctly different categories. Type 1, is one in which almost all the intensity of incident wave is transmitted with very little under reflections, (e.g. steel-copper and Al-S2 glass). This behavior is similar to that of monolithic material where there is nearly no loss of energy during transmission. Such is the case for this group where the acoustic impedance of material A is close to that of B, leading to $I \approx 1$, and $m_2, m_4 \approx 0$. Sharp rise time is

expected in this case as $\frac{\sigma_T}{\sigma_I} \approx 1$.

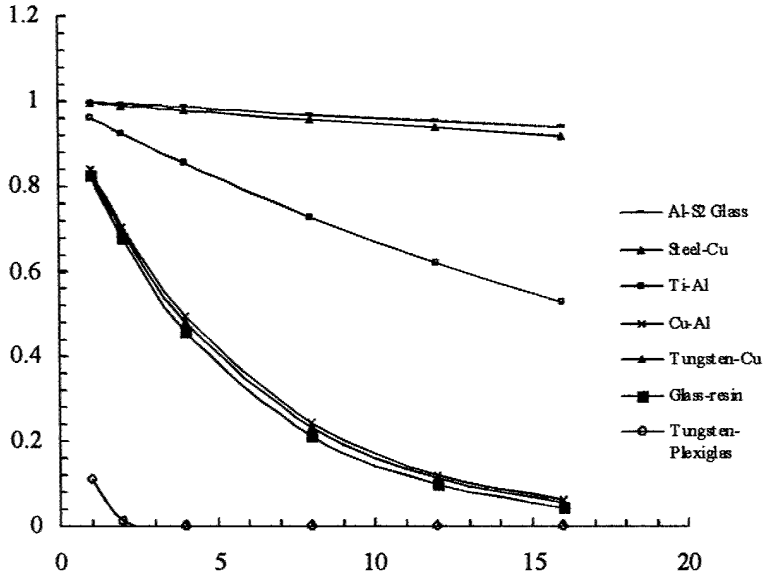

Figure 3-6: Stress intensity of head wave in a layered system

Type 2 represents the other extreme to the Type 1 where we have the head wave with very low values of σ_T (e.g. Tungsten-Plexiglas). In this case $I \approx 0$ with $\mid m_2 \mid \approx 1$ with most of the scattering at the interface resulting in reflection rather than transmission. Peak value of stress σ_T will be much lower than σ_I when some release wave arrives; in any case the beginning slope $\frac{d\sigma}{dt}$ will be very low.

Type 3, is an intermediate case where impedance mismatch I is neither close to 0 nor 1 (e.g., copper-Aluminum, glass-resin). In this case the slope of the rise curve $\frac{d\sigma}{dt}$ will be moderate. Of course, since the head wave intensity decreases with number of layers, the slope will decrease with increase in number of layers.

B. Arrival of second wave train at $x = 2L$

Let us consider a location $x = 2L$ downstream of the incident shock wave which corresponds $L + 1$ layers of A and L layers of B. For the sake of convenience let us also assume that the thickness of the individual layers of A or B is such that the time of flight is identical.

Thus

$$\frac{h_1}{C_A} = \frac{h_2}{C_B} = \frac{h_3}{C_A} = \frac{h_4}{C_B} = \cdots\cdots = \frac{h_{2L-1}}{C_A} = \frac{h_{2L}}{C_B} = t_A = t_B = t^* \tag{3.12}$$

where C_A and C_B are the wave speed in materials A and B respectively. We should also note that in this analysis we neglect the increase in wave speed as a result of prevailing compressive stress in the material. Based on this assumption, the head of the shock wave arrives at $2Lt^*$ from the time of impact when $t = 0$.

As seen in Figure 3-5, the second wave train arrives after one pair of internal reflections within either the material A or B. Thus the number of wave arrival at the station after a time $2Lt^* + 2t^*$ will be $2L$ based on the number of interfaces. We should note that this means the second wave train arrives at the station after an incremental time of $2t^*$ after the arrival of head wave. Since the pair of internal reflections will be of the type $A \longrightarrow B$ and $A \longrightarrow B$ within the material A and $B \longrightarrow A$ and $B \longrightarrow A$ in material B the factor to multiplied for the intensity will be m_2^2 and m_4^2 respectively. While there are L reflections within material B, there will be L reflections within material A. Since the reflection in the first layer A needs to reach the impact surface and then come back, the intensity of this wave depends on equation of state and flyer plate properties. For the sake of simplicity in formulation, we assume the impactor is material B, so that we do not have to distinguish the waves that are reflected inside from the ones that are reflected from impact surface. Thus the stress amplitude of the second wave train are separated into

$$\sigma_{T2L}^{(2)} = (m_2^2 L + m_4^2 L) I^L \sigma_I \tag{3.13}$$

The above equation can be simplified using the identity $m_2 = -m_4$ so that

$$\sigma_{T2L}^{(2)} = 2L \cdot m_2^2 I^L \, \sigma_I \tag{3.14}$$

C. Third and N^{th} wave trains

Proceeding in the similar fashion, the number of waves in the third wave trains that can arrive at $x = L(C_A + C_B)t^*$ at time $2Lt^* + 2(3-1)t^*$ will be any branch of waves

that has exactly two pure reflections in $2L$ layers. We can easily calculate the number $C_R^{(3)}$ of waves that has exactly two reflections in $2L$ layers using the rules of permutations and combinations. If we assume that the number of layers is n, then for n=4, 5, 6, 7, 8 to m, $C_R^{(3)}$ will be 10, 15, 21, 28, 36, ...$[10 + 4 * (m-4) + (1 + 2 + ... + (m-4))]$. However, there is yet another possibility. Here we have one reverse transmission (traveling backwards through two neighboring layers) and then one reflection, and the number for this type is designated as $C_{TR}^{(3)}$ ($C_{TR}^{(3)} = 2L - 1$ in this system). Every transmission always accompany reflection and result in tensile stress waves. So the simplified stress amplitude of the third wave train is given by

$$\sigma_{T2L}^{(3)} = (C_R^{(3)} m_2^{2(3-1)} I^L - C_{TR}^{(3)} m_2^2 I^{L+1}) \sigma_I \tag{3.15}$$

and this wave train arrives at a time lag of $2t^*$ after the second wave or a total elapsed time of $2Lt^* + 2(3-1)t^*$.

Generalizing to the N^{th} wave train, the number of waves will be calculated by considering possible number of reverse transmissions/reflection combinations. For N^{th} wave train, The maximum possible number of reflections in this wave train will be $N-1$, that is, pure reflections without reverse transmissions. In $2L$ layers, the number of such possibility for a given number of reflections K is fixed and assigned to be C_K here. Then the left variable reflections will be $N-1-K$, the number of transmissions in $2L$ layers with K reflections can be designated as C_{TR}. As a result, the total number of waves that go through I reflections and $N-1-K$ reverse transmissions in N^{th} wave train is $C_K C_{TR}$. Obviously, this number is a function of number of layers and wave train number N. Then the total stress amplitude is given by

$$\sigma_{T2L}^{(N)} = \sum_{K=1}^{N-1} (-1)^{N-1-K} C_K C_{TR} m_2^{2K} I^{N-1-K+L} \sigma_I \tag{3.16}$$

with an arrival time lag of an additional $2t^*$ from the previous $(N-1)^{\text{th}}$ wave train with a total elapsed time of $2Lt^* + 2(N-1)t^*$.

The simplified cumulative stress up to N^{th} wave train can be generalized as

$$\sigma_{2L} = I^L \sigma_I + \sum_{W=2}^{N} \sum_{K=1}^{W-1} (-1)^{W-1-K} C_K C_{TR} m_2^{2K} I^{W-1-K+L} \sigma_I \tag{3.17}$$

D. Analytical Solution to the rise time in shock waves

We have in the last few sections succeeded in determining the stress amplitude of successive wave trains arriving at a given plane in regular increments of $\Delta t = 2t^*$. We have thus built a relationship of $\sigma = \sigma(t)$ with the basic assumption that the stress intensity builds up over time as a result of different waves arriving at a section after suffering a series of reflections/transmissions at various interfaces over time. Thus we have $\sigma^{Nt^*} = \sigma^{(N-1)t^*} + \Delta\sigma$ as determined by equation (3.17) resulting in the prediction of rise characteristics in the shock wave signal. The slope $\frac{d\sigma}{dt}$ will of course depend on the material combination (with different m_1, m_2, m_3 and m_4) and the number of layers ($2L$) where the shock signal is being analyzed.

3.1.2. Numerical/Analytical Solution to the Cu/Al multi-layered system

For the purposes of illustration, we select Cu/Al multilayered system with the total number of layers ranging from $2L = 4, 8$ to 16 and apply the above analytical solution for the case of plate impact with Al as the flyer plate. Figure 3-7 (a) shows the schematic of the layers with 5 mm Al flyer plate impacting the layers. The stress profile at the point D (mid point of the 10mm plate) is computed using both the analytical solution and numerical solution using an explicit finite element code (EPIC95 research version). Three different layered systems with different number of layers were studied and the results are shown in Figure 3-7 (b), (c) and (d).

The wave profiles consist of steps and each step represents the arrival of a new wave train at the point D. The horizontal portion of the profile indicates the time delay between the arrival of successive wave train. We can see from the figure that the intensity of the first arrived wave reduces from $2L = 4$ to 8 to 16 (from 2.76 *Gpa* to 1.0 *Gpa*). Also it takes approximately 2 wave trains ($0.89 * 2\mu s$), 2 wave trains ($2 * 0.45\ \mu s$) and 3 wave trains

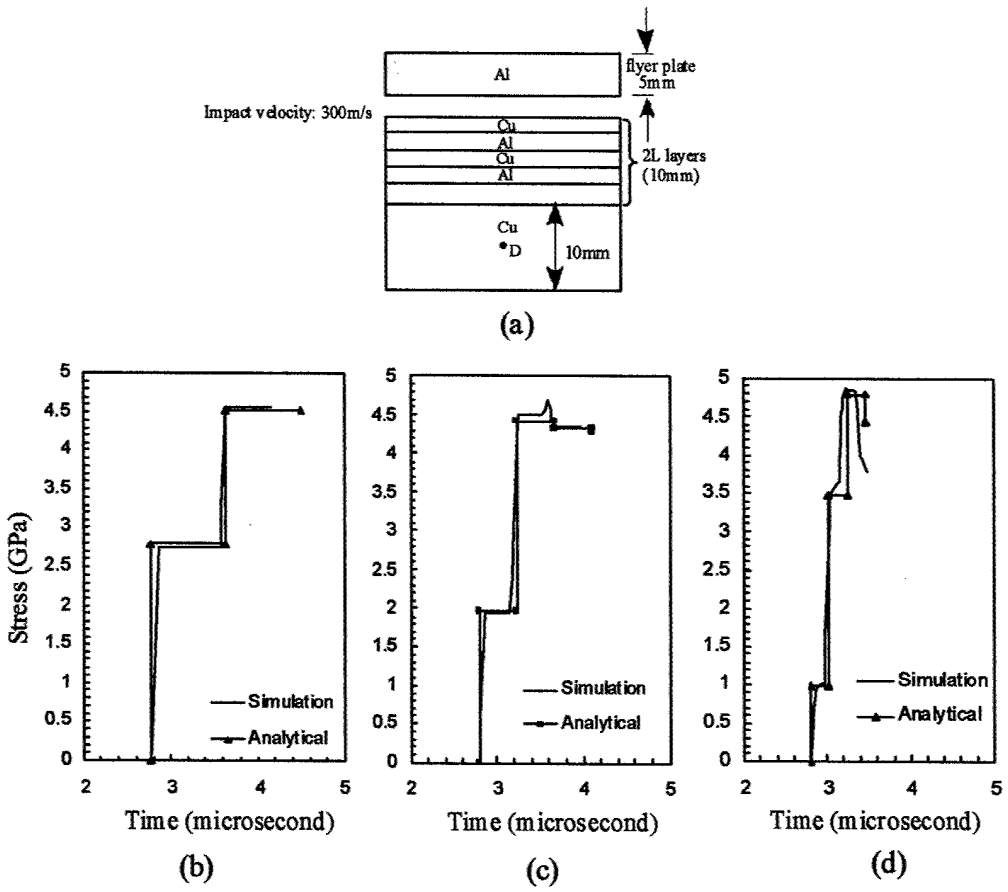

Figure 3-7: Rise characteristics of alternating layered Al - Cu (a) Schematic configuration, (b) 2L=4, (c) 2L=8, (d) 2L=16

(3*0.226μs) to reach the peak value before the release wave arrives from a host of sources. As we extend this observation to a large number of layers, then even the analytical solution will show significant stepped increase making it more or less continuous curve. The analytical solution shows that a given wave arrives at one instant of time thereby producing a vertical segment. It can be seen that the analytical solutions match the numerical simulation very well for 4 and 8 layer cases (Figure 3-7(b) and 3-7(c)), respectively. Numerical simulation shows that a given wave arrives in an incremental time step indicated by the slope of the step. This can be ascribed to the equation of state that predicts that each wave train (except the head wave) comprises many sub-waves with slightly different wave velocities. This effect of wave spreading increases with pressure/wave train number as is seen in the third wave

train of Figure 3-7(d). Agreement between the analytical solution and numerical simulation clearly shows that the stepped stress profiles are due to the scattering processes.

3.1.3. Some consequences of the analytical solution

Based on the above analysis, it is evident that the rise time will be significantly affected by the scattering characteristics and the number of layers in the interfaces.

A. Scattering Characteristics

As the shock wave arrives at an interface, its ability to transmit/reflect is determined by m_1, m_2, and m_3. As discussed already the impedance mismatch factor I determines the strength of the head wave. If $I \simeq 1$ then most of the wave will be transmitted and we expect a sharp rise curve. On the other hand, if $I \simeq 0$ then most of the energy in the wave is spent in internal reflections resulting in a slow build up of stress. Of course the rise of compressive stress will be interrupted at any point when a tensile release wave comes to that point. In such cases, we may be misled by the rise time profile confusing the amplitude reduction with attenuation.

B. Number of layers

As the number of layers increases the rise time slope will be reduced provided the head wave strength is low. If the head wave strength is high ($I \simeq 1$) then a vertical rise occurs irrespective of the number of layers. Figure 3-8 shows the change in the slope (defined in Fig. 3-8(b)) for three different combinations of materials. As indicated in the figure, the systems represent high, medium and low level of impedance mismatch. For a given number of layers, the higher the mismatch (lower the I-value), the slope decreases indicating that it takes a longer time to reach the peak stress value. For a given material system (and hence I), the slope increases (sharper rise time) with increase of the number of layers. It should be noted that in these analyses since the total thickness is fixed, increasing the number of layers decreases the thickness of each layer.

3.1.4. Summary

Shock wave profile in composite systems show marked difference from that of metallic systems. It is postulated that numerous fiber-matrix and lamina-lamina interfaces present in

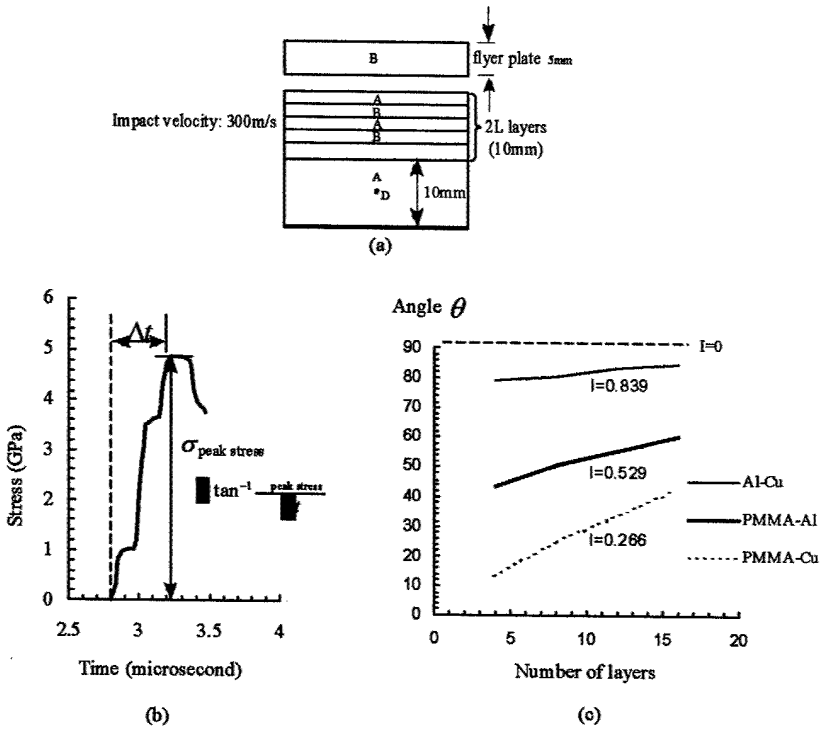

Figure 3-8: (a) Schematic configuration (b) Definition of the rising angle (c) Results

composite systems offer potential sites for scattering; such sites being characterized by materials with acoustic impedance mismatches. Though composites provided motivation, we have analyzed multi-layered heterogeneous systems in this work.

The rise time characteristics is explained as the manifestation of multiple transmission/reflections occurring at the various interfaces resulting in the loss of strength of the head wave. As the waves arrive at a given location with time it results in the slope of stress vs. time signal. An analytical model capturing these processes have been developed. The analytical model predicts the rise time behavior. FEM is then used to corroborate the results for a simple bilaminate system. A good agreement between analytical and numerical results clearly supports the hypothesis that layered systems will suffer rise time slope changes with inherent acoustic impedance mismatch between layers. Other factors that may affect the thermodynamics of the shock front may have to be considered carefully before this assertion can be made conclusively.

3.2. Late time solution to the plate impact problem

3.2.1. Background

Wave propagation in a periodic layered medium has been studied extensively for decades. Historically theoretical work on wave propagation studies in layered systems has followed the mathematical solution to ordinary differential equations with periodic coefficients attributed to Floquet [14] that dates back to 1800s. As early as 1956, Rytov [15] obtained a dispersion relation for one-dimensional longitudinal waves propagating in a periodic laminate. Later Sun, Achenbach and Herrmann [16] obtained the dispersion relations for harmonic wave propagating parallel and normal to the direction of the layering using the effective stiffness theory for a unit step loading at the boundary. Peck and Gurtman [17] studied the wave propagation parallel to the layers and obtained the asymptotic solution through approximation under similar loading conditions. Sve [18], Chen and Clifton [19] predicted the late-time asymptotic solutions and the wave front solution for wave propagation normal to the layers for unit step loading at the boundary.

A schematic of free surface particle velocity of the target measured using a VISAR or the compressive stress measured using an embedded stress gauge is shown in Fig. 3-9. The portion of the plot indicated by the letter A represents the arrival of an elastic shock wave from the impact plane. The material particles are compressed elastically (A-C) until the relatively slow moving plastic shock wave arrives at the given location. Typically, the shape and time duration of the portion A-C depends on the strain rate sensitivity of the material and the distance from the impact plane. If the shock amplitude is below the elastic limit, the profile typically follows the portions AC - CE. The rise time is usually of the order of less than a microsecond for metals and ceramics. If the shock amplitude is above the elastic limit, then the plastic shock takes the particle velocity to the peak between points D and E. The peak level remains the same until the elastic unloading wave arrives from the back of the flyer plate. Therefore, the portion between D and E remains relatively flat. The elastic release (tensile) wave drops the velocity (or stress) to F and the plastic release wave drops the level further to H. Often, the release portion of the wave profile exhibits a typical structure that consists of the elastic release, the transition (F-G), and the plastic release. Fig. 3-9(b) shows the schematic of a typical shock response of a layered composite system. The

Table 3-1: Review of major past work done in studying wave profiles in alternating layered systems under plate impact

	Author/ Year	Material system (target) Experiment/ Simulation configuration	Observations or Results	Method/ Model
1	Lundergan 1971	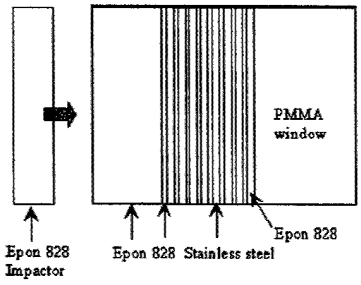	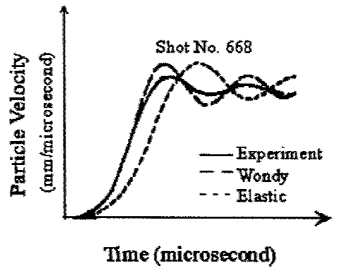	
2	L.M. Barker 1974	PMMA/Al 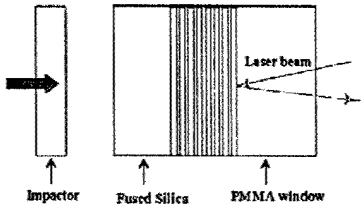	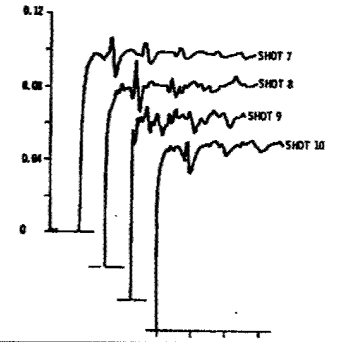	Viscous model (Maxwell model)
3	Y. Oved 1978	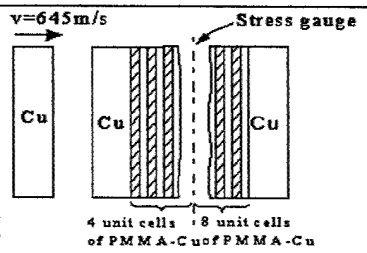	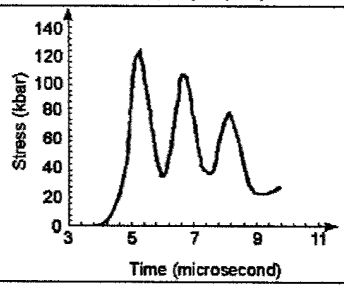	Numerical analysis+ Experi-ments
4	G.I. Kanel 1995	Cu/PE, Al/PE, W/Al N/A	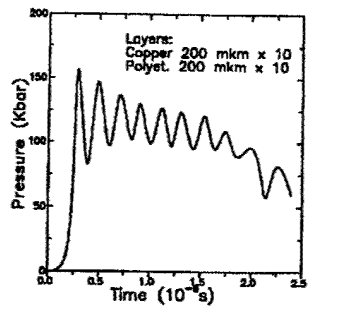	Viscous model based on the Hugoniot curve.

5	B.E. Clements 1996	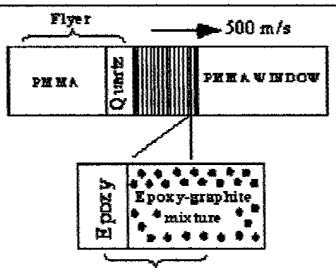	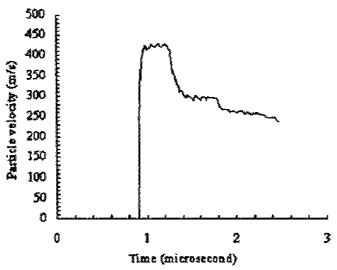	Unit cell method
6	Boteler 1999	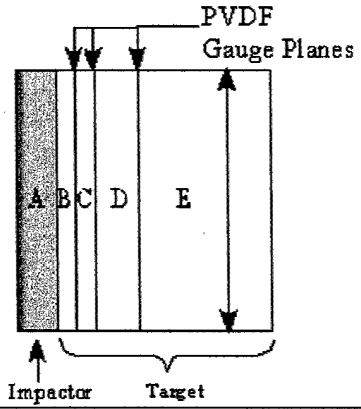	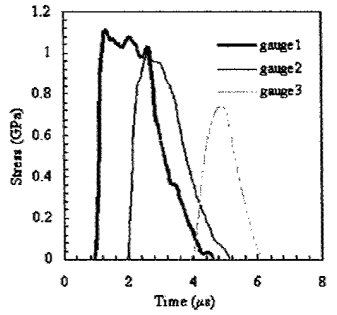	3D Linear viscoelastic model
7	Dandekar*, 1998 Espinosa 2001	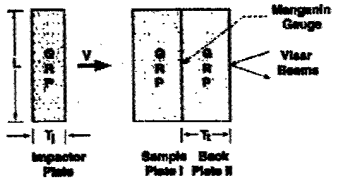	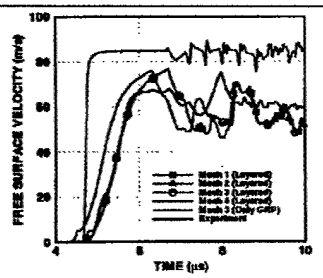	Cohesive zone model + Layered configuration
8	S. Zhuang 2002	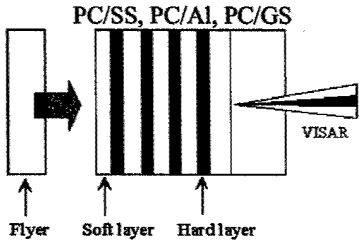	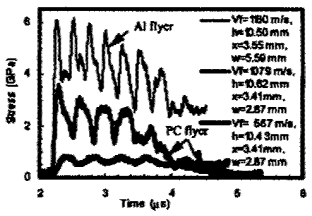	Applying Dremin's mixture theory for analysis

interpretation of this profile is extremely difficult without a wave analysis due to the absence of a clear wave structure. Since the stress or velocity profile is a result of superpositions of numerous wave reflections at the interfaces, the stress level at R_1 is an intermediate stress state. This level is determined by the sequential arrival of many wave trains at the point of measurement. A_1R_1 shows a dispersed wave structure with a longer rise time compared to the rise time in a target plate of a homogeneous material. The oscillatory portion $R_1 - E_1$ at the peak level indicates the arrivals of several release and compressive waves. The pulse duration becomes a function of not only the thickness and wave speed in the flyer plates, but also on the number of interfaces and wave speeds in the heterogeneous system. In layered systems, planar interfaces interact with the incident shock wave generating transmitted and reflected waves, their amplitudes being determined by the impedance mismatch. This factor should be explicitly considered in evaluating the shock response of layered systems. In woven fabric based engineered composite systems, such as the GRP, the interfaces between fiber and matrix and between different laminates, various lay-up sequences with different ply orientations and different forms of fiber arrangements within the matrix (particulate, planar, 2D/3D woven) all contribute to dispersion. It is often very difficult to interpret the measured wave profiles in GRP which lack clear wave structures and exhibit significant wave attenuation and dispersion.

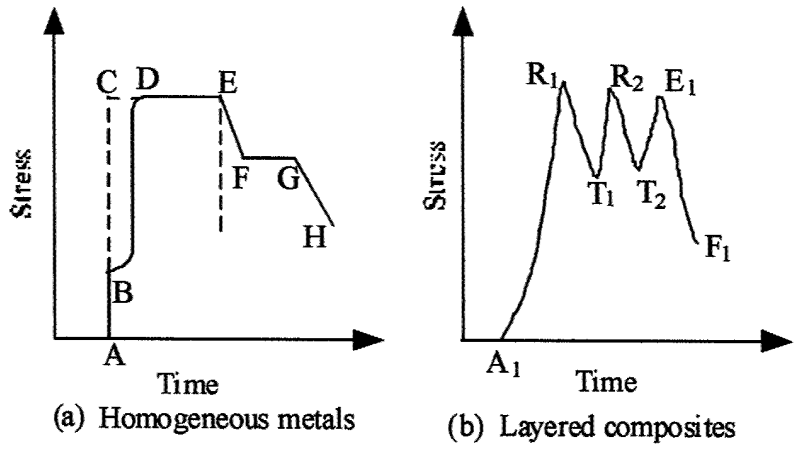

Figure 3-9: Schematic wave profiles of homogeneous metals and layered composites for a finite thickness flyer plate.

Table 3-1 summarizes the major past work in studying wave profiles in alternating layered systems using the plate impact test configuration. Lundergan [20] (1971) numerically simulated the response of a layered material system with varying thickness. The simulated particle velocity response exhibited a slow rise time and an oscillatory peak as observed in the experiments. However, there was a mean stress level about which the stress level oscillated. The idea of replacing the dispersive, heterogeneous composites with an equivalent homogeneous dissipative continuum was first proposed by Barker [21]. A general nonlinear Maxwell (viscous) model was proposed to simulate stress relaxation from an instantaneous state of the mixture to the equilibrium level. In addition, Barker obtained oscillatory stress solutions by explicitly modeling each layer using a stress wave propagation based one-dimensional code. Barker successfully validated the viscous model for the composite equation of state through matching the averaged stress response in the oscillations from the code. In 1974, Barker[22] further validated his theory using results from experiments in which a low volume fraction of aluminum was used in a PMMA/aluminum based layered system. However, in general this model fails to predict the structure of the stress waves (rise time, peak stress and oscillations).

While carrying out impact experiments on layered Cu/PMMA systems, Oved [23] (see Table 3-1) noticed significant oscillations in the stress wave profiles. As can be seen in the corresponding figure, the oscillations occur about a mean value (called mean stress). When the amplitude of oscillations is substantial, Oved pointed out that oscillations do not vanish with distance of propagation in the shock region. Consequently, oscillations should not be ignored but it should be explicitly modeled. More recently Kanel [24] confirmed the harmonic oscillations in experiments on Cu/PE system. He proposed a relaxation model similar to that of Barker, though the physics behind the models were quite different. The main thrust of Kanel's approach was to obtain the nonequilibrium pressure (the difference between the Rayleigh line to the final state and the equilibrium pressure corresponding to the Hugoniot curve) by assuming an empirical kinetic relationship.

Dandekar [25] reported results from plate impact tests on a woven fabric composite. The measured VISAR signal revealed an oscillatory peak stress behavior and a long rise time. Boteler, Rajendran, and Grove [1] further conducted a combined experimental and computational study on stress attenuation and dispersion in S2 glass fiber reinforced plastic

(GRP) laminates. The stress profiles at three different distances from the impact plane were measured using embedded PVDF gauges. They observed that the rise time increased and the average peak stress reduced with propagation distance. Some oscillations were observed at the peak stress in the first gauge, which was closer to the impact plane. The stress histories at locations significantly away from the impact plane showed no oscillatory behavior at the peak level. Their computational modeling using a three dimensional viscoelastic model matched the attenuation of the stress, but failed to reproduce wave dispersions.

Clements [26][27] proposed a modified unit cell method to model wave propagation in alternating Epoxy and Epoxy-graphite system. Only recently, Zhuang [28] conducted a thorough experimental investigation by performing a large number of plate impact experiments in selected material systems involving alternate units of either polycarbonate and stainless steel or polycarbonate and glass. In his experiments, both the quasi-harmonic oscillations and the finite rise time were observed in different systems. The effects of impedance mismatch, interface density, propagation distance as well as loading strength were examined as the basic parameters in his experiments.

In the study of wave propagation in solids, scattering, dispersion and attenuation play a critical role in determining the thermomechanical response of the media. These phenomena can be attributed to a number of nonlinearities arising from the wave characteristics, loading conditions and material heterogeneity (measured at various spatial scales ranging from nanometers to a few millimeters). The nonlinear effects in general can be ascribed to impedance (and geometric) mismatch at various length scales as often encountered in composite material systems. In addition, material nonlinearities (inelastic effects) can arise due to void nucleation and growth, microcracking, and delamination. The strong shock waves generated under high velocity impact loading often induce nonlinear effects in the deformation and failure behaviors (Nesterenko [29]).

Present authors (2002) showed that the observed structures in the measured stress wave profiles in layered systems under low velocity impact loading condition could be explained through modeling the scattering effects at planar interfaces. However, under high velocity impact loading where strong shocks are generated, it is fully realized that material nonlinear effects may play a key role in altering the basic structure. Therefore, it is important that models that describe the wave structures include equation of state for each material in the

periodic layered system.

3.2.2. Problem formulation and solution methods

Consider two semi-infinite bodies $\Omega_1(-\infty < y, z < \infty, 0 \leqslant x < \infty)$ and Ω_2 $(-\infty < y, z < \infty, -\infty < x < 0)$ such that they are initially separated and then impact each other with velocity $\overrightarrow{v} = v_0 \overrightarrow{i}$ in the x direction. As shown in Fig. 3-10(a), without loss of generality we can assume Ω_1 to be fixed in space and Ω_2 impacting on the entire $x = 0$ plane. Upon impact, stress waves are generated on a plane parallel to the impact plane and travel in the negative x direction in Ω_2 and positive x direction in Ω_1 with wave velocities determined by the material properties of these two bodies. The amplitude or strength of the stress wave is determined by the velocity of impact v_0 and the acoustic impedances of Ω_1 and Ω_2. As the waves propagate away from the impact plane, the bodies Ω_1 and Ω_2 are in compression with a uniaxial state of strain $\varepsilon_x \neq 0$ and all other components $\varepsilon_{ij} = 0$ (for $i, j = 1, 2, 3$ except $i = j = 1$). The problem is to find the state of strain and stress in the compressed region given the velocity of impact and the material properties of the two bodies.

This plate impact problem has long been well understood and successfully modeled when Ω_1 and Ω_2 are homogeneous. What we seek here is a solution to the problem when Ω_1 is laminated as shown in Fig. 3-10(c) as a precursor to the practical plate impact test shown in Fig. 3-10(b). In the plate impact test (Fig. 3-10(b)), Ω_2 is called the flyer plate or the impactor impacting on Ω_1 termed the target plate. The target plate is made of alternating layers of materials A and B with the impactor made of a homogeneous material C. All the materials (layers) are assumed to be homogeneous and damage free with known mechanical (E, υ), physical (ρ, and Equation of State) and acoustic properties. Though the bulk of the paper assumes a constitutive relationship of linear elastic, isotropic form, extensions to very high stress regions are formulated by invoking the equation of state.

In this work, we seek solution to the stress history in Ω_1 as posed in Fig. 2(b). This problem is identical to the problem in Fig. 2(c) if the thickness of the flyer plate (d_f) and the target plate (d_t) are much smaller compared to the lateral dimensions (radius of the plates). In other words, due to the geometry the strain state remains strictly one dimensional for the solution time duration. Also both the thickness d_f and d_t are large enough not to permit

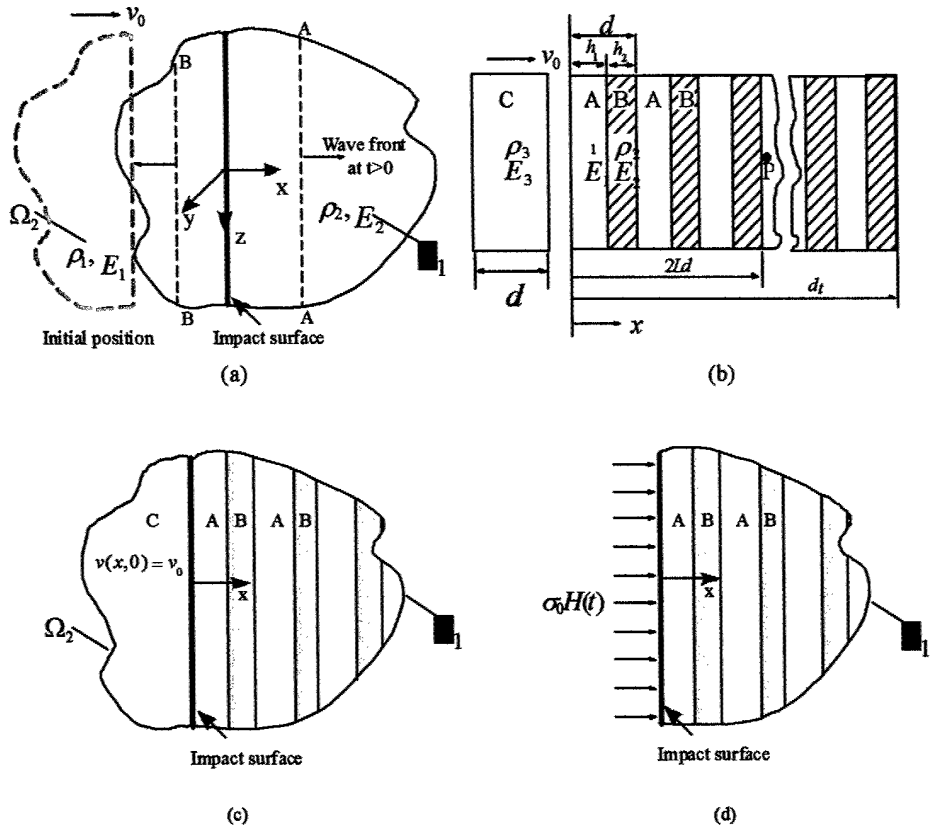

Figure 3-10: Schematic of the configuration for impact problem(a) two half spaces of homogeneous materials, (b) general plate impact problem of layered systems (c) plate impact problem of two half spaces with target being layered (d) The layered media under unit step loading.

wave reflections from the free surfaces to interfere with the solution.

The governing equations can be written as follows:

Equation of Motion:

$$\frac{\partial \sigma(x,t)}{\partial x} = \rho_i \frac{\partial^2 u(x,t)}{\partial t^2} \tag{3.18}$$

Velocity continuity:

$$\frac{\partial \varepsilon}{\partial t} - \frac{\partial v(x,t)}{\partial x} = 0 \tag{3.19}$$

Constitutive relation (Elastic laminates):

$$\sigma(x,t) = E_i^e \varepsilon(x,t) \tag{3.20}$$

where $\sigma(x,t), u(x,t), v(x,t)$ and $\varepsilon(x,t)$ denote the longitudinal stress, displacement, velocity and strain respectively. As shown in Fig. 3-10(b), the constants ρ_i and $E_i\,(i=1,2,3)$ represent the material densities and the elastic moduli for the uniaxial strain of materials A, B and C respectively.

Initial boundary condition:

Stress, displacement and strain are zero at $t = 0^-$:

$$\begin{cases} \sigma(x,0) = 0 \\ u(x,0) = 0 \quad \text{for } -\infty < x < \infty \\ \varepsilon(x,0) = 0 \end{cases} \tag{3.21}$$

Initial loading condition:

$$v(x,t) = v_0 \text{ for } x < 0 \tag{3.22}$$

Stress and velocity continuity (at all interfaces):

For wave propagation in a layered medium, the stress and displacement continuity should be maintained at all interfaces:

(a) stress continuity at $x = h_1 + Ld$:

$$\sigma_a(h_1 + Ld, t) = \sigma_b(h_1 + Ld, t) \tag{3.23}$$

where L is positive integer representing number of unit cells and $h_i\,(i=1,2)$ are the thickness of layer 1 and layer 2, and the d is the thickness of the unit cell with $d = h_1 + h_2$.

(b) Stress continuity at $x = Ld$:

$$\sigma_a(Ld, t) = \sigma_b(Ld, t) \tag{3.24}$$

In the same manner, velocity continuity at $x = h_1 + Ld$ and $x = Ld$:

$$v_a(h_1 + Ld, t) = v_b(h_1 + Ld, t) \tag{3.25}$$

$$v_a(Ld, t) = v_b(Ld, t) \tag{3.26}$$

Take Laplace transform of Eqs (3.18), (3.20) and (3.19):

$$\frac{\partial \overline{\sigma}(x,s)}{\partial x} = \rho_i s \overline{v}(x,s) \tag{3.27}$$

$$\overline{\sigma}(x,s) = E_i^e \overline{\varepsilon}(x,s) \tag{3.28}$$

$$\frac{\partial \overline{v}(x,s)}{\partial x} - s\overline{\varepsilon}(x,s) = 0 \tag{3.29}$$

The solution of equations of Eqs (3.27)-(3.29) are in the form

$$\overline{v}(x,s) = a_i e^{E_i x} + b_i e^{-E_i x} \tag{3.30}$$

$$\overline{\sigma}(x,s) = a_i \left(\frac{s\rho_i}{k_i}\right) e^{k_i x} + b_i \left(-\frac{s\rho_i}{k_i}\right) e^{-k_i x} \tag{A.5}$$

where

$$k_i = k_i(s) = \left[\frac{\rho_i s}{\overline{E}_i(s)}\right]^{\frac{1}{2}} \tag{3.31}$$

$$k_i = k_i(s) = \frac{s}{c_i} \tag{3.32}$$

where c_i is phase velocity and can be obtained by

$$c_i = \left[\frac{E_i^e}{\rho_i}\right]^{\frac{1}{2}}$$

For ordinary differential equations with periodic coefficients, Floquet theory can be applied

$$\overline{\sigma}(x,s) = e^{k(s)d}\overline{\sigma}(x-d,s) \tag{3.33}$$

$$\overline{v}(x,s) = e^{k(s)d}\overline{v}(x-d,s) \tag{3.34}$$

By considering the stress and velocity continuity across $x = h_1$,let $l = 0$ in Eqs (3.23) and (3.25):

$$a_1 e^{k_1 h_1} + b_1 e^{-k_1 h_1} = a_2 e^{k_2 h_1} + b_2 e^{-k_2 h_1} \tag{A.10}$$

$$a_1\left(\frac{\rho_1}{k_1}\right)e^{k_1 h_1} - b_1\left(-\frac{\rho_1}{k_1}\right)e^{-k_1 h_1} = a_2\left(\frac{\rho_2}{k_2}\right)e^{k_2 h_1} - b_2\left(-\frac{\rho_2}{k_2}\right)e^{-k_2 h_1} \tag{A.11}$$

Stress and velocity continuity across $x = d$:

$$e^{kd}(a_1 + b_1) = a_2 e^{k_2 d} + b_2 e^{-k_2 d} \tag{A.12}$$

$$e^{kd}\left(a_1\frac{\rho_1}{k_1} - b_1\frac{\rho_1}{k_1}\right) = a_2\frac{\rho_2}{k_2}e^{k_2 d} - b_2\frac{\rho_2}{k_2}e^{-k_2 d} \tag{A.13}$$

Eqs (3.35)-(3.35) have non-trivial solutions for only when the determinant of the coefficients is equal to zero. This condition yields the transcendental dispersion relation:

$$\cosh kd = \cosh k_1 h_1 \cosh k_2 h_2 + \frac{1}{2}\left(\frac{\rho_1 c_1}{\rho_2 c_2} + \frac{\rho_2 c_2}{\rho_1 c_1}\right)\sinh k_1 h_1 \sinh k_2 h_2 \tag{A.14}$$

where k is wave number for the laminates, k_1 and k_2 are frequencies for layer A and layer B, where h_1, h_2 and c_1, c_2 are the thickness and the longitudinal wave velocities of the layers respectively. And d is the thickness of the unit cell, with $d = h_1 + h_2$, as shown in Fig. 2(c).

For steady wave with frequency s, the dispersion relation can be written as

$$\cosh kd = \cosh\frac{s}{c_1}h_1 \cosh\frac{s}{c_2}h_2 + \frac{1}{2}\left(\frac{\rho_1 c_1}{\rho_2 c_2} + \frac{\rho_2 c_2}{\rho_1 c_1}\right)\sinh\frac{s}{c_1}h_1 \sinh\frac{s}{c_2}h_2 \tag{A.15}$$

Therefore, the phase velocity for zero-frequency limit c_0 is obtained

$$c_0 = \frac{d}{\left\{\left(\frac{h_1}{c_1}\right)^2 + \left(\frac{h_2}{c_2}\right)^2 + \left(\frac{\rho_1 c_1}{\rho_2 c_2} + \frac{\rho_2 c_2}{\rho_1 c_1}\right)\frac{h_1 h_2}{c_1 c_2}\right\}^{\frac{1}{2}}} \tag{3.35}$$

In order to get the solution for plate impact loading, as will be discussed later, it is convenient and necessary to show the solution for the problem of unit step loading. For unit step loading, the flyer plate vanishes and the boundary condition for the target plate can be written as

$$\sigma(0,t) = \sigma_0 H(t) \tag{3.36}$$

Its corresponding Laplace transform is

$$\sigma(0,s) = \frac{\sigma_0}{s} \tag{3.37}$$

The transformed stress at distance $x = 2ld$ can be obtained by Floquet theory

$$\sigma(2Ld,s) = e^{k(s)}\frac{\sigma_0}{s} \tag{3.38}$$

The late-time solution can be obtained by the asymptotic evaluation of the integral

$$\sigma(2Ld,t) = \frac{1}{2\pi i}\int_{\gamma-i\infty}^{\gamma+i\infty} \overline{\sigma}(2Ld,s)\, e^{st} ds \tag{3.39}$$

Now introduce a small time scale

$$\delta = t - x/c_0 \tag{3.40}$$

By introducing δ, we remove the variable x in the stress function in Eq. (3.39). Substitute Eqs (3.40) and (3.38) to Eq. (3.39) and assume $p(t,\delta)$ is the stress function with t and δ being the variables.

$$p(t,\delta) = \frac{\sigma_0}{2\pi i}\int_{\gamma-i\infty}^{\gamma+i\infty} \frac{e^{-\delta g(s)} e^{th(s)} ds}{s} \tag{3.41}$$

where

$$\begin{aligned} g(s) &= k(s)\, c_0 \\ h(s) &= g(s) + s = k(s)\, c_0 + s \end{aligned}$$

For late time solution, we seek an asymptotic representation of $p(t,\delta)$ for $t \to \infty$ with fixed δ. Such representation can be obtained by making the integration path follows a path of steepest descent though the saddle point s_0 at which $h'(s) = 0$. This happens when $s \to 0$. The expansion of about the saddle point will yield (for elastic case)

$$h(s) = \frac{h'''(0)}{3!}s^3 \tag{3.42}$$

where

$$h'''(0) = \frac{(c_0)^2}{d^2}\left\{\left(\frac{h_1}{c_1}\right)^2\left(\frac{h_2}{c_2}\right)^2\left[\frac{1}{4}\left(\frac{\rho_1 c_1}{\rho_2 c_2}+\frac{\rho_2 c_2}{\rho_1 c_1}\right)^2 - 1\right]\right\} \tag{3.43}$$

So the integral of Eq. (3.41) becomes

$$p(t,\delta) = \frac{1}{3}\sigma_0 + \frac{\sigma_0}{2\pi i}\int_\Gamma \frac{e^{\delta s \frac{h'''(0)}{3!}s^3}}{s}ds \tag{3.44}$$

Evaluation of the integral in Eq. (3.44) will finally give an integral of the Airy function.

$$\sigma(x,t) = \sigma_0\left[\frac{1}{3} + \int_0^B Ai(-s)ds\right] \tag{3.45}$$

where

$$B = \left(t - \frac{x}{c_0}\right)\left(\frac{2}{h'''(0)t}\right)^{\frac{1}{3}} \tag{3.46}$$

The above solution for unit step loading follows Chen and Clifton's (1975) work. Also, it should be noted that Sve (1972) evaluated an integral analogous to Eq. (3.41) and obtained the same final result.

Eq. (??) provides the solution to the stress profile of a laminated system subjected to a unit step loading. Though it is tempting to specify the amplitude of this step as the stress at the impact plane at the time of impact, it will be shown later that this is not correct. Despite this, the stress response of a unit step loading on bilaminates qualitatively displays all the essential features found in plate impact tests. Consider the case of bilaminates with material A as PMMA with $h_1 = 0.26mm$ and B as copper with $h_2 = 0.36mm$. When subjected to

unit step loading given by Eq. (3.36), the stress history at $x = 10mm$ can be calculated using Eqs (3.45) and (3.46). Fig. 3-11 shows the stress history. It should be noted that in the figure that the effective speed of c_0 corresponds to the propagating speed of $\frac{1}{3}\sigma_0$. It can be seen that the stress rises with a specific slope (as opposed to a vertical rise for a homogenized material). Then the stress oscillates about an average stress equivalent to the applied stress σ_0. In addition, the oscillations are almost harmonic with the amplitude of oscillations decaying with time.

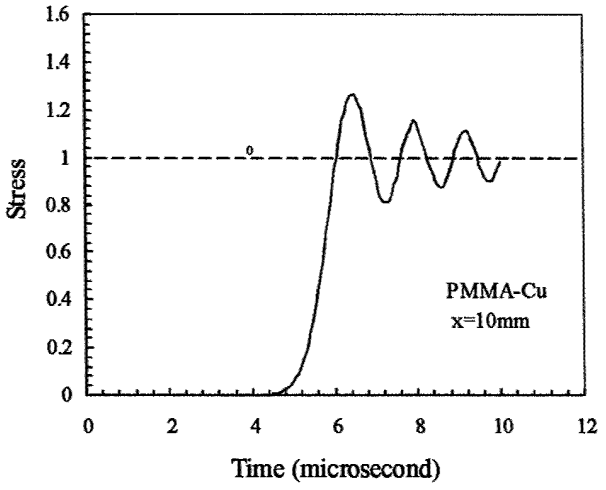

Figure 3-11: Solution to the Unit step loading condition in PMMA-Cu.

3.2.3. Solution to the plate impact problem

Problem as shown in Fig. 3-10(c) describes the plate impact problem while late-time solution in the previous section pertains to problem in Fig. 3-10(d). For a plate impact test, the body Ω_2 is continuously in contact with Ω_1 imposing initially a velocity boundary condition at $x = 0$ and at $t = 0$ identical to the constant stress boundary condition in Fig. 3-10(d). However, for problems in Fig. 3-10(c) the magnitude of loading on the boundary of the target plate keeps changing due to wave reflections in the target plate. Let us suppose σ_0 be the stress induced at the time of impact between C and A. As shown below, additional stress increments are induced at the impact plane due to wave reflections from interfaces.

In this section, we formulate the stress increments as a function of impedance mismatch between the material A and B and between C and A.

Incident wave:

Upon initial impact of Ω_2 on Ω_1, the incident wave with magnitude σ_0 is generated at the impact instant, and the magnitude σ_0 is given by

$$\sigma_0 = \frac{\rho_3 c_3 \rho_1 c_1 v_0}{\rho_3 c_3 + \rho_1 c_1} \tag{3.47}$$

Second wave train:

Fig. 3-12(a) shows the schematics of the wave traveling within the target body Ω_1. The incident wave first travels in material A. As it reaches the interface A-B, part of it is reflected back and the rest of it is transmitted (shown in dotted line only for wave train a). This reflected wave arrives back at the impact plane after a time $t_{\sigma_1} = 2t_a = 2h_1/c_1$. Stress at the impact plane is altered by this new wave arrival given by

$$\Delta\sigma_1 = r_{A-B}\left(1 + r_{A-C}\right)\sigma_0 \tag{3.48}$$

where $r_{A-B} = \frac{\rho_2 c_2 - \rho_1 c_1}{\rho_1 c_1 + \rho_2 c_2}$ and $r_{A-C} = \frac{\rho_3 c_3 - \rho_1 c_1}{\rho_1 c_1 + \rho_3 c_3}$, denoting reflection ratios at interface A-B and C-A respectively. Here C is the flyer plate. The cumulative stress level up to the second wave train at $x = 0$ at $t_{\sigma_1} = 2t_a = 2h_1/c_1$is

$$\sigma_1 = \sigma_0 + \Delta\sigma_1 = \left[r_{A-B}\left(1 + r_{A-C}\right) + 1\right]\sigma_0 \tag{3.49}$$

Third wave train:

The propagation path of the third wave train depends on the ratio of the transit time in layer A (t_a) and that in layer B (t_b).

a) If $t_a = \left(\frac{h_1}{c_1}\right) > t_b = \left(\frac{h_2}{c_2}\right)$, then the third wave train comes from the branch that has one reflection in layer B and reaches the boundary at $t = 2t_a + 2t_b$, which is represented as path b in Fig. 3-12(a). The stress variation due to the wave train that follows this path can be calculated as

$$\Delta\sigma_2 = \left[r_{A-B}\left(1 - r_{A-B}^2\right)\left(1 + r_{A-C}\right)\right]\sigma_0 \tag{3.50}$$

So, the overall stress magnitude up to the third wave train (still at the impact plane) is

$$\sigma_2 = \sigma_1 + \Delta\sigma_2 \tag{3.51}$$

b) If $t_a = \left(\frac{h_1}{c_1}\right) < t_b = \left(\frac{h_2}{c_2}\right)$, then the third wave train follows path c, which goes through two reflections in layer A and reaches the impact plane at time $t_{\sigma_2} = 4h_1/c_1$:

$$\Delta\sigma_2' = r_{A-B}^2 r_{A-C}\left(1 + r_{A-C}\right)\sigma_0 \tag{3.52}$$

The overall stress is

$$\sigma_2 = \sigma_1 + \Delta\sigma_2' \tag{3.53}$$

c) When $t_a = \left(\frac{h_1}{c_1}\right) = t_b = \left(\frac{h_2}{c_2}\right)$,the propagating path of the wave trains is independent of the materials. So the third wave train comprises waves that follow path b and waves that follow path c. As a result, the increment of this wave trains $\Delta\sigma_2''$ are the sum of Eq. (3.50) and Eq. (3.52), so we have:

$$\sigma_2 = \sigma_1 + \Delta\sigma_2'' = \sigma_1 + \Delta\sigma_2 + \Delta\sigma_2' \tag{3.54}$$

Fourth wave train:

The propagation path of the fourth wave train that reaches the boundary of the target plate still depends on the transit times t_a and t_b. For example, If $t_a > 2t_b$, then the fourth wave train follows path d and arrives at the boundary at time $t_{\sigma_3} = 2t_a + 4t_b$, as shown in Fig. 3-12.

$$\Delta\sigma_3 = \left[r_{A-B}^3\left(1 - r_{A-B}^2\right)\left(1 + r_{A-C}\right)\right]\sigma_0 \tag{3.55}$$

And the overall stress up to the third wave train σ_3 is

$$\sigma_3 = \sigma_2 + \Delta\sigma_3 \tag{3.56}$$

Also, if $t_a = t_b$, then the fourth wave train contains the waves that follow either path d or

path e.

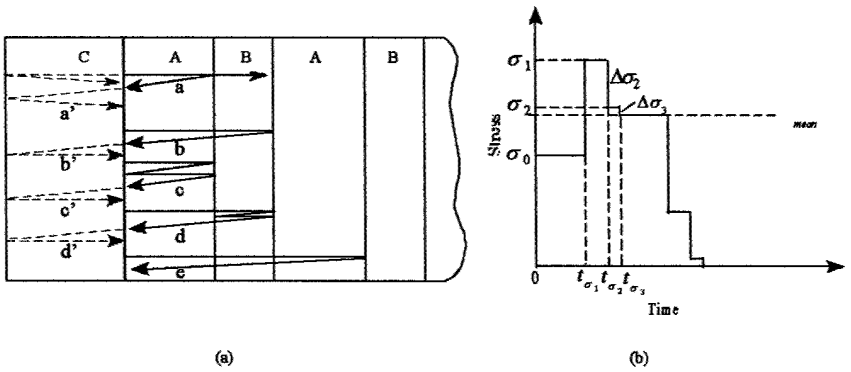

Figure 3-12: Multi-step loading method (a) The wave trains that reach the impact plane from inside of the target due to reflections.

The fifth, the sixth and additional wave trains that are generated later lead to stress increments $\Delta\sigma_4, \Delta\sigma_5$... Obviously the above analysis shows that the boundary conditions to be imposed on the target body Ω_1 is not a constant but varies with time as a result of reflected waves coming from the interfaces. Thus boundary condition at $x = 0$ comprises impact stress σ_0 (called the head wave), followed by the second wave train $\Delta\sigma_1$ after time $t_{\sigma_1} = 2t_a$, then the third wave train $\Delta\sigma_2$ at $t_{\sigma_2} = 2t_a + 2t_b$ (if $t_a > t_b$) or at $t_{\sigma_2} = 4t_a$ (if $t_a \leqslant t_b$), the fourth wave train $\Delta\sigma_3$ at t_{σ_3} and so on. The exact solution should consider all these stress increments with specific time delays as the loading condition at $x = 0$. Since the formulation is linear, the late-time solution to plate impact problem can be obtained by the method of superposition of unit step loadings with steps corresponding to incremental stress and specific time delays.

Mean stress σ_{mean} In the present problem, the target and the impactor materials are assumed to be of infinite thickness and hence the back surfaces do not exist. Waves continue to travel in the positive $x-$direction in the target and negative $x-$direction in the impactor. Waves that arrive at the plane of the impact are those that have suffered multiple interactions in the target plate. The energy content of the newly arriving waves will in general decrease with time as more energy is being diffused away from the plane of the impact. Thus the incremental stress contribution by late arriving waves will continue to decrease and eventually

vanish signalling the steady state conditions. One can always identify the sequence n of arriving waves that correspond to any given arbitrarily low stress level ϵ Thus

$$\left| \sum_{i>n}^{\infty} \Delta\sigma_i \right| < \epsilon, \tag{3.57}$$

It can be clearly seen that for a given value of ϵ, the value of n will depend on a number of geometric and material parameters. The above analysis indicates that a steady state stress value is reached at the plane of the impact (in reality throughout the domains $\Omega_1$and Ω_2) and this value will be designated as σ_{mean} in the present study.

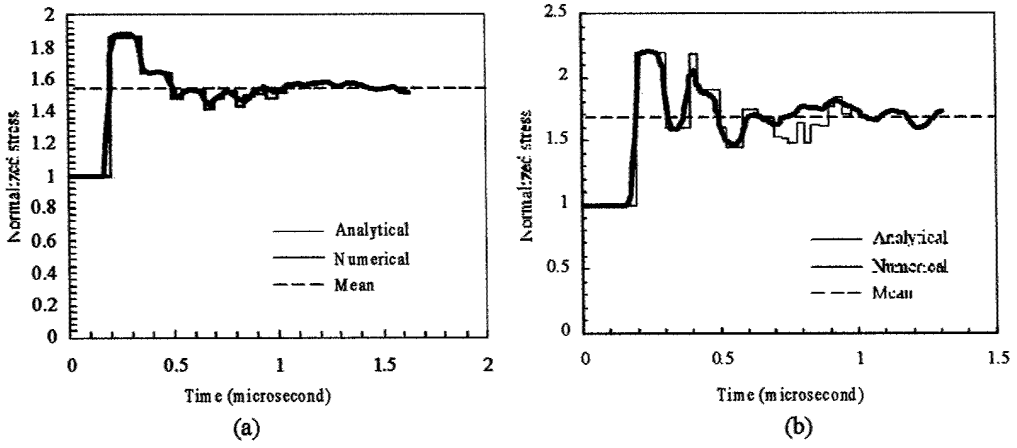

Figure 3-13: Comparison of the stress history at the boundary of the layered systems between analytical solution and

In order to confirm the existence of σ_{mean} or Eq. (3.57), we can examine the plate impact tests of two different material systems comprising PMMA/Cu and PMMA/Al both being impacted by PMMA. Fig. 3-13(a) is the example of PMMA impacting PMMA/Cu with the thickness $h_1 = 0.26mm$ and $h_2 = 0.36mm$, while Figure 3-13(b) shows the stress history of aluminum impacting PMMA/Al. In both cases, the incremental stress levels in the first few steps are significantly larger than the subsequent steps and the total stress finally oscillates about a steady stress state (marked in dotted line). The analytical results were also compared with numerical results using an explicit FEM code. The FEM results (shown in thick dark lines) indicate very similar trend in the incremental stresses all the way to the steady state.

This validates the existence of σ_{mean} and possible hypothesis given inEq. (3.57). Thus it is possible to use the superposition of the first few steps to obtain the value of steady state stress σ_{mean}.

It should be noted that σ_0 is the stress at the instant of impact in a homogenous (as well as heterogenous) system, and is also the steady state value for the homogenous system. For a heterogeneous system the steady state value is σ_{mean}.The ratio $\frac{\sigma_{mean}}{\sigma_0}$ represents the amplification factor induced due to the heterogeneity of the body Ω_1. Obviously this ratio is unity if Ω_1 were to be homogeneous. Since the above procedure of computing σ_{mean} is tedious and not elegant, herein we explore other means of obtaining the same result.

The existence of the steady state suggests rule of mixture as a possible effective medium theory. Thus invoking mixture theory, the density of the target body can be written as

$$\widetilde{\rho}_0 = \eta\rho_1 + (1-\eta)\,\rho_2 \tag{3.58}$$

where η is the volume fraction of the first component (Material A). For low velocity loading, we can assume that η is constant with the relation

$$\eta = \frac{h_1}{d} \tag{3.59}$$

Since c_0 represents the effective sound velocity in the laminates, the equivalent impedance of the mixture is $\widetilde{\rho}_0 c_0$. From the stress continuity at the impact surface, we have

$$\sigma_{mean} = \rho_3 c_3 \left(v_0 - u_p\right) = \widetilde{\rho}_0 c_0 u_p \tag{3.60}$$

where u_p is particle velocity. By eliminating u_p, the mean stress can be written as

$$\sigma_{mean} = \frac{\rho_3 c_3 \widetilde{\rho}_0 c_0 v_0}{\rho_3 c_3 + \widetilde{\rho}_0 c_0} \tag{3.61}$$

From Eq. (3.47) and (3.61) we can obtain the normalized mean stress as

$$\frac{\sigma_{mean}}{\sigma_0} = \frac{\rho_f c_f + \rho_1 c_1}{\rho_f c_f + \widetilde{\rho}_0 c_0} \frac{\widetilde{\rho}_0 c_0}{\rho_1 c_1} \tag{3.62}$$

The above relation has also been plotted in Figures 3-13(a) and 3-13(b) and show that equation (3.62) is capable of determining σ_{mean} without actually computing many incremental stress levels.

Multiple-steps loading The determination of σ_{mean} though very useful in computing the steady state response of heterogeneous material, still cannot capture the wave structure that precedes the steady state value. For this we still need to use multiple steps as outlined below. We can now propose a solution that comprises n steps due to first n wave trains. In order to make the final steady state reach σ_{mean}, we set

$$\Delta\sigma_{n-1} = \sigma_{mean} - \sigma_{n-2} \tag{3.63}$$

For example, for a four-step method (when $n = 4$), the fourth step is specified by

$$\Delta\sigma_3 = \sigma_{mean} - \sigma_2 \tag{3.64}$$

The whole loading history at the impact plane is shown in Fig. 3-12(b) and the solution can be written as:

$$\sigma(x,t) = \begin{cases} \sigma(x,t)\mid_{\sigma_0} & \frac{x}{c_0} \le t < t_{\sigma_1} + \frac{x}{c_0} \\ \sigma(x,t)\mid_{\sigma_0} + \Delta\sigma_1(x,t)\mid_{\sigma_1} & t_{\sigma_1} + \frac{x}{c_0} \le t \le t_{\sigma_2} + \frac{x}{c_0} \\ \sigma(x,t)\mid_{\sigma_0} + \Delta\sigma_1(x,t)\mid_{\sigma_1} + \Delta\sigma_2(x,t)\mid_{\sigma_2} & t_{\sigma_2} + \frac{x}{c_0} < t < t_{\sigma_3} + \frac{x}{c_0} \\ \sigma(x,t)\mid_{\sigma_0} + \Delta\sigma_1(x,t)\mid_{\sigma_1} + \Delta\sigma_2(x,t)\mid_{\sigma_2} + \Delta\sigma_3(x,t)\mid_{\sigma_3} & t_{\sigma_3} + \frac{x}{c_0} < t \end{cases} \tag{3.65}$$

where

$$\sigma(x,t)\mid_{\sigma_0} = \sigma_0 \left[\frac{1}{3} + \int_0^B Ai(-s)\,ds\right]$$

$$\Delta\sigma_j(x,t)\mid_{\sigma_i} = \Delta\sigma_j \left[\frac{1}{3} + \int_0^B Ai(-s)\,ds\right],\ j = 1,2,3,4 \tag{3.66}$$

The above equations can be solved similar to Eqs (??-??).

Application of the analytical solution The late time solution predicts the stress history from the contribution of the main disturbance which is when $s \rightarrow 0$. So theoretically the late time solution is only valid when $t \rightarrow \infty$ and also is only valid in the infinity ($x \rightarrow \infty$). However, if we decompose the incident square wave into Fourier series, it is obvious that the coefficients of the terms with higher frequencies become monotonically smaller. Also, equation of dispersion relation means that the phase velocities for waves with higher frequencies are slower. These two facts make sure that when x is sufficiently large the head of the pulse can be approximated by Eq. (3.65) with good accuracy since high frequency terms die out and cannot reach a certain location x at a given time. Based on this phenomenon, we can postulate that x^* where head wave dies out can be considered as a reference location for applying the analytical solution. Though rigorous proof is not provided, our numerical results compares well with the analytical solution based on this assumption. With this reference location x^* for application, we propose that for $x < x^*$, it is suggested that superposition not be used and routine stepwise incremental stress calculation should be performed, as shown in previous paper (Chandra et al.,2002). Since the head wave in systems with low impedance mismatch dies down much slowly compared with systems with high impedance mismatch, the values of x^* of such systems are relatively large.

It is also important to explore the least number of steps n for obtaining the stress response with acceptable accuracy. At a fixed location, our independent study shows that the accuracy depends on $\left|\sum_{i>n}^{\infty} \Delta\sigma_i\right|$ which is in turn governed by material heterogeneity. One major heterogeneity factor is impedance mismatch and it is shown that systems with very high impedance mismatch between A and B (equivalent to high r_{A-B}) and small impedance mismatch between A and C (small r_{A-C}) in general yields small $\left|\sum_{i>n}^{\infty} \Delta\sigma_i\right|$. So we propose a simple one step loading method ($n = 1$) for such systems, by assuming the equivalent loading condition

$$\sigma(0,t) = \sigma_{mean} H(t) \tag{3.67}$$

Though σ_0 is the impact stress at $t = 0$ and the loading magnitude reaches σ_{mean} at time $t > 0$, Eq. (3.67) ignores the time effect. Substituting σ_0 by σ_{mean} in the late-time solution

Eq. (??) we obtain the solution for plate impact as

$$\sigma(x,t) = \sigma_{mean}\left[\frac{1}{3} + \int_0^B Ai(-s)ds\right] \tag{3.68}$$

In order to validate the above ideas, we select PMMA/Al system with a high impedance ratio of $r_{A-B} = 0.71$ and examine the effect of number of loading steps n on the accuracy of the solution. Fig. 3-14 shows the stress response at $x = 10mm$ (impact conditions identical to that in Fig. 3-13(b)), using1, 3 and 5 steps. Numerical results using an explicit finite element code is also presented for comparison purposes. Fig. 3-14 clearly shows that 1 step solution gives sufficiently accurate results for this case. Though the results are not shown here, when impedance ratio r_{A-B} is small (for example, below 0.4), the use of one-step method may not be sufficient and higher number of steps are needed.

All the analyses presented so far, assume that the impact process generates a single elastic wave that travels away from the impact plane. When velocity of impact increases, the wave enters an elastic-plastic regime and with further increase the wave becomes a shock wave. For both these cases, the approaches presented above need to be modified. For the case of shock wave, we present the necessary modifications in the next section.

3.2.4. Approximate Solution for shock loading

In plate impact tests, the loading strength is usually much higher than the Hugoniot Elastic Limit (HEL). In this case, the shock wave is generated. For laminated systems under shock loading, the shock waves propagates with supersonic velocity depending on the pressure. Therefore, it is necessary to relate shock velocity, density and volume to the particle velocity by means of Equation of State (EOS). A general EOS takes the form

$$U_s = C_0 + S_1 u_p + S_2 u_p^2 + S_3 u_p^3 + ... \tag{3.69}$$

where S_1, S_2 and S_3 are empirical parameters. C_0 is the sound velocity in a given material under zero pressure. For most metals (without porosity and phase transformation), linear

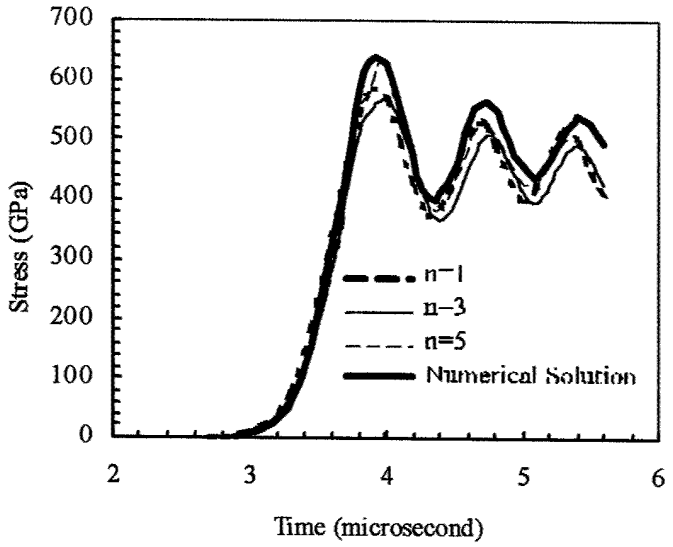

Figure 3-14: Comparison of solutions for Al impacting PMMA26/Al36 at x=10mm. Comparison between FEM results and Analytical solutions using n=1,3,5 respectively.

relationship between U_s and u_p is sufficiently accurate and EOS is in the form

$$U_s = C_0 + S_1 u_p \tag{3.70}$$

For materials other than metals, such as polymers, EOS with higher orders is necessary. The density under high pressure (ρ_i') can no longer be approximated as the original density. It is directly related to the loading strength u_p:

$$\rho_i' = \frac{1}{1 - \frac{u_{pi}}{U_{si}}} \rho_{0i}, i = 1, 2, 3 \tag{3.71}$$

In the same way, the volume under high pressure (V_i') is related to u_p by:

$$V_i' = \left(1 - \frac{u_{pi}}{U_{si}}\right) V_{0i}, i = 1, 2, 3 \tag{3.72}$$

Therefore, in plate impact problem, according to this equation, the thickness under shock loading condition (h_i') will be

$$h_i' = \left(1 - \frac{(u_p)_i}{(U_s)_i}\right) h_{0i},\ i = 1, 2 \tag{3.73}$$

New impedance ratio is approximately (Assume that material 2 is harder than material 1):

$$R' = \frac{\rho_2' U_{s2}}{\rho_1' U_{s1}} \tag{3.74}$$

It can be seen from Eqs (4.6), (3.70), (3.71) and (3.73) that wave velocity, thickness and density for the laminates subjected to shock loading all depend on the particle velocity. While for elastic response, they remain constant. There is yet another difference between the shock response and the acoustic response. Across the front of the strong disturbance which is generated by extremely strong impact loading, velocity is not continuous. In other words, Eq. (3.19) is no longer valid. However, under low pressure to moderate, the shock wave is weak and the wave front is not very steep. So in this analysis we assume that this governing equation is still valid for systems under low to moderate pressure. Therefore, by substituting the U_{si}, ρ_i' and h_i' $(i = 1, 2)$ into Eq. (??), we obtain the late time velocity for shock loading condition ($\widetilde{U}_s$):

$$\widetilde{U}_s = \frac{h_1' + h_2'}{\left[\left(\frac{h_1'}{U_{s2}}\right)^2 + \left(\frac{h_2'}{U_{s2}}\right)^2 + \left(R' + \frac{1}{R'}\right)\frac{h_1' h_2'}{U_{s1} U_{s2}}\right]^{\frac{1}{2}}} \tag{3.75}$$

Similarly, we obtain the mean stress level for layered systems (σ'_{mean}) corresponds to the steady state solution by assuming that the layered systems is equivalent to the mixture with impedance $\widetilde{\rho}_0 \widetilde{U}_s$. Similar to Eqs (3.60) and (3.61), we have

$$\sigma'_{mean} = \widetilde{\rho}_0 \widetilde{U}_s \widetilde{u}_p \tag{3.76}$$

where

$$\widetilde{u}_p' = \frac{\rho_3' U_{s3}'}{\rho_3' U_{s3}' + \widetilde{\rho}_0 \widetilde{U}_s} v_0 \tag{3.77}$$

We have obtained the σ_{mean} so far, now we need to get the solution for the whole stress history. As is mentioned earlier the significant difference between shock wave and acoustic wave lies in the fact that the velocity increase and impedance mismatch varies depending on the pressure. For an observer at a given location, the head wave propagates with longitudinal velocity in uncompressed media. So for a given location x, the arrival time of the head wave is

$$t_{\sigma_0'} = \frac{\eta x}{C_{01}} + \frac{(1-\eta)\, x}{C_{02}} \tag{3.78}$$

where C_{01}, C_{02} are the sound velocities in material A and B under zero pressure and η is given by Eq. (3.59). Immediately behind the head wave, the high pressure σ_0' is achieved

$$\sigma_0' = \frac{\rho_3 U_{s3} \rho_1 U_{s1} v_0}{\rho_3 U_{s3} + \rho_1 U_{s1}} \tag{3.79}$$

So the high pressure due to the impact instant with magnitude given by Eq. (3.79) is generated behind the head wave, the successive wave trains travel faster than the head wave. As shown in Fig. 3-12(a), the second wave train is generated by one reflections inside first layer (in Material A). This wave train reaches the impact surface after $\Delta t'$ from initial impact:

$$\Delta t' = \frac{h_1}{C_{01}} + \frac{h_1'}{U_{s1}} \tag{3.80}$$

As shown in Eq. (3.80), the time interval between the second wave train and the head wave is determined by the thickness and wave velocity of the first layer before and after the arrival of the head wave, which are all affected by the loading strength v_0. The time t_{σ_1} when the second wave train arrives at location x is approximately given by

$$t_{\sigma_1} = \Delta t' + \frac{\eta x}{(U_{s1})_{\sigma_0'}} + \frac{(1-\eta)\, x}{(U_{s2})_{\sigma_0'}} \tag{3.81}$$

Comparing with Eq. (3.81) and Eq. (3.78), we can see that the second wave train overtakes the wave front at a sufficiently large propagation distance x when the initial time delay $\Delta t'$ is relatively negligible due to $(U_{si})_{\sigma_0'} > C_{0i}$ $(i = 1, 2)$. In the same manner, it is also possible that the subsequent wave trains can catch up with the first and second wave train depending

additionally the properties of layer B.

Thus the steps in the analytical procedure for determining the stress response under shock loading conditions are as follows:

1. The shock velocities U_{si}, and the thickness h_i' should be calculated by considering EOS, as shown in Eqs (4.6)-(3.73).

2. The mean stress σ'_{mean} should be computed using Eqs (3.75) and (3.76).

3. By considering the EOS effect, incident stress σ_0 is given by Eq. (3.79), incremental stress values at the impact plane $\Delta\sigma_0', \Delta\sigma_1'$... should be calculated similar to Eqs (3.49) and (3.51). Unless modification of reflection ratio is needed based on velocity variation with pressure.

4. In order to take into account the 'overtaking' effect and thus to predict the peak stress accurately, the number of steps n should be more than the steps it takes to reach the peak stress. First we need to determine if the second wave has overtaken the first for the given location x under consideration. If the second (and subsequent) wave has not overtaken then σ_0' and $\Delta\sigma_1'$ should be superimposed successively with proper time interval $\left|t_{\sigma_1'} - t_{\sigma_0'}\right|$ At a given location where the head wave is overtaken by the second wave train, then the new wave front travels with the second wave front. The first stress increment σ_0'' is the sum of the strength of the initial head wave and that of the initial second wave front

$$\sigma_0'' = \sigma_0' + \Delta\sigma_1' \tag{3.82}$$

   Similar corrections due to 'overtaking' effect can be made to subsequent steps if necessary.

5. Superposition of results based on time dependent stress increments, similar to Eq. (3.65).

3.2.5. Results and discussions

In this section we apply the developed method to solve a few additional plate impact problems and examine the impact of our solution procedure. We first demonstrate the need to use σ_{mean} for solving plate impact problems rather than σ_0 which is truly valid only for unit step loading. Next we show that if the impact velocity is low such that the material response is within the elastic regime, then we can use the elasticity approach. However, if the impact velocity is very high, the material enters the shock regime when we need to invoke equation of state to represent the material behavior.

Mean stress σ_{mean} It should be noted that σ_0 is the stress produced at the time of impact and remains constant in homogeneous materials compared to σ_{mean} the steady state stress obtained in a heterogeneous target material (see sections 3.2). In some sense $\frac{\sigma_{mean}}{\sigma_0}$ represents the heterogeneity of the target system. The Eq. (3.62) can be visualized from Fig. 3-15, which shows the magnitude of $\frac{\sigma_{mean}}{\sigma_0}$ of PMMA (matrix) based composites systems. Various polymer and metallic materials are used to reinforce the composites. The figure shows the variation of $\frac{\sigma_{mean}}{\sigma_0}$ with varying volume fraction of PMMA in the composites. Two sets of data are shown in the figure: the data in the solid line are for cases when the flyer plate is PMMA, while the data in the dashed lines are for the cases when the flyer plate is aluminum. It can be seen from the figure that $\frac{\sigma_{mean}}{\sigma_0}$ can vary as much as 0.9 to 4.8. While σ_0 is the stress induced at the time of impact (both in the flyer and the target plates), σ_{mean} represents the steady state stress reached in flyer and the target at sufficiently long time and is the result of multiple reflections at the various heterogeneous interfaces. Thus this $\frac{\sigma_{mean}}{\sigma_0}$ ratio represents the amplification in the stress levels reached within the material compared to that at the time of impact, and the figure shows that the ratio can be very high. Thus in order to correctly predict the stress levels we should use σ_{mean} and not σ_0. It should be noted that while σ_0 is dictated by the heterogeneity at the impact surface (materials A and C) and of course the impact velocity, the magnitude of σ_{mean} depends additionally on the impedance mismatch of the components of the target materials (B and C) and their volume fraction.

Since the magnitude of σ_{mean} uniquely determines the steady state stress in the materials subjected to plate impact loading, it is interesting to explore whether other theories can lead to the same result. For this purpose we examine Dremin's mixture theory. As shown in

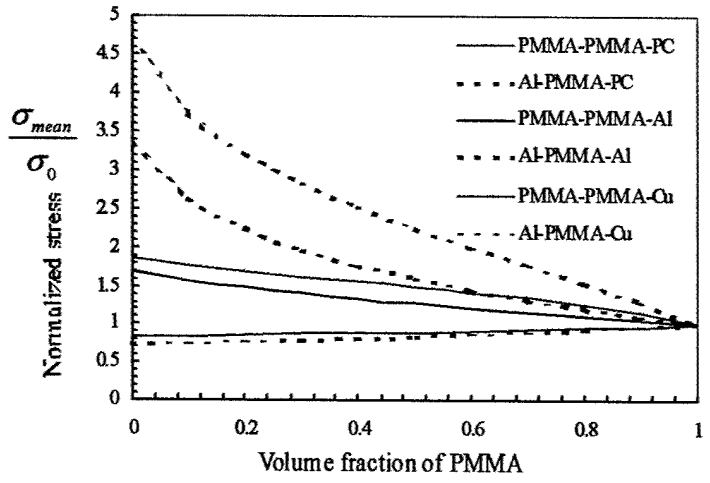

Figure 3-15: The normalized mean stress as a function of volume fraction in different systems.

Appendix B, the same effective sound speed for the equivalent mixture can be obtained based on this theory. So by obtaining the same effective density and sound velocity in the mixture, the same expression of mean stress can be obtained by applying Eqs (3.60) and (3.61). However, as is mentioned in section 2, except the mean stress the structure of the wave cannot be obtained simply through mixture theory.

The effect of Equation of State The method described in section 3, and shown in Eq. (3.68) is valid when the material behavior is within elastic regime. However, when the impact velocities are high leading to stress levels higher than the HEL, it is then required to use EOS as the appropriate constitutive equation. Though it is easy to apply EOS for a single material system, when the target plate is made up of multiple materials with their individual EOS, the application of EOS of the system is not straightforward. EOS can be expressed in many forms including as a variation of shock velocity with particle velocity. Fig. 3-16(a) shows shock velocity, U_s as a function of particle velocity, u_p for a few materials of interest. The slope of the curve $\frac{\partial U_s}{\partial u_p}$ is different for different materials; typically the slope varies linearly for metals and nonlinearly for polymers. Thus the parameter S_1 in Eq. (3.70) determines the slope for metals. While S_1 plays a major role, S_2 and S_3 or even higher orders cannot be neglected for polymers. It is clear from that figure that the slope $\frac{\partial U_s}{\partial u_p}$ increases the fastest for polycarbonate (PC) while there is negligible slope for glass. The slopes of Cu,

Al and PMMA show only moderate values.

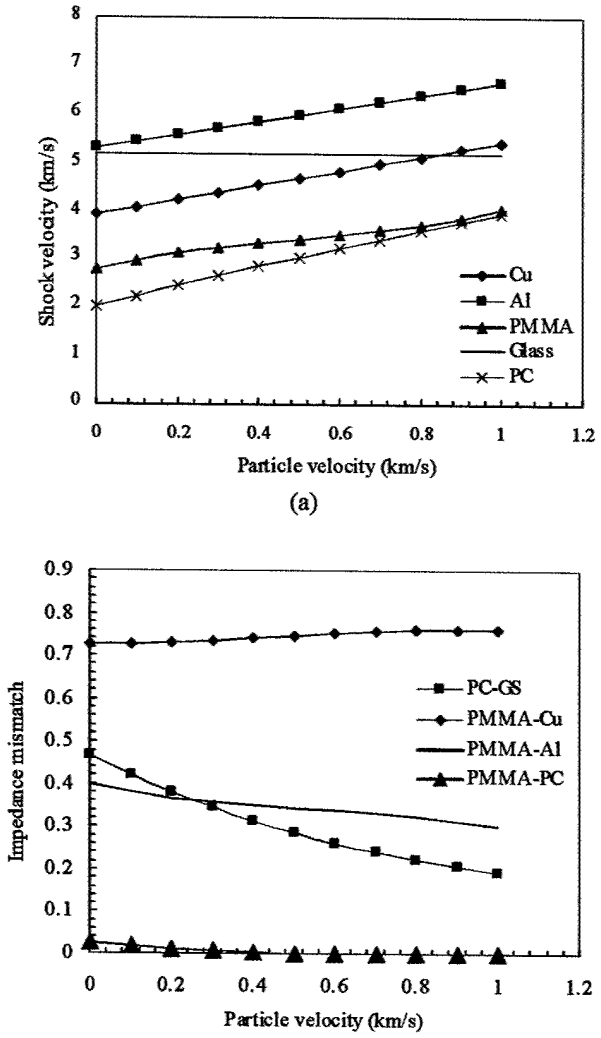

Figure 3-16: The effect of EOS in velocity and impedance mismatch.

It should be noted that the impedance mismatch of a pair of given materials not only depends on the relative magnitudes of shock velocities but on the densities at a given state. For the materials under shock loading conditions, apart from the velocities there is a concurrent increase in densities with particle velocity. Since impedance is the product of density and shock velocity and since both increase with particle velocity, absolute value of the impedance of a given material increases. However, since $\frac{\partial U_s}{\partial u_p}$ and the rate of density change is different for

different materials, impedance *mismatch* of a given pair materials may increase or decrease. Fig. 3-16(b) shows the impedance mismatch of combinations of materials (described in Fig 3-16(a)) with particle velocities. It can be clearly seen from the figure that the impedance mismatch is not a constant for a given material combination and is a function of particle velocity and hence the velocity of impact. For example, the impedance of PC-GS reduces significantly with the increase in particle velocity. However, for other systems considered here the variation is less significant.

The method of using EOS (section 3.2.3) has been used to simulate a plate impact test that corresponds to an experimental data available in the literature. Fig. 3-17(a) shows the comparison of the experimental result (Zhuang, 2002) with the analytical solution. In this experiment, a flyer made of PC impacts on a target made of alternating PC and glass (GS) with velocity of 1079 m/s, as shown in Table 2. It can be seen that the mean stress obtained from analytical solution agrees well with the experimental result. It should be noted that by incorporating EOS, the shock velocity and the density generally increase depending on the loading strength. As a result, the mean stress level obtained based on section 3.2.3 can be significantly higher than the mean stress obtained using just elastic analysis (showed in dotted line). The elastic solution does not even come close to the experimental results validating the need to use EOS as the right constitutive model.

Experiments	A	B	C	Impact velocity	h_1	h_2	x
1	PC	Glass	PC	1079	0.37	0.20	6.44
2	PC	Glass	Al	1160	0.37	0.20	3.55

Table 3.1: Configurations of Experiment 1 and 2

There is yet another critical difference between elastic and shock loading conditions in terms of the peak stress. While in the elastically loaded condition, the first peak has a magnitude of $1.274\sigma_{mean}$ when the impact stress is σ_{mean}, the same is not true for shock loading. It is important to note that peak stress may be more critical than mean stress in determining the fracture or damage of materials. Fig. 3-17(a) shows that the peak stress is much higher than the factor of 1.274 compared to the mean stress. This anomaly can be explained by the fact that wave trains in compressed media travel faster and the second wave

may be able to overtake the first wave depending on the distance of propagation. Thus using a single step method may not be adequate for shock loaded cases while it may be acceptable for elastic loadings. The matching of experimental and analytical results is quite good, in terms of arrival time, peak stress, frequency of the oscillations and mean stress. Yet another experimental comparison is shown in Fig. 3-17(b), this time the impactor being a metal on a polymer/ceramic composite system. Here Al impacts on PC/GS with 1160 m/s. Again the overall agreement is good and similar observations can be made.

3.2.6. Summary

In this section, an analytical solution to the problem of plate impact in layered heterogeneous material systems has been developed. The solution to the plate impact problem (Fig. 2(c)) is quite different from that of a unit step loading. The stress boundary condition at the plane of the impact, continuously varies for a heterogeneous layered target plate, due to the reflections inside the target plate.

- A steady state stress value has been identified for the case of heterogeneous target system. This σ_{mean} is different from the value at the time of impact σ_0, and the difference depends on the degree of material heterogeneity. σ_{mean} was obtained using wave dispersion relation and it was further shown that Dremin's mixture theory can also be used to get the same value.

- A late time solution to the problem of plate impact on a heterogeneous layered material system has been formulated. The applicability of the spatial range of the late time solution has been identified.

- The solution procedure for elastic loading has been formulated using multiple steps. Conditions for using a single step have also been identified.

- The solution method for shock loaded cases have also been described.

- The developed method has been validated by comparing the analytical results with numerical and experimental data. The comparison is good.

Appendix: Dremin's theory in finding effective wave speed

In this theory, it is assumed that the specific volume of the shock-compressed mixture is equal to the sum of the specific volume of its components, obtained at the same pressure by separate shock compression

$$\widetilde{V} = \alpha V_1(P) + (1-\alpha) V_2(P) \tag{A.1}$$

where P is the pressure or stress, $\widetilde{V}, V_1$and V_2 are the specific volumes of the mixture, materials 1 and 2, respectively. α is the mass fraction of component 1. Differentiating the above equation with respect to pressure P, we obtain

$$\frac{d\widetilde{V}}{dP} = \alpha \frac{dV_1}{dP} + (1-\alpha)\frac{dV_2}{dP} \tag{A.2}$$

In the above equation $\frac{d\widetilde{V}}{dP}$ represents the slope of Hugoniot curve of the mixture which can then be equated as follows.

$$\frac{d\widetilde{V}}{dP} = -\frac{\widetilde{V}^2}{\widetilde{U}_s^2} \tag{A.3}$$

The above equation (A.3) can be written for each of the constituent materials 1 and 2, and that of the mixture. Now using those definitions in Eq. (A.2) we obtain the shock velocity $\widetilde{U}_s$ of the mixture

$$\widetilde{U}_s = \frac{\widetilde{V}}{\left[\frac{\alpha}{(\rho_1 U_{s1})^2} + \frac{(1-\alpha)}{(\rho_2 U_{s2})^2}\right]^{\frac{1}{2}}} \tag{A. 4}$$

In elastic region, the effective volume in the above equation is given by

$$\widetilde{V} = \frac{1}{\widetilde{\rho}_0} = \frac{h_1 + h_2}{\rho_1 h_1 + \rho_2 h_2} \tag{A. 5}$$

Also, conservation of mass holds for each constituent as well as for the mixture, so the mass fraction of the material 1 is given by $\alpha = \frac{\rho_1 h_1}{\rho_1 h_1 + \rho_2 h_2}$. By substituting α and the specific volume

$\widetilde{V}$ in Eq. (A. 5) into Eq. (A. 4), we have

$$\widetilde{U}_s = \frac{h_1 + h_2}{\left[(\rho_1 h_1 + \rho_2 h_2)\left(\frac{\rho_1 h_1}{\rho_1^2 c_1^2} + \frac{\rho_2 h_2}{\rho_2^2 c_2^2}\right)\right]^{\frac{1}{2}}} \tag{A. 6}$$

By expansion of the terms in the denominator and rearrangement of these terms, it is found that

$$\widetilde{U}_s = \frac{h_1 + h_2}{\left[\left(\frac{h_1}{c_1}\right)^2 + \left(\frac{h_2}{c_2}\right)^2 + \left(\frac{\rho_1 c_1}{\rho_2 c_2} + \frac{\rho_2 c_2}{\rho_1 c_1}\right)\frac{h_1 h_2}{c_1 c_2}\right]^{\frac{1}{2}}} = c_0 \tag{A. 7}$$

In the same manner, it can be shown that under shock loading condition the same velocity is also obtained through these two different theories.

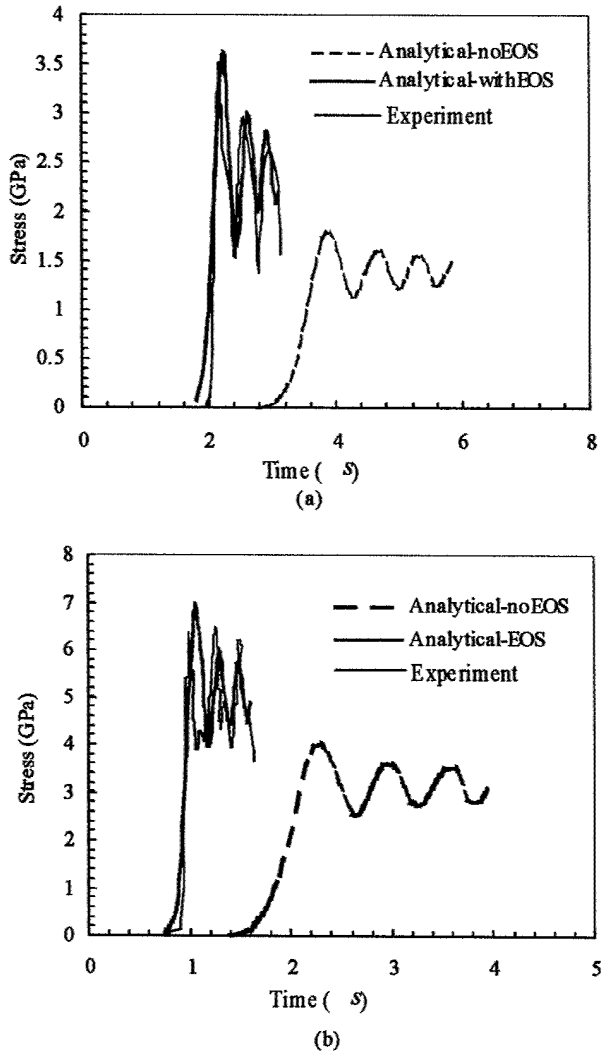

Figure 3-17: Comparisons of the experimental data and the analytical solutions in layered PC/GS. (a) Experiment 1, and (b) Experiment 2.

Chapter 4

Controlling parameters for layered materials

4.1. Material Heterogeneity factors

For a typical laminated composite, the impact response depends on the loading condition and also the structure of the composites. The loading condition generally involves the geometry of the impactor (bullet, plate, or ball...), impact direction (normal or oblique) and impact velocity. The interaction of waves with an interface are relatively less complicated when the impact angle is normal and also when the impact surface is simple. This suggests that normal plate impact remains to be a practically simple test configuration. For plate impact tests, the impact velocity is a critical factor and it determines whether the material response falls into elastic, elastic-plastic or hydrodynamic region. On the other hand, there are various characteristic parameters that determine the structure of a laminated composite. Take the glass reinforced polyester (one type of GRP) for illustration: the material properties of the constituents include: Young's modulus, density, Poisson's ratio, strength (both tensile and compressive), and toughness... In addition, the geometric properties consist: the form of the fiber (roving, woven, chopped strand...), the volume fraction, thickness of laminates, stacking sequence and interface density, and preexisting flaws such as voids... Fig. 4-1 shows a plain weave GRP composite used in practice. The GRP plate comprise $0°/90°$ crossplied laminates, and in each laminate, plain weave of fiber is coated by polyester resin by the

weight of 32%. For such woven composites, there are a large number of spatial variations in geometry and material properties. As a result, when subjected to high velocity plate impact tests, the wave scattering in GRP is very complex. To simplify the structure of the composite so that it is feasible to study wave propagation in the system, we can ignore the curved shape of the fiber fabric and the difference between the laminates, and consequently when the wave travels inside GRP, it travels through strictly periodic layers of pure matrix and fiber fabric. In this way, we obtain the same model as shown in Fig. 3-10(c). As shown in Fig. 3-10(c), the controlling parameters for flyer plate are thickness d_f, impact velocity v_0 and impedance of the flyer plate $\rho_3 c_3$ (homogeneous monolithic material is assumed). The controlling parameters for target plate are densities ρ_1 and ρ_2, and velocities c_1 and c_2, number of layers $2L$, and thickness for constituent A and B h_1 and h_2, respectively.

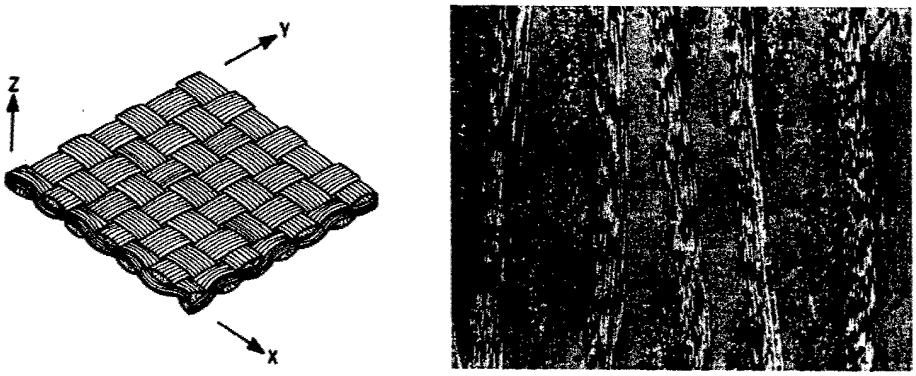

(a) (b)

Figure 4-1: Structure of 2D woven GRP. (a) Fiber fabric, (b) micrograph of the lay-up structure

From both the past work (Chandra et al, 2002) and the analytical solution in our latest paper, it is easily seen that the origin of the observed structure of the stress waves can be attributed to material heterogeneity at the interfaces. The level of heterogeneity of a layered system depends mainly on impedance mismatch between A and B, impedance mismatch between A and C, characteristics of geometry arrangement (such as total target thickness, thickness ratio between two component materials, number of layers, stacking sequence). Here we present three major factors that define material heterogeneity in layered systems: impedance mismatch, number of layers, and the thickness ratio.

4.1.1. Impedance mismatch

In the previous work (X. Chen, Scotland 2002), we defined impedance mismatch factor I as

$$I = 1 - \frac{4Z_1Z_2}{(Z_1+Z_2)^2} \tag{4.1}$$

where Z_1 and Z_2 are impedance of A and B, respectively. Since the second term on the right represents the transmitted strength of waves after one unit cell, I represents the fraction of the incident stress that is not transmitted (reflected back) as the wave passes through a pair of A/B and B/A interfaces. Also, $I = 1$ represents infinite impedance mismatch and $I = 0$ leads to no mismatch. By rearranging the above equation, we can also get the following relation

$$I = \left(\frac{\rho_1 c_1 - \rho_2 c_2}{\rho_1 c_1 + \rho_2 c_2}\right)^2 = r^2 \tag{4.2}$$

where r is the reflection ratio at A/B or B/A interface.

As we know, the impedance ratio ($R = \frac{(\rho c)_{hard}}{(\rho c)_{soft}}$, i.e. the ratio of the impedance of the hard layer over that of the soft layer) is conventionally used to represent the level of impedance mismatch. From the definition (shown in the bracket), it is easily found that R is within the range of one and infinity theoretically. When $R = 1$, there is no impedance mismatch across the interface, and infinite R represents infinite impedance mismatch. The relation between I and R is given by

$$I = \left(\frac{R-1}{R+1}\right)^2 \tag{4.3}$$

The relation by Eq. (4.3) is plotted in Fig. 4-2. From this figure, it is clearly shown that the impedance ratio R has a one-to-one correspondence relationship with impedance mismatch I. The higher the impedance ratio R, the higher I it corresponds to. However, quantitatively the relation is highly nonlinear. When the impedance ratio changes from 1 to 20, the corresponding impedance mismatch varies from 0 to 0.82. But when the ratio

continues to change from 20 to 40, the impedance mismatch varies little by from 0.82 to 0.90.

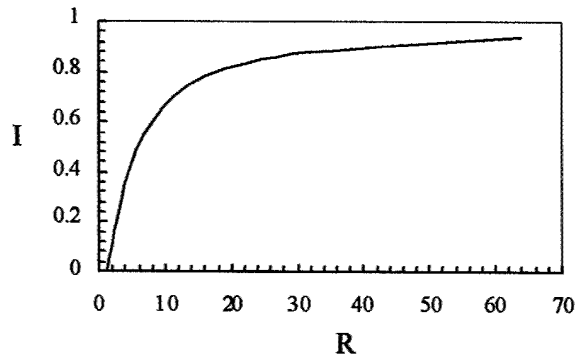

Figure 4-2: The relation between impedance mismatch I and impedance ratio R.

After defining impedance mismatch I, it is convenient to formulate the strength of the wave trains. The magnitude of transmitted wave after $2L$ interactions for a system comprising alternating L layers of A and L layers of B is given by

$$\sigma_{T2L} = (1 - I)^L \sigma_0 \tag{4.4}$$

where σ_{T2L} represents the strength of the head wave after propagating through L unit cells. The second wave train that arrives at $x = 2Ld$ is given by

$$\sigma^{(2)}_{T2L} = 2L \cdot I\,(1 - I)^L \sigma_0 \tag{4.5}$$

where $\sigma^{(2)}_{T2L}$ represents the strength of the second wave train. Also, if we stay at the impact plane, we also find that I is directly related to the strength of the incremental waves such as in Eq. (3.48). From these equations, I seems to be better than impedance ratio R for giving a clear quantitative indication of the level of impedance mismatch though they are equivalent qualitatively.

When designing layered structures to resist impact, it is important to choose the right material combinations from the usual engineering materials. Table 2 lists the impedance mismatch values of 153 material combinations from 18 materials, including organic materi-

als and metals. The materials are listed in such an order that the impedance R increases from left to right and from top to bottom. As a consequence, the impedance mismatch factors are distributed in the following order: I increases from top to bottom in the same column and decreases from left to right in the same row. Since the combination that has maximum impedance mismatch is Tungsten-Polyethylene with $I = 0.933$ and the corresponding impedance ratio is about 57.6, we can expect that the impedance ratio for combinations of engineering materials will generally fall within the range of 1 and 60. On the other hand, Epoxy-Nylon, 2024Al-S2Glass, Pb-Titanium, 304Steel-Cu, Nickel-Steel and Platinum-Molybdenum have almost the same impedances with $I \approx 0$. The scattering effect in these systems is expected to be very limited. In addition, it is clearly seen that the impedance mismatch values are randomly distributed between 0 and the maximum value 0.933.

4.1.2. Number of layers/Interface density

Let us define the interface density as the number of layers per unit width. If the thickness of the target is fixed, then the interface density is directly proportional to the number of layers and hence the two terms will be used interchangeably in our discussions.

It is known that the strength of the head wave will keep decreasing when traveling through more unit cells (or when L increases) with the relation shown in Eq. (4.4). This equation shows that for a system with fixed impedance mismatch, i.e., for a given material combination more interfaces can dampen the strength of the head wave. The different laminar acoustic dampers and anti-meteorite shields are made based on the amplitude decay of the head wave (Riney 1970). When based on dampening of the head strength, it is preferred that the impedance mismatch of the selected material combination be as high as possible. However, as will be shown later, more interfaces will not necessarily result in more attenuation of the peak stress due to the arrival of more wave trains after the head wave. These secondary wave trains (wave trains that follow the head wave) can play an important role by strengthening the wave trains when a location of interest is far from the impact surface (L is large). This is due to the fact that more interfaces results in more number of waves in successive wave trains, as shown in Eq. (4.5). In this equation, it can be seen that the impedance mismatch I arises as a base, while the number of layers L appears both as an exponent and as the

coefficient. Thus the quantitative effects of the two factors are quite different.

Fig. 4-4 shows the normalized strength of the first two wave trains and the corresponding cumulative stress up to the 2nd wave train as a function of impedance mismatch at a point downstream of L unit cells. It can be seen that the head wave decreases drastically as impedance mismatch increases. When the impedance mismatch is as high as about 0.5, the strength of the head wave is negligibly low. However, as Eq. (4.5) shows, the number of waves in the second wave train is proportional to the number of layers. The overall strength of the second wave train increases with impedance mismatch when I is very low, then it reaches a peak when I is about 0.11. It can be seen that the strength of the cumulative stress up to the second wave train is larger than 1 for small I. It should be noted that the stress overshooting can occur for systems with higher impedance mismatch when cumulative stress for more wave trains are considered since more steps are needed to reach the peak stress value. The overshooting indicates that the laminates may not necessarily result in stress decay. This surely contradicts with the common sense that more interfaces will result in more amplitude decay of the stress. In addition, as shown in our previous paper, for a given systems (a given combination with fixed thickness ratio), the rise time become less due to the stronger secondary wave trains that arrived at a shorter time interval for systems with higher interface density.

It has been mentioned before that EOS should be considered for shock response. A general EOS in in the form

$$U_s = C_0 + S_1 u_p + S_2 u_p^2 + S_3 u_p^3 + ... \tag{4.6}$$

where S_1, S_2 and S_3 are empirical parameters. C_0 is the sound velocity in a given material under zero pressure. U_s is the sound velocity in the material with particle velocity u_p. In general, U_s increase with increase of u_p. As a result, the secondary wave trains can overtake the head wave since they travel faster in a loaded material. Also, it was shown in the companion paper that this 'overtaking' effect was the key for the ratio of peak stress over mean stress to increase and the oscillation frequency to increase. So below is more detailed analysis about the condition when this phenomenon occurs. From EOS, the magnitude of the difference between C_{01} and U_{s1},and between C_{02} and U_{s2} depend on the pressure. For an

observer at a given location, the head wave propagates with original longitudinal velocity. So at a given location x, the arrival time of the head wave is given by Eq. (3.78). This time interval between the head wave and the second wave train is given by Eq. (3.80) and the second wave train arrives at location x at time t_{σ_1} and t_{σ_1} is given by Eq. (3.81). So it can be seen that the overtaking occurs when

$$t_{\sigma_1} \leq t_{\sigma_0} \tag{4.7}$$

It can be seen from Eq. (3.78) to (4.7) that when the interface density is high (so that Δt is negligible) and the distance of observation x is far enough

4.1.3. Thickness ratio

For a periodic bilaminated system, thickness ratio can be defined by $\frac{h_1}{h_2}$, and this quantity represents the volume fraction of the constituents in plate impact configuration. The effect of thickness ratio on the scattering process is to change the pattern of wave trains by altering the transit time and total internal reflection sequences of the wave trains in each of the layers. Thus for a given elapsed time the number of waves traveling within the layers A or B is also a function of the thickness ratio. For the general case, we need to assume that one of the layers, say A has a longer transit time (t_a) than that of layer B (t_b). There is no change in the arrival of the first wave train and it is independent of the thickness ratio. The second wave train includes waves that go through one reflection in first layer A only. The content of subsequent wave trains depends on the specific value of the ratio of $\frac{t_a}{t_b}$. Take for instance, the third wave train; if the ratio $\frac{t_a}{t_b} > 2$, then the third wave train comprises waves that go through two reflections in layer B. If however, $\frac{t_a}{t_b} < 2$, the third wave train comprises of waves that go through one reflection in layer A. Since the sequence of wave train is different, the observed slope and the oscillations are also different. It can be seen that the absolute value of $\frac{t_a}{t_b}$ indicates the wave train pattern more directly than $\frac{h_1}{h_2}$. Fig. 4-5 shows the numerical simulation of the effect of thickness ratio on the stress history downstream of 4 unit cells of Al-Cu system (configuration is shown in Fig. 4-5(a)). In this figure, when $\frac{h_1}{h_2}$ is moderate, (i.e. the case of $\frac{h_1}{h_2} = 1.5$ and $\frac{h_1}{h_2} = 4$), the stress increase in three steps in the rise slope. The time intervals between the steps are obvious. On the contrary, when $\frac{h_1}{h_2}$ is very small or very

large (i.e. the case of $\frac{h_1}{h_2} = 0.11$ or $\frac{h_1}{h_2} = 9$), the stress wave profiles show smooth rise part. In this case, the shape of the stress profile in the rise part and duration part is very similar to the case of Barker's experiment (shown in row 2, Table 3-1), where the volume fraction of one constituent is very small with $\frac{h_1}{h_2} = 0.05$.

If $\frac{h_1}{h_2}$ is very small, the second wave train, the third, the fourth... arrive at a given location through reflections only in layer A. However, if $\frac{h_1}{h_2}$ is very large, then these wave trains go through reflections in layer B only. For both cases, these wave trains are positive. On the other hand, since the time intervals between these wave trains are very small. As a result, the rising slope is sharp and the slope gradually decrease till a flat portion is reached. Evidently, we can see that the sharp rising slope is not due to small viscosity of the laminates as indicated in Barker's model.

Barker proposed that when the thickness of the layers were randomized, the stress oscillations will largely be removed. This phenomenon can be explained by the disturbance of the wave trains. When the structure is completely randomized, the wave trains includes both tensile and compressive waves. Besides, the magnitude and the arrival times of these waves are totally randomized. In other words, the wave pattern is randomized. As a consequence, stress oscillations are no longer periodic or significant.

4.2. Numerical analysis of elastic-plastic response of layered systems

Figure ?? shows one example of wave attenuation generated by interfaces. In this resin/glass system (A is resin and B stands for glass, the thickness ratio is 0.64/0.36), resin was modeled as elastic plastic and glass was modeled as elastic. Figure ?? (a), (b) and (c) are stress profiles at x=2.5, x=5, x=10 and x=15 respectively. It is noted that x=15 is equivalent to point D in Figure ??. Both spatial dispersion and wave attenuation can be observed in this case, very similar to experimental wave profiles shown in Figure ??. One important reason for phenomena generated in the simulation is the impedance mismatch at last interface glass/resin, since glass has larger impedance than resin, the compressive waves will keep being reflected as tensile waves back to the layers on the left and hence release the compressive

stress in those layers and result in shorter duration and lower peak stress value; at the same time, the peak stress in the last layer is also reduced. It is obvious that this idea is very useful to design integral armor.

This simulation result contains important information: wave attenuation can be also caused by scattering knowing that viscoelasticity is one possible reason. Also,when we relate this simulation result with wave profiles observed in real composites, interface effect may contribute uniquely to the wave profiles of composite by causing wave dispersion and slowing the rising slope. However, even when layered configuration will be used to model the layered composites, the last big monolithic layer does not exist, this indicates that there are some other sources for the consecutive releasing waves. Progressive damage evolution seems to be extremely possible. First, it is known that, delamination and degradation of material properties will initiate and starts to grow under high velocity impact. Once damage happens, the releasing waves will be sent out in both directions from the damaged zone. In this case, releasing waves from left to right will be the overall dominant releasing effect. At high pressure, considerable damage occurs and this will sending strong releasing waves to significantly reduce the total releasing time which is not the case in Figure ??.

Effect of yield stress

In order to know the effect of yield stress in layered geometry, the effect is simulated in monolithic material first. Figure ?? shows the result of Al (6.5mm) impacting resin (32mm) with impact velocity 273m/s. Each graph shows stress profiles at two positions for comparison: x=2.0mm and x=14.0mm in the target plate. For a fixed impact velocity, the yield stress of resin is varied from the normal value to a value when the material starts to behavior as elastic.

For the rising part, the sharp elastic wave front increases stress magnitude with the increase of yield stress, it is followed by a curved elastic-plastic transition part and then a sharp plastic part till the peak stress; it can be seen from Figure ?? (c) that there is an intermediate stage when the transition part becomes significant and the plastic part disappears. In addition, when then yield stress is high enough, the rising part tends to be only elastic wave front as can be seen in Figure ?? (d). For the purpose of comparison, Fig. 4-8 shows the response of a target plate made up of pure resin. We can clearly see that

both the elastic front and the pulse duration part are vertical, which are different from the ramped rising part and the oscillation part in Fig. ??.

4.3. Structure of the stress wave profiles of periodic layered structures

It has been shown in Fig. 3-9 that a typical stress profile in a periodic layered heterogeneous system includes a finite rise portion, an oscillatory portion in the steady state and then the pull-back signal. This section will examine the rise characteristics and the pulse duration part based on the analytical solution developed in last chapter.

4.3.1. Rise characteristics

Rise time

Fig. 4-9 shows the whole normalized stress wave profiles at a fixed location x=10mm (i.e. $\frac{\sigma(10,t)}{\sigma_{mean}}$) for PMMA-PC with impedance mismatch I=0.03, PMMA-Al with I=0.507 and PMMA-Cu with I=0.743. PMMA is the flyer plate in Fig. 4-9(a) and Al is the flyer plate in Fig. 4-9(b). The thickness ratio is also fixed with $\frac{h_1}{h_2} = \frac{0.26mm}{0.36mm}$. If we define the rise time as the time difference between the time of arrival of the head wave and the time when the first peak stress value is reached, it can be seen from Fig. 4-9 that the rise time is largely determined by impedance mismatch. The system with higher impedance mismatch has longer rise time. In addition, the rise time seems to be independent of the choice of the flyer plate and the impact velocity for elastic response. However, the rise time will significantly reduce in the shock response of the layered structure, which has been verified in experiments. It should be noted that this statement is only valid for elastic case. It can also be seen from Fig. 4-9 that rise time is close to the period of oscillations (without proof), discussion about the effects of heterogeneous factor on the oscillation frequency can be seen in the next subsection.

First peak

In general, the first peak of the stress wave profiles (such as point R_1 in Fig. 3-9) can be considered as the end of the rise portion. At the same time, it is found that this first peak is usually the highest peak in the pulse duration segment. When the peak stress is close

to the averaged steady state value, Barker pointed out that the peak stress is not critical. However, for general cases, the peak stress can be much higher than the steady state stress. Since the peak stress is often more suitable than the mean stress for evaluating the material response, such as damage initiation, it is necessary to obtain the peak stress rather than just the averaged stress based on homogenization. It has been recognized by our work that the peak stress is a consequence of wave scattering and R_1 is a point where the strength of the coming wave train is compressive. For elastic analysis, as is shown in chapter 3, the mean stress σ_{mean} exists and the first peak stress will be close to $1.274\sigma_{mean}$ based on the features of the solution shown in Eq. (3.68), because the Airy function for any systems has fixed maximum and minimum values of oscillations. As discussed in the previous paper, the ratio of 1.274 is valid at a moderate distance in a system with large impedance mismatch between A and B. For this type of system, the first peak stress can be approximated as

$$\sigma_{peak} \approx 1.274\sigma_{mean} = 1.274\frac{\rho_3 c_3 \widetilde{\rho}_0 c_0 v_0}{\rho_3 c_3 + \widetilde{\rho}_0 c_0} \tag{4.8}$$

Consequently, the linear relationship between σ_{peak} and σ_{mean} ensures that the effects of factors on the peak is the same as that on the mean stress. So it is convenient as well as necessary to review the effects of heterogeneity factors on mean stress σ_{mean}, which have been presented in the last paper. The effect of stacking sequence: from Fig.4-9 and from Eq. (3.62), it can be seen that stacking sequence can in general determine whether the value $\frac{\sigma_{mean}}{\sigma_0}$ is larger or smaller than one: when $\frac{\rho_1 c_1}{\rho_2 c_2} < 1$, $\widetilde{\rho}_0 c_0 > \rho_1 c_1$. Otherwise, $\frac{\sigma_{mean}}{\sigma_0} > 1$. The effect of flyer plate: the comparison between Fig. 4-9(a) and 4-9(b) shows that harder flyer plate results in higher $\frac{\sigma_{mean}}{\sigma_0}$ (when A is softer than B, otherwise, $\frac{\sigma_{mean}}{\sigma_0}$ is smaller). In other words, the mean stress deviate more from 1. The effect of impedance mismatch is obvious: When the flyer plate and the thickness ratio is fixed, the system with higher impedance mismatch will result in higher mean stress. The effect of volume fraction/thickness ratio: the more the harder material, the higher the normalized mean stress. This can be understood by looking at the expressions of effective density $\widetilde{\rho}_0$ (Eq. (3.58)) and effective velocity c_0 (Eq. (??)). With the increase of the thickness ratio of the hard layers, $\widetilde{\rho}_0$ monotonically increase. Though c_0 can decrease a little bit, since the minimum value and its neighbor appear in the region when the volume fraction of the hard layer is very large. Therefore, the overall

effective impedance $\widetilde{\rho}_0 c_0$ still increase when increasing the volume fraction of the hard layers. The effect of interface density on the stress wave profiles can also be understood from Eq. (3.58) and (3.35). Both $\widetilde{\rho}_0$ and c_0 are independent of interface density, so the mean stress level in a given bilaminates is independent of interface density. As will be shown later,this is only true for low velocity impact. If the mean stress is considered as the quasi equilibrium state of the system since this mean stress is also independent of propagation distance, this equilibrium state is achieved by the reflections of wave both in the target and at the impact surface. Combining the effect of impedance mismatch of the target and the flyer plate, it can be postulated that the ratio depends on the reflected energy in the layered system because head wave, which go through pure transmissions, does not contribute to the increase of mean stress.

The above quantitative analysis about mean stress is valid for elastic response of the materials. It should be noted that practically there is strictly no mean stress value in shock response which can be clearly evidenced in experiments. The stress tends to oscillation about decreasing values, or the mean stress "decreases" with time (see experiments by Oved and Zhuang). This behavior can be due to some time dependent dissipation mechanisms and this needs further investigation. However, it is noticed from the experimental data that the mean stress only decrease slightly. Besides, the second, the third peak and more are lower than the first peak. Hence we ignore this phenomenon for the time being and define the initial mean stress of the first peak as the mean stress for the whole wave profile. On the other hand, equation of state was shown to be necessary and even critical for shock response. When material is under shock, the density and wave velocity of each constituent are much higher than original values. Also, the thickness of each layer is smaller than the original value. As a result, the effective shock velocity (Eq. (3.75) and the mean stress (Eq. (3.76) are higher than elastic prediction. In addition, the second wave train catches up with the head wave as long as the thickness of the first layer is small and the location of interest is far enough. When the overtaking happens, the ratio of the first peak stress over mean stress can be much higher than 1.274, which has been validated in previous paper by matching a couple of experiments (Zhuang, 2002).

However, for systems with very little impedance mismatch, only negligible oscillations are generated and most energy is contained in the head wave at moderate distance, so Eq.

(4.8) is not good for such systems either and we can assume that $\sigma_{peak} \approx \sigma_{mean}$.

For the purpose of illustration, let us examine the rise characteristics seen in the experimental data by Clements (1997) (solid curve in Fig. 4-10(a)) with the configuration shown in Table 1, row 5. The data represents the particle velocity history of an epoxy and epoxy-graphite mixture layered system subjected to a plate impact test. As it happens the mismatch in the acoustic of these two material systems is very small with I very close to 0, similar to that of a homogeneous material. As a result, rise part is steep and the oscillations in the pulse duration period are minor. The solid curve in Fig. 4-10(b) was the experimental data by Oved (Configuration shown in Table 3-1, row 3). The impedance mismatch for Copper and PMMA is 0.743 and this high mismatch resulted in low rising slope. It should be noted that the dashed lines in two figures are the numerical results for both experiments modeled by us using elastic analysis with EOS considered. In both cases, the rising slopes are very well matched. This verified the idea that solution in section 2 is good enough for predicting the fundamental characteristics of wave profiles.

4.3.2. Oscillations

Amplitude of oscillations

From the Eq. (3.68), it is also clear that the peaks always decay in the same manner in the pulse duration: the first peak is about 1.274 and the first valley is 0.81, the second peak is about 1.152.... In the shock response, it is shown in section 4.1 that the mean stress decays. So far there is no analytical solution is available for evaluating this behavior, so amplitude of each individual oscillation is beyond quantitative understanding. Qualitatively, the observation from past experiments as shown in table 3-1 appears to suggest that the amplitudes of oscillations generally decay slower than the 1.274, 1.152 pattern. Again, this is not true for systems with negligible impedance mismatch such as Epoxy/Epoxy-graphite in Fig. 4-10(a). In addition, when the impact response is in elastic-plastic region, the two-wave-structure seems to reducing the amplitudes, which is also mentioned in Kanel's study. Without doubt, viscous behavior is another source to reduce the amplitude of oscillations, as shown in Barker's work. However, for general material systems Barker's prediction about the disappearance of oscillations under strong shock was invalidated both by experiments

(Oved, Zhuang) and by our analytical analysis.

Period of oscillations

It is found that the rise time is roughly proportional to the oscillation period, so the trend of period of oscillations that is discussed below will be applicable for the trend of rise time. Fig. 4-10 show that the period of the oscillations vary from system to system and system with higher impedance mismatch will result in longer rise time and low oscillation frequency. It can be seen from Eq. (3.46) that B is the only factor that determines the nondimensional oscillation frequency. In Eq. (3.46), the first term can be thought of as time difference between t and the characteristic time τ_{c_0} ($\tau_{c_0} = \frac{x}{c_0}$). Therefore, this term cannot be used to distinguish the rise time of oscillation frequency of oscillation. In the second term of Eq. (3.46), $h'''(0)$ is a fixed quantity for a given material system. So $\frac{2}{h'''(0)}$, which is in frequency dimension, is the factor that can characterize the oscillation behavior. The higher $\frac{2}{h'''(0)}$ will represent higher frequency, so it is termed in this paper as the frequency factor and the effects of impedance mismatch, interface density and thickness ratio due to Eq. (3.43) in a few systems (Volume fraction of PMMA is used as the variable) are plotted in Fig. 4-11. It can be seen in the figure that the effect of thickness ratio is not significant on the frequency of oscillations whenever the volume fraction of either material is not negligibly low. In other words, two extreme systems with almost all PMMA or nearly no PMMA will both result in high oscillation frequency and a quasi-homogeneous material behavior is expected. The much more important factor that affects the oscillation frequency is impedance mismatch (between A and B): Low impedance mismatch, such as PMMA-PC, will result in high frequency factor and short rise time, as shown in Fig. 4-9. With the increase of the impedance mismatch, the frequency becomes lower. Also, the effect of interface density can be as critical as impedance mismatch for oscillation frequency: With the increase of interface density, the oscillation frequency gets higher. With this, we can postulate that a laminates with extremely high interface density will also acts like a homogeneous mixture.

4.4. Velocity c_0 and Arrival time

Zhuang's experiments and numerical solutions showed the 'abnormal' phenomenon that the shock velocities of the PC(polycarbonate)-Glass and PC-SS systems were even lower than

that of PC. This indicates that

$$c_0 < c_1 \text{ and } c_0 < c_2 \tag{4.9}$$

the arrival time of the wave at a location in the laminates can be later than either components. When arrival time of stress wave is considered, the averaged longitudinal velocity is usually immediately examined

$$c_L = \frac{d}{\frac{h_1}{c_1} + \frac{h_2}{c_2}} \tag{4.10}$$

c_L' represents the wave front velocity which is given by the weighted averaged velocity. Eq. (4.10), can explain the phenomenon of the increase of the velocity c_L with the increase of the hard layer. It also predicts that the velocity of the layered media will without exception falls in between two components. On the other hand, for systems with big impedance mismatch, the wave front quickly dies out. Since velocity c_0 will determines the arrival time of the main part of the stress wave at late time, c_0 is the critical factor for the arrival time of a given systems. The actual arrival time is slightly earlier than this value. From equation 3.35, c_0 is always slower than for a layered medium when $\rho_1 c_1 \neq \rho_2 c_2$. Obviously, when $\rho_1 c_1 \approx \rho_2 c_2$, we will get $c_0 \approx c_L$. Fig. 4-12 is the velocity plot of three systems with PMMA-PC, PMMA-Al and PMMA-Cu. The longitudinal velocity of PC, PMMA, Al and Cu are 1.85, 2.66, 6.473 and 4.74, respectively according to Eq. (3.35). Very interesting trend is observed. For systems with very close impedance such as PMMA-PC, the velocity of the corresponding laminates stay in between of this two materials, with an almost linear relationship. However, the concave shaped curves are generated for PMMA-Cu and PMMA-Al. When the volume fraction of PMMA is zero, the velocities of PMMA-Cu and PMMA-Al equal that of Cu and Al respectively. With the increase of the volume fraction of PMMA, c_0 starts to decrease and become smaller than either of the materials at a certain value(At A for PMMA-Al and point B for PMMA-Cu). It is obvious from the plot that the volume fraction of PMMA at B is much smaller than that at A. This effect can be directly seen from the equation 3.35, the third term of the denominator is proportional to the impedance mismatch. The higher this term, the slower the c_0 will be. After c_0 reaches the minimum value, then it starts to

increase again and finally reaches the velocity of PMMA. The minimum c_0 also corresponds to smaller volume fraction of the softer materials (In this case, PMMA) for systems with higher impedance mismatch.

It should also be noted that c0 corresponds to the propagation speed of the main disturbance, so it does not corresponds to the stress at the arrival of the wave profiles.

Table 2: Impedance mismatch of various combinations of solids

	PE	PC	Epoxy	Nylon	PMMA	Mg	Fused silica	S2 Glass	2024 Al	Lead	Ti	Silver	Cu	Steel	Ni	Mo	Pt	Tungsten
Polyethelene																		
Polycarbonate	0.013																	
Epoxy	0.033	0.005																
Nylon	0.062	0.019	0.005															
PMMA	0.082	0.031	0.012	0.002														
Magnesium	0.494	0.409	0.356	0.303	0.272													
Fused silica	0.570	0.491	0.440	0.388	0.357	0.012												
S2 Glass	0.642	0.572	0.524	0.476	0.447	0.051	0.014											
2024 Al	0.680	0.614	0.571	0.525	0.496	0.084	0.034	0.005										
Lead	0.752	0.698	0.661	0.622	0.597	0.177	0.106	0.047	0.022									
Titanium	0.762	0.710	0.674	0.636	0.612	0.194	0.120	0.057	0.030	≈ 0								
Silver	0.832	0.793	0.766	0.737	0.718	0.341	0.256	0.170	0.125	0.046	0.037							
Copper	0.848	0.812	0.787	0.760	0.743	0.382	0.297	0.208	0.160	0.071	0.060	0.003						
304 Steel	0.857	0.824	0.800	0.774	0.758	0.409	0.324	0.234	0.184	0.089	0.077	0.008	0.001					
Nickel	0.868	0.837	0.814	0.790	0.775	0.439	0.355	0.264	0.214	0.112	0.099	0.017	0.006	0.002				
Molybdenum	0.895	0.869	0.851	0.831	0.818	0.525	0.446	0.356	0.303	0.191	0.174	0.060	0.037	0.025	0.014			
Platinum	0.904	0.881	0.865	0.846	0.834	0.560	0.484	0.396	0.343	0.228	0.221	0.086	0.059	0.044	0.029	0.003		
Tungsten	0.933	0.916	0.904	0.891	0.882	0.671	0.607	0.530	0.482	0.369	0.351	0.203	0.166	0.142	0.117	0.054	0.033	0

Figure 4-3: Impedance mismatch of selected material combinations

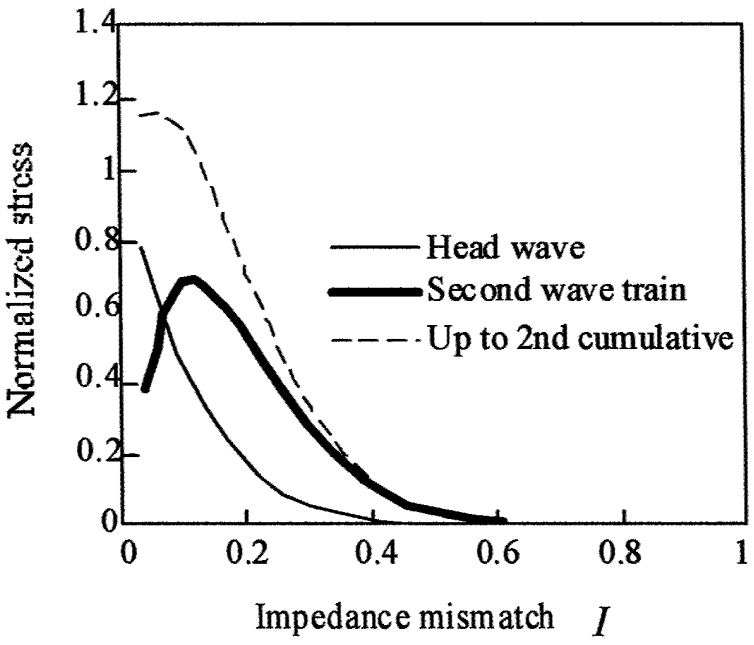

Figure 4-4: The strength of the head wave and the second wave train as a function of I with 2L=16.

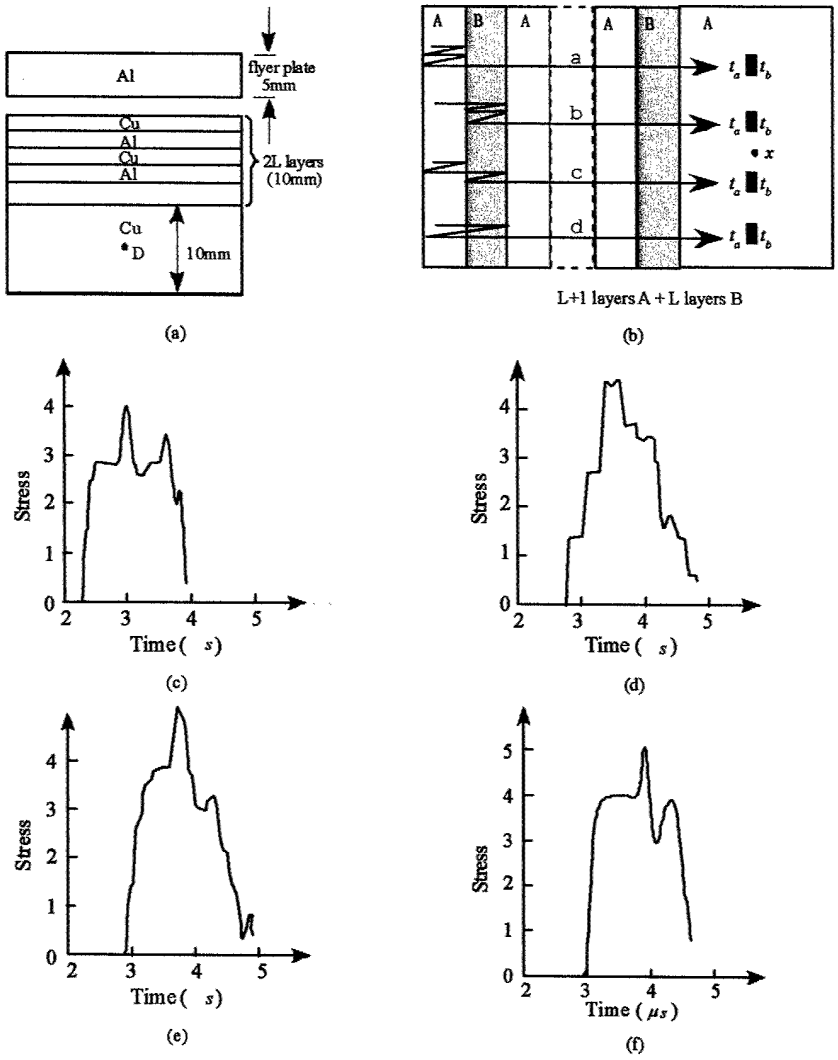

Figure 4-5: The effect of thickness ratio on the rise characteristics of Al-Cu structures. (a) Configuration, (b) The third wave trains of different ratio, (c) (d) , (e) , and (f)

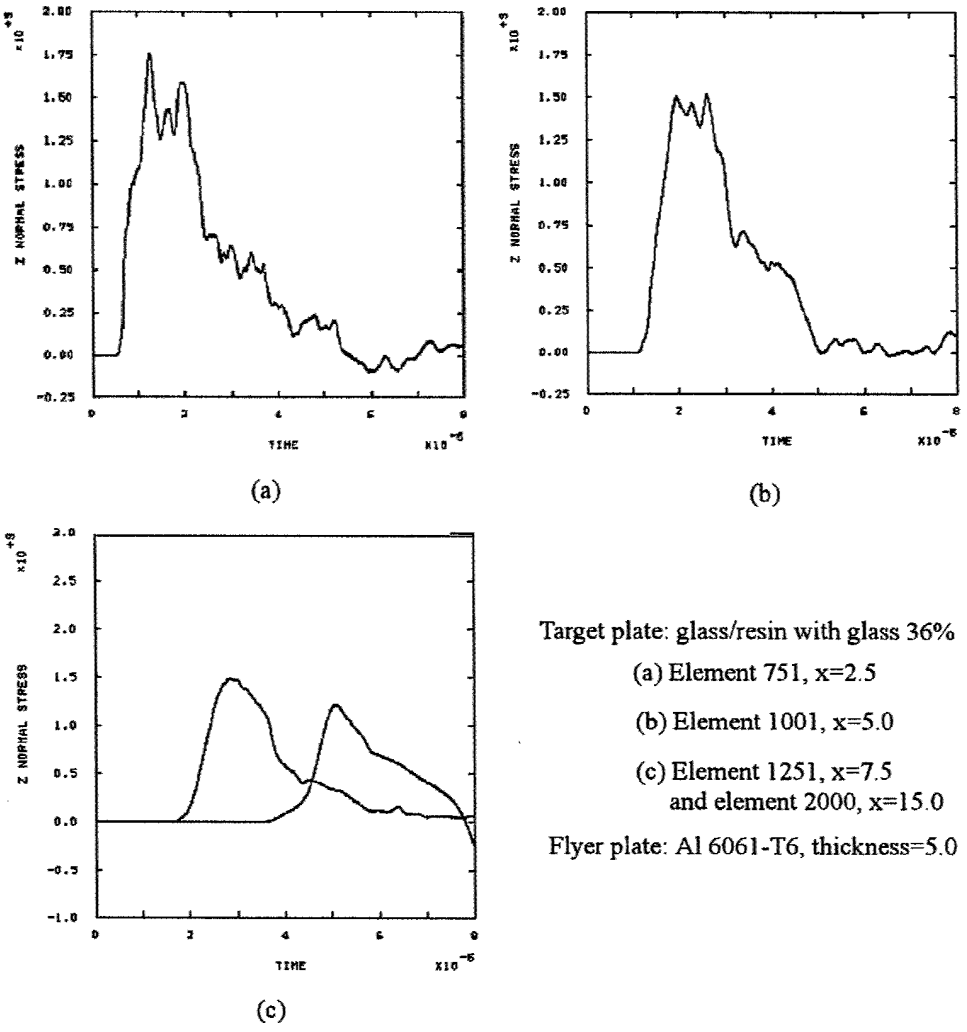

Figure 4-6: The effect of interface on spatial wave dispersion and attenuation in alternating glass/resin system.

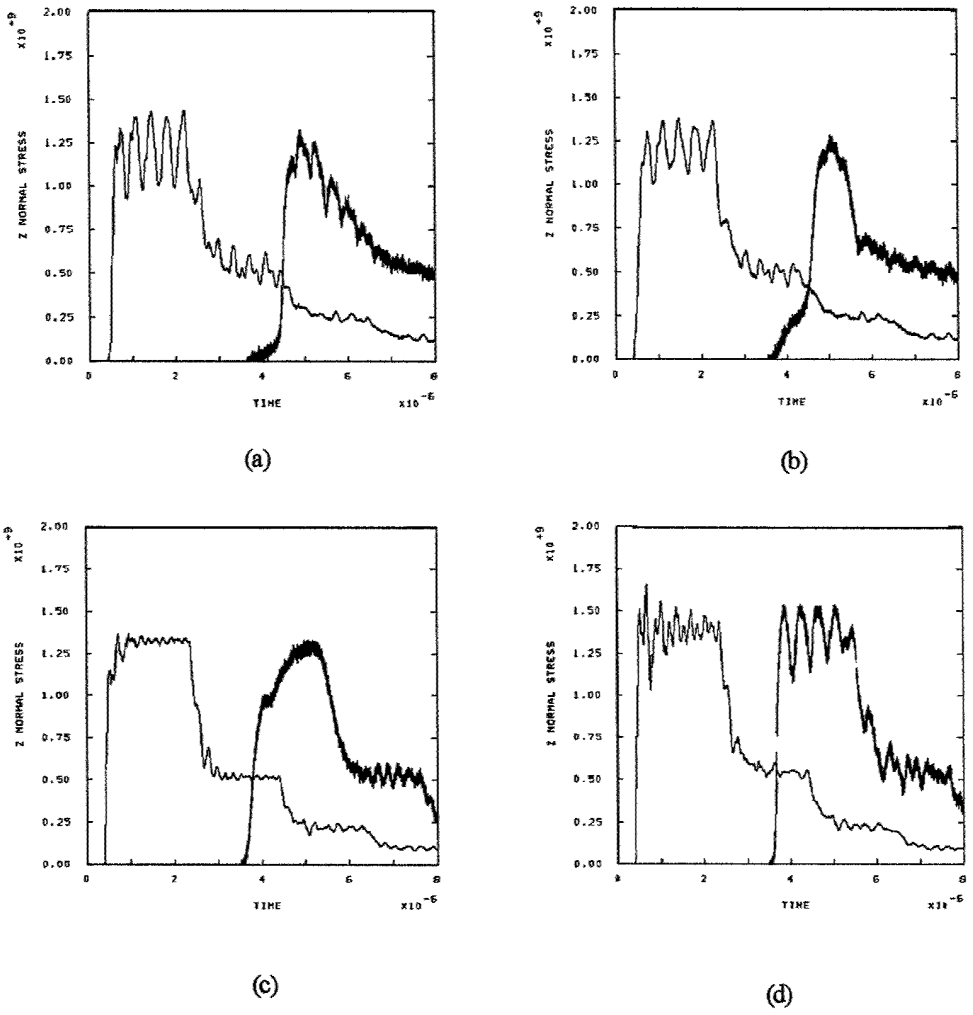

Figure 4-7: The effect of yield stress/strength on wave profile for fixed Young's modulus, failure strain and strain hardenging coefficient. Impacting velocity 273m/s. (a)1.0×10^7 Pa, (b) 1.0×10^8 Pa, (c) 5.0×10^8 Pa, (d) 1.0×10^9 Pa.

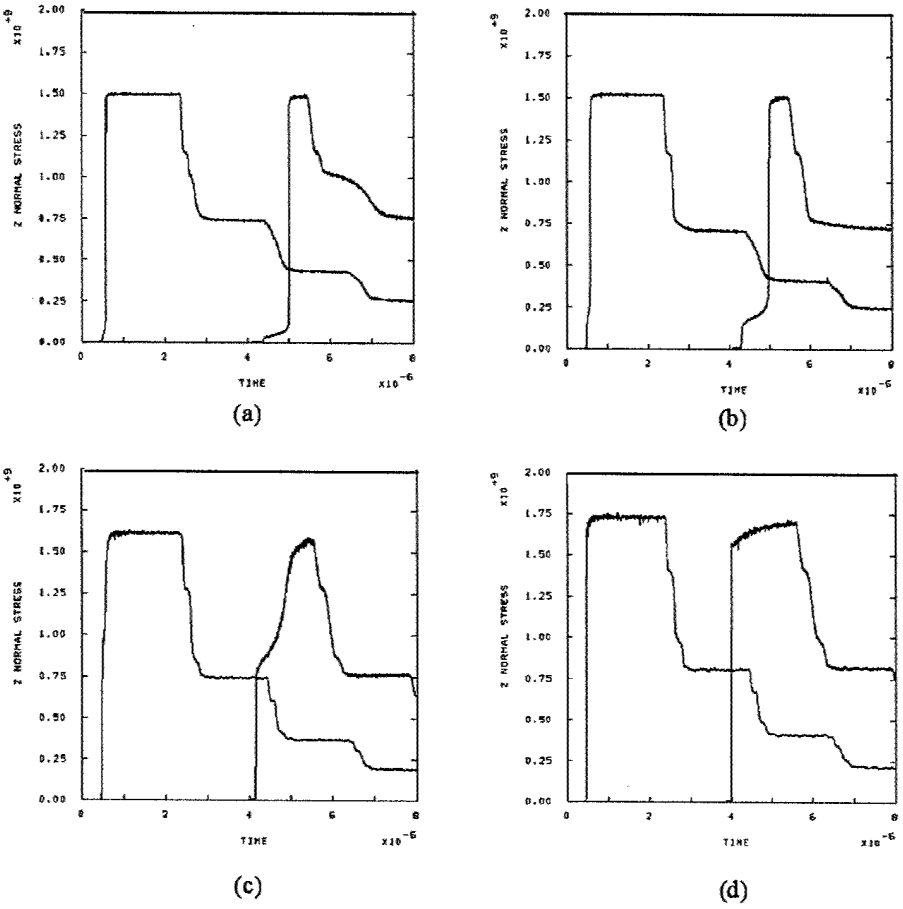

Figure 4-8: The elastic-plastic response of homogeneous resin.

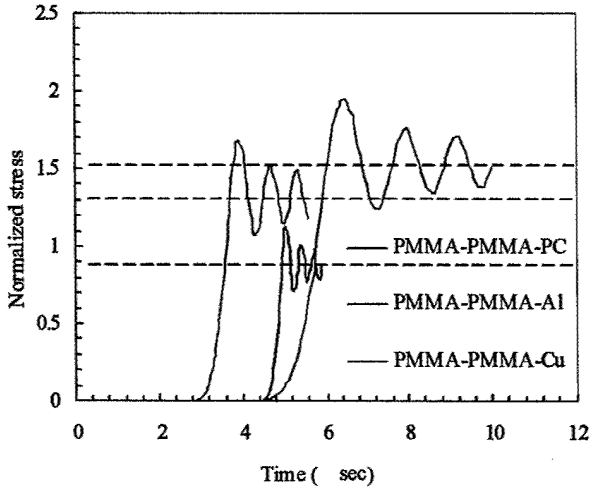

(a)

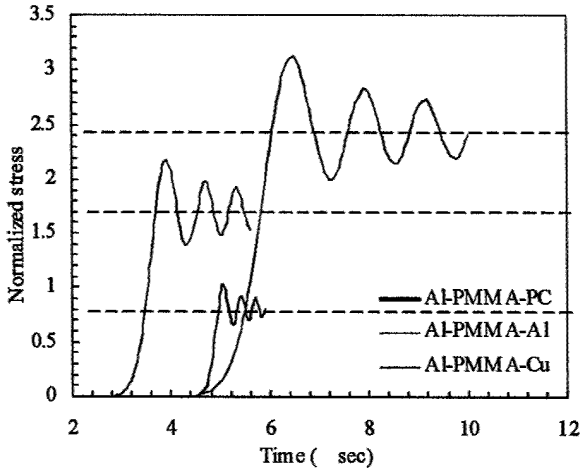

(b)

Figure 4-9: The analytical solutions to the normalized stress history (with respect to in PMMA-PC, PMMA-Al and PMMA-Cu. (a) Flyer plate is PMMA and (b) Flyer plate is Al.

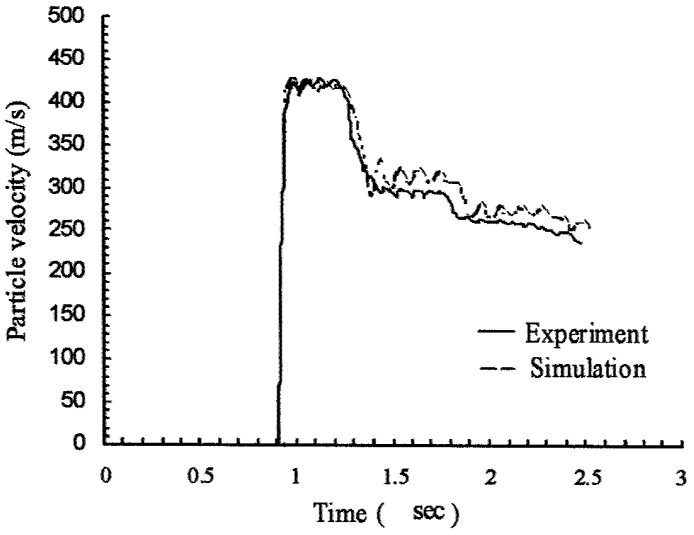

(a)

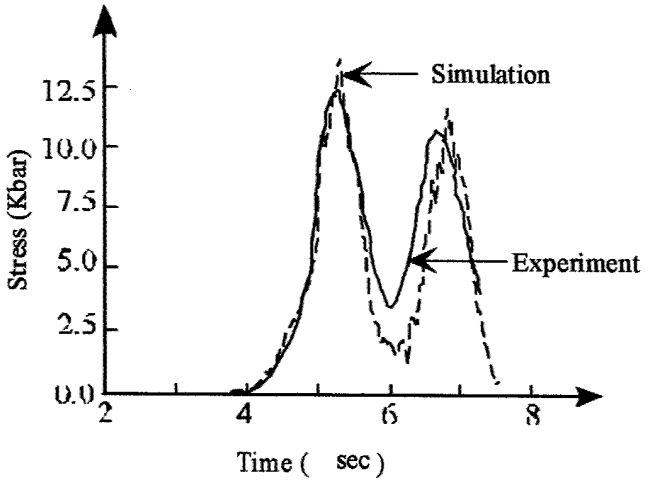

(b)

Figure 4-10: The shock responses of two material systems. (a) Epoxy/Epoxy-graphite by Clements et al, (b) Cu-PMMA by Oved et al.

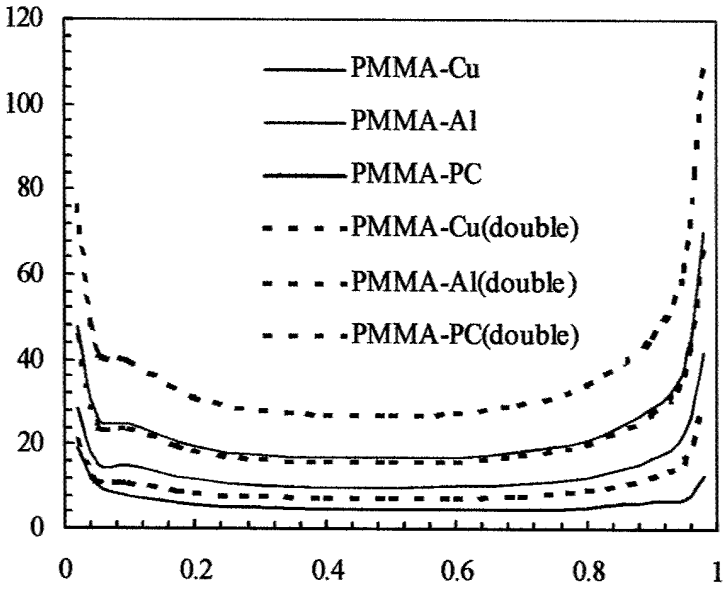

Figure 4-11: The frequency factors of different systems.

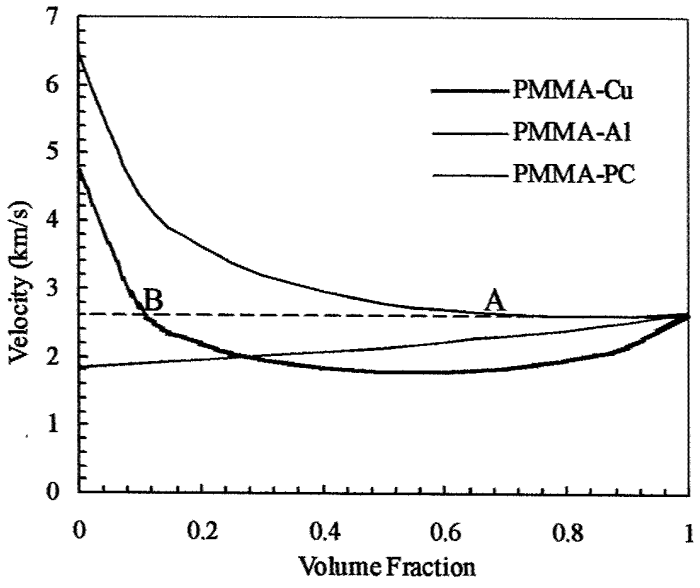

Figure 4-12: The effective velocity of different systems.

Chapter 5

Composites

Wave propagation in homogenous, isotropic media has been widely investigated. Now, more interest [5, 6] is focused on the wave propagation in anisotropic, heterogenous media such as composites. The mechanical behavior of composites have been extensively investigated using homogenization approaches. Micromechanics based analysis of composites has been conducted for constitutive modeling and failure analysis. So in this chapter a brief introduction of the constitutive relation of the orthotropic composites is given. The effective sound velocity for these type of materials has been developed for the state of uniaxial strain. One numerical example is given for the purpose of validation. Then a review of failure modes of composites is provided and this is followed by a numerical analysis of the damage evolution in homogeneous composites.

Since the built-in defect of the approaches by neglecting explicitly the interfaces, this approach showed much limitations in examing the impact behavior, where wave interactions can play critical roles in the response. As mentioned before, researchers have used periodically layered (planar planes) configuration to study the wave propagation for decades. However, the applicability of this planar model in place of complex engineering composites, such as woven composites, has not been carefully evaluated. It is necessary to determine the effective matrix/fiber fabric material properties for out-of-plane loading conditions. The current author proposed a preliminary 1D effective layered model for GRP, though more work is needed in this issue.

5.1. Constitutive Relation

For an orthotropic elastic solid (we assume the material is homogenous), the symmetric compliance matrix with nine independent is:

$$\begin{bmatrix} E_{11} \\ E_{22} \\ E_{33} \\ E_{23} \\ E_{31} \\ E_{12} \end{bmatrix} = \begin{bmatrix} \frac{1}{E_1} & -\frac{\nu_{21}}{E_2} & -\frac{\nu_{31}}{E_3} & 0 & 0 & 0 \\ -\frac{\nu_{12}}{E_1} & \frac{1}{E_2} & -\frac{\nu_{32}}{E_3} & 0 & 0 & 0 \\ -\frac{\nu_{13}}{E_1} & -\frac{\nu_{23}}{E_2} & \frac{1}{E_3} & 0 & 0 & 0 \\ 0 & 0 & 0 & \frac{1}{G_{23}} & 0 & 0 \\ 0 & 0 & 0 & 0 & \frac{1}{G_{31}} & 0 \\ 0 & 0 & 0 & 0 & 0 & \frac{1}{G_{12}} \end{bmatrix} \begin{bmatrix} T_{11} \\ T_{22} \\ T_{33} \\ T_{23} \\ T_{31} \\ T_{12} \end{bmatrix} \tag{5.1}$$

This can also be inverted to stiffness matrix:

$$\begin{bmatrix} T_{11} \\ T_{22} \\ T_{33} \\ T_{23} \\ T_{31} \\ T_{12} \end{bmatrix} = \begin{bmatrix} C_{11} & C_{12} & C_{13} & 0 & 0 & 0 \\ C_{21} & C_{22} & C_{23} & 0 & 0 & 0 \\ C_{31} & C_{32} & C_{33} & 0 & 0 & 0 \\ 0 & 0 & 0 & C_{44} & 0 & 0 \\ 0 & 0 & 0 & 0 & C_{55} & 0 \\ 0 & 0 & 0 & 0 & 0 & C_{66} \end{bmatrix} \begin{bmatrix} E_{11} \\ E_{22} \\ E_{33} \\ E_{23} \\ E_{31} \\ E_{12} \end{bmatrix} \tag{5.2}$$

In the case of plate impact, when the state of uniaxial strain is still valid, if wave propagates along E_{11}, the wave velocity by using equation of equilibrium is

$$C_L = \sqrt{\frac{(1 - v_{23}\nu_{32})E_1}{\rho V}} \tag{5.3}$$

where $V = [1 - v_{12}\nu_{21} - v_{23}v_{32} - v_{31}v_{13} - 2v_{21}v_{32}v_{13}]$

When the composite is transversely isotropic, there are 5 independent elastic constants. copper impacts an orthotropic elastic plate

When the target plate is orthotropic elastic rather than isotropic, the elastic wave velocity

is in more complicated form:

$$C_L = \sqrt{\frac{(1 - v_{13}^2 E_3/E_1)E_2}{\rho V}} \tag{5.4}$$

where $V = [1 - v_{12}\,(v_{12}E_2/E_1 + 2v_{23}v_{13}E_3/E_1) - v_{13}^2 E_3/E_1 - v_{23}^2 E_3/E_2]$

A copper plate impacting an fiber-reinforced composite plate (in transverse direction) is simulated using orthotropic elastic material model. The material is unidirectional CFRP t300/914. $E_1 = 139e9(Pa)$, $E_2 = E_3 = 9.4e9(Pa)$, Poison's ratio $v_{12} = v_{13} = 0.0209$ and $v_{23} = 0.33$. Since for this kind of materia v_{12} and v_{13} are very small, the higher order of them can be neglected. And also, the ratio of E_2/E_1 and E_3/E_1 is also very small, so in this case, $V \simeq [1 - v_{23}^2]$

Material properties of CFRP T300/914 [30] is shown in the following table:

Material properties of CFRP T300/914

Young's modulus in three directions	In fiber direction	E_1:	139 (Gpa)
	In normal direction	E_2:	9.4 (Gpa)
	In transverse direction	E_3:	9.4 (Gpa)
Poison's ratios		v_{12}:	0.0209
		v_{23}:	0.33
		v_{13}:	0.0209
Shear modulus		G_{12}:	4.5 (Gpa)
		G_{23}:	2.98 (Gpa)
		G_{13}:	4.5 (Gpa)
Tensile strength	In fiber direction	X_T:	2.07 (Gpa)
	In normal direction	Y_T:	74 (Mpa)
	In transverse direction	S_N:	74 (Mpa)
Compressive strength in transverse direction		Y_C:	237 (Mpa)
Bulk modulus of failed material		K_f:	2.0 (Gpa)
Shear strength		S_{12}:	64 (Mpa)
		S_{23}:	64 (Mpa)
		S_{13}:	86 (Mpa)
Mass density		ρ:	1.58 ($kg.m^5$)

Figure 5-1: Material properties of CFRP T300/914

Elastic wave speed under the state of uniaxial strain:

Figure 5-2: Copper impacting an elastic orthotropic plate

$$C_L = \sqrt{\frac{(1 - v_{13}^2 E_3/E_1)E_2}{\rho V}} \simeq \sqrt{\frac{E_2}{\rho\,(1 - v_{23}^2)}} = 2585m/s$$

Using the same method as before, we can get the stress within composite right after impact:

$$v = (300)\left(\tfrac{8.9\times4.56}{8.9\times4.56+1.58\times2.585}\right) = 272m/s$$

$$\sigma = \rho c v = (1.58e3)\,(2585)\,(272) = 11.1kbar$$

It needs to be noted that in the above wave speed is just for the elastic, uniaxial strain state and uncompressed material. Since after the material has been compressed, the density of the material after the wave front increases, the release wave tends to move faster than the original compressive wave speed.

The above is just for macroscopically homogeneous, elastic orthotropic composites. For any real composites, the wave scattering, dispersion due to fibers, voids or some particles in the matrix can significantly influence the whole deformation behavior and result in very complicated situation.

5.2. Modes of failure of composites

In the second section, literature on damage of composites (mainly under impact loading) was reviewed. Also, some preliminary simulation results on the damage of composites were shown and discussed. The goal of this section was to investigate the failure modes and damage evolution of material under impact loading rather than quasistatic loading. LS-DYNA3D is used to simulate different cases in plate impact.

A great variety of deformation modes can lead to failure of the composite. The operative failure mode depends, among other things, on loading conditions and the microstructure of a particular composite system. By microstructure we mean fiber diameter, fiber volume fraction, fiber distribution, and damage resulting from thermal stresses that may develop during fabrication.

A. Strain rate effect on failure of materials [31]

Generally, impacts are categorized into either low or high velocity (sometimes hypervelocity), there is no clear transition between categories. Very low-velocity impact can be treated as quasi-static, the upper limit of which can vary from one to tens of ms^{-1}depending on the target stiffness, material properties and the impactor's mass and stiffness. The dynamic structural response of the target is of utmost importance as the contact duration is long enough for the entire structure to respond to the impact and in consequence more energy is absorbed elastically.

Higher-velocity impact (much less than ballistic limit) response is dominated by stress wave propagation through the materials, in which the structure does not have time to respond., leading to very localized damage. Boundary condition effects can be ignored because the impact event is over before the stress waves have reached the edge of the structure.Low-velocity impact is characterized by delamination and matrix cracking.

Hyper-velocity impact and perforation of composite laminates are of interest for a wide rand of engineering applications. In this type of loading, the impact velocity exceeds the ballistic limit. (Ballistic limit is defined as the minimum impact velocity required by the projectile to completely perforate the target).Compared with low velocity impact, high velocity impact tends to induce a more localized form of target response, resulting in the dissipation of energy over a comparatively small region [32].

B. Different failure modes

1. *Matrix damage*

   Matrix damage is the first type of failure induced by transverse low-velocity impact,usually takes the form of matrix cracking but also debonding between fibre and matrix. Matrix cracks occur due to property mismatching between the fibre and matrix, and are usually oriented in planes parallel to the fibre direction in unidirectional layers. In an FRP, the polymeric matrix provides several key functions: it transfers the load to the fibres, protects the fibres from damaging themselves and aligns/stabilizes the fibres. The majority of structural applications employ epoxy resins as they meet the hot/wet compressive strength requirements. However, epoxy is brittle and has poor resistance to crack growth (i.e. delamination).

2. *Delamination*

   A delamination is a crack which runs in the resin-rich area between plies of different fibre orientation and not between lamina in the same ply group. Liu [33] explained that delamination was a result of the bending stiffness mismatch between adjacent layers, i.e., the different fibre orientations between adjacent layers. Delamination is an initiation and growth process. After initiation, the delamination can undergo stable growth. Eventually, unstable growth, interaction with in-plane failure modes, result in final fracture [34].O'Brien [35] proposed a prediction criterion by the strain energy release rate approach.

3. *Fiber failure*

   This damage mode generally occurs much later in the fracture process than matrix cracking and delamination. Fibre failure is a precursor to catastrophic penetration mode. Fibre failure occurs under the impactor due to locally high stresses and indentation effects (mainly governed by shear forces) and on the non-impacted face due to high bending stresses. Fibres are the main load-bearing constituent, providing the composite with the majority of its strength and stiffness. The most common fibres are glass, carbon and Kevlar. For resistance to low-velocity impact, the ability to store energy elastically in the fibres is the fundamental parameter [36].

Figure 5-3: Failure modes of composites

4. *Penetration*

   Penetration is a macroscopic mode of failure and occurs when the fibre failure reaches a critical extent, enabling the impactor to completely penetrate the materials. El-Habak tested a variety of glass fibre-reinforced plastic (GFRP) composites at penetration loads and conclude that the glass fiber treatment played a key role in determining the perforation load. Dorey [36] provided a very simplified analytical model of penetration to give the energy absorbed.

5.3. Simulating composite damage under impact using LS-DYNA3D

The composite failure material model of DYNA3D is based on Chang-Chang failure criteria. With the delamination criterion proposed by Brewer and Lagack. These criteria are formulated as below.

1. Fiber failure:

$$e_f^2 = \left(\frac{\sigma_{11}}{X_T}\right)^2 + \left(\frac{\sigma_{12}}{S_{12}}\right)^2 \geqslant 1 \tag{5.5}$$

2. Matrix cracking

In the case of $\sigma_{22} \geqslant 0$,

$$e_m^2 = \left(\frac{\sigma_{22}}{Y_T}\right)^2 + \left(\frac{\sigma_{12}}{S_{12}}\right)^2 \geqslant 1 \tag{5.6}$$

3. Matrix crushing

In case of $\sigma_{22} < 0$,

$$e_d^2 = \frac{1}{4}\left(\frac{-\sigma_{22}}{S_{12}}\right)^2 + \frac{Y_C^2\sigma_{22}}{4S_{12}^2} - \frac{\sigma_{22}}{Y_C} + \left(\frac{\sigma_{12}}{S_{12}}\right)^2 \geqslant 1 \tag{5.7}$$

4 Delamination

$$e_1^2 = \left(\frac{\sigma_{33}}{S_n}\right)^2 + \left(\frac{\sigma_{23}}{S_{23}}\right)^2 + \left(\frac{\sigma_{31}}{S_{31}}\right)^2 \geqslant 1 \tag{5.8}$$

Where:

σ_{11} - stress in the fibre direction;

σ_{22} - stress in the transverse direction;

σ_{33} - stress in the through-thickness direction;

σ_{12} - shear stress in the plane of fibre and transverse directions;

σ_{23} - shear stress in the plane transverse and through-thickness plane;

σ_{31} - shear stress in the plane of through-thickness and fibre directions;

X_T - tensile strength in the fibre direction;

Y_T - tensile strength in the transverse direction;

Y_C - tensile strength in the fibre direction;

S_{12} - shear strength in the fibre and transverse plane;

S_{23} - shear strength in the transverse and through-thickness plane;

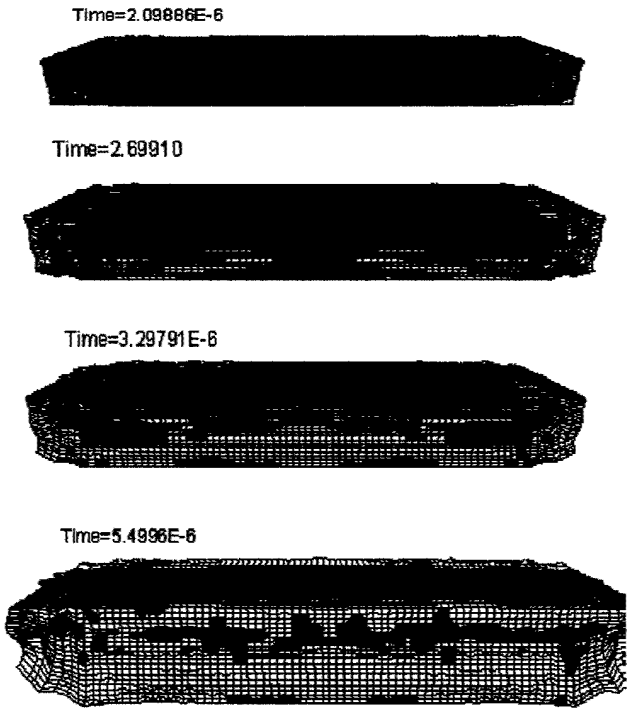

Figure 5-4: The failure evolution including fiber failure and matrix crack

Damage of composites by plate impact (modeling)

In this section, LS-DYNA3D was used to model four failure modes of composite under plate impact using Materials model 22 and the through thickness direction changed to Z according to the convention used in the failure criteria. The objective of simulating composite damage is to understand the redistribution of stress after damage happens and thus study the interaction between different failure modes.

Example: when X_T and Y_T are set to real values of the strengths of the given materials while setting all other values high enough to elastic region, then according to the failure criteria used, only two failure modes happen: fibre failure and matrix crack.(impacting velocity=600m/s)

The configuration is shown in Figure For the target plate, it is made up of two layers: the top layer is composite (with damage) and the bottom is copper (elastic).Adding another

Figure 5-5: Damage modes and the corresponding stresses update

copper is because of the need to get more information from the damaged composites.

The material model 22 is for a macroscopically homogenous orthotropic material. In this model, fiber properties,fiber volume fraction, and interface cohesion are not directly related to the input.

The current material failure criteria implemented in LS-DYNA3D suffers the following shortcomings: First of all, only plane stresses, such as σ_{11}, σ_{12}, σ_{22}, are considered in the criteria for fibre failure, matrix cracking and matrix crushing. Thus, in the cases when the out-of plane are significant, the damage prediction may not be satisfactory. Secondly, inter-laminar shear stresses caused by matrix cracking and fibre failure are very important causes of delamination in impact events [30]. Actually, these failure should act as stress raisers at the adjacent interface [37]. In LS-DYNA3D code, related stresses are reduced after failure (see table 5-1), so the local stresses close to the damage cannot be modelled realistically. Thus, their interaction between different failure modes are not properly modelled. Finally, the through-thickness compression stress is taken to have exactly the same effect as the through-thickness tension stress on delamination, which is obviously not satisfactory [30].

Therefore, it is necessary to modify the failure criteria and also some input of material properties (such as equation of state [38], fiber properties, some parameters for heterogeneity).

5.4. Modeling the engineering GRP as layered structures

A series of shock experiments were conducted on S2-glass reinforced polymeric matrix composites (PMC) and the shock wave profile history showed marked departure in the stress history response from that typically observed in metallic systems in a number of ways [1]. A schematic geometry of the experiment in Reference [1] is shown in Figure 5-6(a). The PMC laminates composed of S-2 glass woven roving in a polyester resin matrix with a resin content of 32 % by weight were subjected to plate impact tests with an initial velocity of 0.273 $mm/\mu sec$. The target comprised four layers with thickness of about 3mm, 3mm, 7mm and 20 mm; three PVDF gages were placed in between the layers to measure the stress history response. The stress response at each of those gages is shown in Figure 5-6(b). Gauge 1 in the figure corresponds to the interface between layers B and C (see Figure 5-6) while gauge 2 is the one between layers C and D, and gauge 3 that between D and E. In order to obtain a clear comparison of the three stress profiles, the starting points of the curves are overlapped as shown in Figure 3.

Apparent difference can be seen between these three stress profiles in the figure; the peak stress levels at gauges 1, 2 and 3 decrease with wave propagation, the rise time increases and pull back time decreases significantly as wave propagates. Also, the duration of the pulse as denoted by the resident time at the peak pressure reduces from 1 to 2 to 3. In addition, time of arrival of the release wave at gauges (when the peak pressure starts to decline) does not coincide with the rarefaction wave from the flyer plate. It is very important to relate the various underlying physics of the phenomenon to the dynamic behavior of the materials before such materials can be effectively used in future applications. An attempt in this direction was made in reference [1] to explain some of these features in terms of viscoelastic relaxation behavior of the materials. However in that work only attenuation levels could be matched but other important characteristics like the rise and pull back behavior as well as the release wave arrival times could not be explained.

In general, many computational simulations use homogenized properties of the composites while considering various material components. We believe that this approach may lead to erroneous results for modeling high velocity impact problems, since this approach neglects the

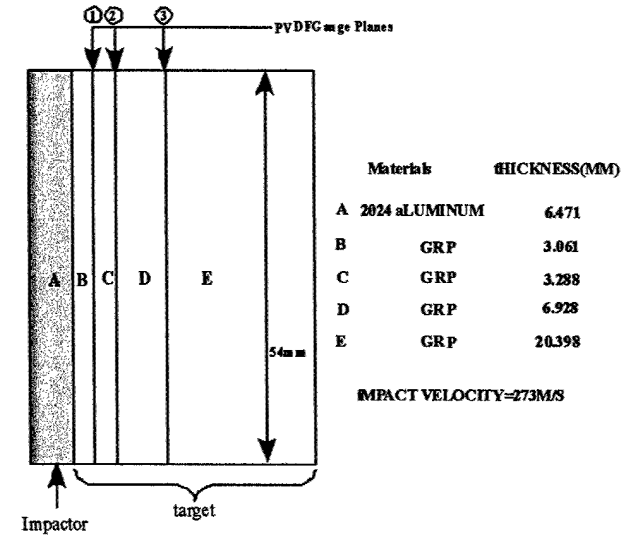

(a)

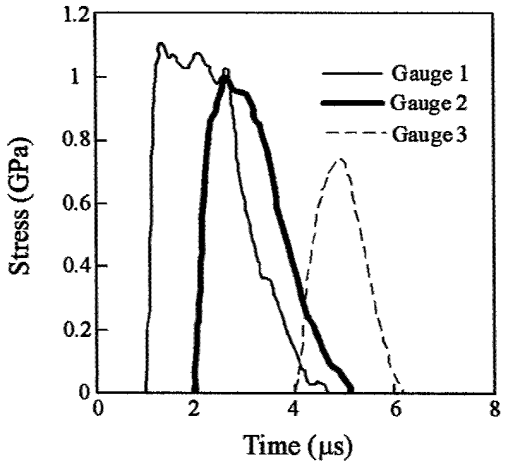

(b)

Figure 5-6: Experimental results of GRP subjected to plate impact [1].

presence of interfaces which are the root causes for scattering. When the loading rate is high enough such that the wavelength is comparable to the size of material heterogeneity, then the scattering process should be explicitly considered for obtaining valid results [16][7][8][39][40].

In order to study the effect of planar interfaces, as is the case in laminated composite systems, it is appropriate to simulate a layered configuration, and this approach is taken in this work. Then the problem becomes how to obtain the equivalent layered structure. For a general periodic system, it is necessary to determine the thickness, density, material properties for each constituent so that the macroscopic material properties are identical to the measured data that are available. From the microstructure, we propose an alternating resin/fiber fabric system. If we assume that the thickness of the resin layer is h_1, then h_2 can be obtained by

$$h_1 + h_2 = 0.68 \tag{5.9}$$

from the weight ratio of resin, we have

$$(h_1\rho_1 + \rho_2 h_2) * 0.32 = h_1\rho_1 \tag{5.10}$$

From the effective wave speed

$$c_0 = \frac{d}{\left\{\left(\frac{h_1}{c_1}\right)^2 + \left(\frac{h_2}{c_2}\right)^2 + \left(\frac{\rho_1 c_1}{\rho_2 c_2} + \frac{\rho_2 c_2}{\rho_1 c_1}\right)\frac{h_1 h_2}{c_1 c_2}\right\}^{\frac{1}{2}}} = c_L \tag{5.11}$$

where c_L is given by Eq. (5.4). It should be noted that the measured velocity can vary due to the method used, so the experimental data is not used.

For resin, c_1 is straightforward with E_1,ρ_1 and υ_1 known. It should be noted that fiber fabric is assumed to be homogeneous, so we need to determine E_2, and υ_2.

$$\upsilon_2 = \upsilon_1\alpha_1 + \upsilon_2\left(1 - \alpha_1\right) \tag{5.12}$$

where α is the volume fraction of resin in the fiber fabric and can be obtained by relating to

ρ_2

$$\rho_2 (1 - \alpha_1) + \alpha_1 \rho_1 = \rho_2 \tag{5.13}$$

Young's modulus of fiber fabric

$$\frac{1}{E_3} = \frac{h_1/(h_1 + h_2)}{E_1} + \frac{h_2/(h_1 + h_2)}{E_2} \tag{5.14}$$

From the above equations, the effective layered structure can be constructed. It should be noted that the above planar model is based on simplified micromechanics based analysis. One of the objective of building such model is to analyze the effect of wave interactions on the impact response of laminated composites.

It is fully realized that, however, GRP is a 2D woven structure, so the weaving effect should be investigated for a simplified one-dimensional analysis. For a simple unit cell model of the plain weave composites as shown in Fig. 5-7(a), the angle between the warp tow and the resin is not a constant. So the incident longitudinal wave reach the fiber/matrix interface with an angle and both longitudinal and transverse waves will be generated in fiber and matrix, as shown in Fig. 5-7(b). So the second question is how to get effective properties of 2D woven structure for 1D analysis? In order to clearly understand this effect, micromechanics based analysis is necessary. When we take a close look at a single lamina as shown in Fig. 5-7(a), it is clear that some geometric ratios are critical for the applicability of the layered model. For example, it is easy to understand that thickness ratio of warp/fill tows b vs the width of the unit cell l determines the angle of incident waves. When b/l is very small, the impact is almost normal. As a result, the amplitude of the shear waves are negligible and the majority strength is contained in longitudinal wave. It is also clear that both reflected longitudinal and transverse waves are almost perpendicular to the fiber tows. In fact, general $b/l < 0.15$, the corresponding angle α is about 8.5° [41]. Though this justifies the 1D approximation over one unit cell, the woven effect cannot be neglected for long wave propagation distance.

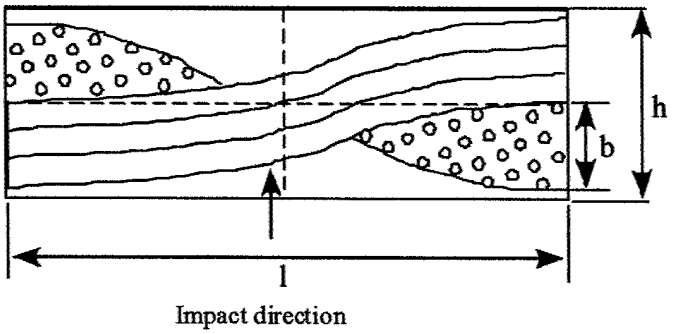

(a)

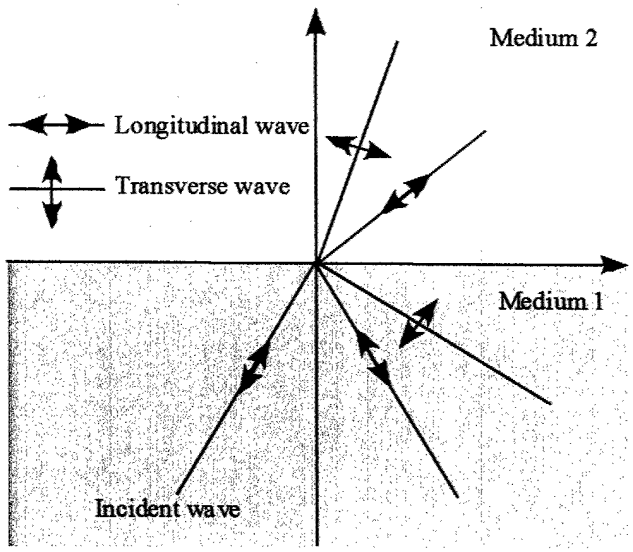

(b)

Figure 5-7: Lamina of 2D woven GRP and wave refelctions in a curved interface.

Chapter 6

Conclusions

The high velocity impact response of engineering composites is very complicated. The measured stress wave profiles often don't exhibit clear or regular structure when compared with homogeneous metals or ceramics. However, due to the length scales of laminated composites, wave interactions can play critical role in forming the observed profiles. Periodic layered configuration has been recognized as an ideal model for investigation of wave propagation inside the laminated composites. As a result, most effort of this work has focused on the impact response of layered heterogeneous materials subjected to plate impact loading.

In this work, the plate impact problem has been formulated. As shown in Fig. 3-10 the plate impact problem is different from the problem of unit step loading, for which the analytical solution has long been available. The loading conditions of the target plate, which is a heterogeneous layered medium, varies continuously due to the reflections inside the target plate. The steady state σ_{mean} has also been identified to be directly related to multiple wave interactions at interfaces. Consequently, besides following the case of unit step loading by applying Floquet theory and the late time approach. the proposed solution methodology meanwhile takes into account of the details of the wave reflections by using multistep loading. The mixture theory as well as dispersion relation is invoked to derive σ_{mean} inside the target system. Then the solution is obtained by means of superposition of stress increments over time, as shown in Eq. (3.65). The spatial applicability of the late time solution is also identified. For systems with large impedance mismatch and high interface density, the solutions are found to be good at relatively small distance. In addition,

the solution based on elastic analysis is extended for shock loading condition by taking into account of EOS and also the 'overtaking effect' between the wave trains. This approach is validated by matching two experimental data and the comparison is good.

Having developed the analytical solution for the stress response in layered systems, analysis of the material heterogneity factors and their effects on the stress structures are examined in chapter 4. It confirms our previous idea that the origin of the observed structure of the shock waves can be attributed to material heterogeneity at the interfaces. The level of heterogeneity of a layered system depends on material property mismatch (for elastic cases, mainly the impedance mismatch) and the characteristics of geometry arrangement (such as total target thickness, thickness ratio between two component materials, interface density or number of layers with the target of a certain thickness, stacking sequence). As a result, the proposed analytical solution in this paper and together with the heterogeneity factors are all critical for designing the optimum layered armor systems. The solution in section 3.2.2 and that in section 3.2.3 are for linear elastic response and shock response, respectively. When the loading strength is such that the material response falls into elastic-plastic region, both elastic wave and plastic waves are induced. Therefore, the effect of yielding strength on stress response was studied numerically.

Failure modes are essential to the dynamic response of composites besides wave interaction. The current homogenized material model may not be adequate or capable of modeling the failure modes of fiber, matrix and interphase reasonably. So a layered model has the advantage of capturing the different damage mechanisms inside the heterogeneous materials. It has been demonstrated that the proposed solution predicts reasonably well about the stress history inside a layered system at a moderate distance for both elastic response and shock response. The applicability of the layered model and the corresponding solution to the real engineering composites (such as GRP) has been evaluated and seems to be practical for thin target plates. However, it is fully recognized that more work needs to be done for modeling 2D woven composites, especially for wave interactions through curved microstructure.

Bibliography

[1] J. Boteler, A. Rajendran, and D. Grove, "Shock wave profiles in polymer matrix composite," *Shock Compression of Condensed Matter* , pp. 563–566, 1999.

[2] O. Sherby, S. Lee, R. Koch, T. Sumi, and J. Wolfenstine, "Multilayered composites based on ultrahigh carbon steel and brass," *Materials and Manufacturing Processes* **5**, pp. 373–376, 1990.

[3] H. Mahfuz, Y. Zhu, A. Haque, A. Abutalib, V. Vaidya, S. Jeelani, B. Gama, J. Gillespie, and B. Fink, "Investigation of high-velocity impact on integral armor using finite element method," *International Journal of Impact Engineering* **24 (2)**, pp. 203–217, 1999.

[4] B. Fink, "Performance metrics for composite integral armor," *Journal of Thermalplastic Composite Materials* **13 (5)**, pp. 417–431, 2000.

[5] E. DeLuca, J. Prifti, W. Betheney, and S. Chow, "Ballistic impact damage of s2-glass-reinforced plastic structural armor," *Composites Science and Technology* **58**, pp. 1453–1461, 1998.

[6] D. Grady, "Shock-wave compression of brittle solids," *Mechancis of Materials* **29**, pp. 181–203, 1998.

[7] S. B. A. Mal, "Elastic waves in a fiber-reinforced composite," *Journal of the Mechanics and Physics of Solids* **22**, pp. 217–229, 1974.

[8] S. Datta, H. Ledbetter, and R. Kriz, "Calculated elastic constants of composites containing anisotropic fibers," *International Journal of Solids and Structures* **20**, pp. 429–438, 1984.

[9] A. Mal and A. Chatterjee, "The elastic moduli of a fiber-reinfored composite," *Journal of Applied Mechanics* **99**, pp. 61–67, 1977.

[10] T. Nicholas and A. Rajendran, *Material Behavior at High Strain Rates*, Short Course Notes, Monterey, California, 1994.

[11] D. Grady, "Scattering as a mechanism for structured shock waves in metals," *Journal of Mechanics and Physics in Solids* **46 (10)**, pp. 2017–2032, 1998.

[12] T. Nicholas and A. Rajendran, "Materials behavior at high strain rates,"

[13] Z. Chen and X. Xin, "An analytical and numerical study of failure waves," *International Journal of Solids and Structures* **36**, pp. 3977–3991, 1999.

[14] J. Ferreira, J. Costa, P. Reis, and M. Richardson *C.R. Acad. Sci. Paris* **91**, pp. 880–882, 1880.

[15] S. Rytov, "Acoustical properties of a thinly laminated medium," *Soviet Physics and Acoustics* **2**, pp. 68–80, 1968.

[16] C. Sun, J. Achenbach, and G. Herrmann, "Time harmonic waves in a stratified medium propagating in the direction of the layering," *Journal of Applied Mechanics* **90 E**, pp. 408–411, 1968.

[17] J. Peck and G. Gurtman, "Dispersive pulse propagation parallel to the interfaces of a laminated composite," *Journal of Applied Mechanics* , pp. 479–484, 1969.

[18] C. Sve, "Stress wave attenuation in composite materials," *Journal of Applied Mechanics* , pp. 1151–1153, 1972.

[19] C. Chen and R. Clifton, "Asymptotic solutions for wave propagation in elastic and viscoelastic bilaminates, developments in mechanics," *Proceedings of the 14th Midwestern Mechanics Conference, University of Oklahoma* **8**, pp. 399–417, 1975.

[20] C. Lundergan and D. Drumheller, "Propagation of stress waves in a laminated plate composite," *Journal of Applied Physics* **42**.

[21] L. Barker, "A model for stress wave propagation in composite materials," *Journal of Applied Mechanics* **5**, pp. 140–162, 1971.

[22] L. Barker, P. C. C.D. Lundergan, and M. Gurtin, "Nonlinear viscoelasticity and the evolution of stress waves in laminated composites: A comparison of theory and experiment," *Journal of Applied Mechanics* .

[23] Y. Oved, G. Luttwak, and Z. Rosenberg, "Shock wave propagation in layered composites," *Journal of Composite Materials* **12**, pp. 84–96, 1998.

[24] G. Kanel, M. Ivanov, and A. Parshikov, "Computer simulation of the heterogeneous materials response to the impact loading," *International Journal of Impact Engineering* **17**, pp. 455–464, 1995.

[25] D. Dandekar and P. Beaulieu, "Shots 518 and 521-1," *AMD* **48**, pp. 63–70, 1995.

[26] B. Clements, J. Johnson, and R. Hixson, "Stress waves in composite materials," *Physics Review E* **54**, pp. 6876–6888, 1996.

[27] B. Clements, J. Johnson, and F. Addessio, "wave propagation in an epoxy-graphite laminate," *Journal of Applied Physics* **82 (10)**, pp. 4831–4837, 1997.

[28] S. Zhuang, "Shock wave propagation in periodically layered composites," *PhD Dissertation* .

[29] V. Nesterenko, *Dynamic of Heterogeneous Materials*, Springer Verlag, Berlin, 2001.

[30] J. Hou, "Prediction of impact damage in composite plates," *composite science and technology* **60**, pp. 273–281, 2000.

[31] W. Stronge and S. Matemilola, "Rate effect for impact damage initiation in cfrp laminates," *Journal De Physique IV* , pp. 225–230, 1994.

[32] W. Cantwell and J. Morton, "The influence of target geometry on the high velocity impact response of cfrp," *Composite Structures* **10**, pp. 247–265, 1988.

[33] L. D, "Impact-induced delamination - a view of bending stiffness mismatching," *Journal of Composite Materials* **22**, pp. 674–692, 1988.

[34] J. C. Brewer and P. A. Lagace, "Quadratic stress criterion for initiation of delamination," *Journal of Composite Materials* **22 (12)**, pp. 1141–1151, 1988.

[35] T. O'Brien, "Characterization of delamination onset and growth in composite laminate," *American Society for Testing and Materials* .

[36] G. Dorey, "Impact damage in composites-development,consequences and prevention," *6th Int. Conf. On Composite Materials and 2nd European Conf. On Composite Materials* **3**, pp. 3.1–3.26, 1988.

[37] A. Davies, X. Zhang, and D. Hitchings, "Modeling impact damage in laminated composites," pp. 1216–1231, 1997.

[38] J. K. Chen, F. Allahdadi, and T. C.Carney, "High-velocity impact of graphite/epoxy composite laminates," *Composites Science and Technology* **57**, pp. 1369–1379, 1997.

[39] A. Mal, "Wave propagation in layered composite laminates under periodic surface loads," *Wave Motion* **10**, pp. 257–266, 1988.

[40] H. Espinosa, S. Dwivedi, and H. Lu, "Modeling impact induced delamination of woven fiber reinforced composites with contact/cohesive laws," *Computer Methods in Applied Mechanics and Engineering* **183: (3-4)**, pp. 259–290, 2000.

[41] J. Kuhn and P. Charalambides, "Elastic response of porous matrix plain weave fabric composites: Part i-modeling," *Journal of Composite Materials* **32**, pp. 1427–1471, 1998.